

UNIVERSITY OF KWAZULU-NATAL

**DENSITY FUNCTIONAL THEORY STUDIES OF THE NON-
CATALYTIC AND CATALYTIC OXIDATIVE
DEHYDROGENATION REACTION OF n-HEXANE TO 1-
AND 2-HEXENE**

2017

NKULULEKO E. DAMOYI

DENSITY FUNCTIONAL THEORY STUDIES OF THE NON-CATALYTIC AND CATALYTIC OXIDATIVE DEHYDROGENATION REACTION OF *n*-HEXANE TO 1- AND 2-HEXENE

by

NKULULEKO E. DAMOYI

Submitted in fulfilment of the academic requirements for the degree of Master of Science in the School of Life Sciences, University of KwaZulu-Natal, Westville campus.

The chapters in this thesis are written as a set of three research papers, Chapter 2 to 4, with all-inclusive Chapter 1 and Chapter 5. The three papers will be published in internationally recognized, peer-reviewed journals.

As the candidate's supervisors, we have approved this thesis for submission.

Supervisor:

Signed:----- Name: **Prof. H.B. Friedrich** Date:-----

Co-Supervisor:

Signed:----- Name: **Prof. H.G. Kruger** Date:-----

Co-Supervisor:

Signed:----- Name: **Dr D. Willock** Date:-----

ABSTRACT

One of the important areas in the present petrochemical industry is the catalytic production of olefins that have wide applications, including as starting materials for many valuable products, like polymers. Although the choice and advancement in the development of appropriate catalysts for such processes is a challenging effort, catalytic oxidative dehydrogenation (ODH) methods potentially provide for energy-favourable transformation of widely available hydrocarbon feedstocks into a variety of products, including olefins. The aim of this study was to use Density Functional Theory (DFT) methods to model the non-catalytic and catalytic (VMgO) ODH conversion of *n*-hexane hydrocarbon to 1- and 2-hexene, which are products that were characterised and obtained in low yields (< 20%) in our laboratory experiments. All the reaction pathways were modelled under experimental conditions of 573, 673 and 773 K and the relative total energies (ΔE^\ddagger , ΔE , ΔG^\ddagger and ΔG) were determined and in order to elucidate the non-catalytic and catalytic radical mechanisms for the reaction.

In Chapter 2 of the thesis, the kinetically and thermodynamically most favourable non-catalytic reaction pathways were determined, with the rate-determining step (RDS) proposed as the interaction of the *n*-hexane and the O₂ molecules through β -H abstraction ($\Delta E^\ddagger = +42.4$ kcal/mol) at 573 K. The most stable intermediates were found to be the alkoxy (C₆H₁₃O) and hydroxyl (OH) radicals. The propagation steps that lead to 1- and 2-hexene were proposed as likely to involve the two intermediate radicals, although the C₆H₁₃O radical may also contribute to side reactions that produce undesired oxygenates. Chapters 3 and 4 discuss the catalytic radical mechanisms of the interaction of *n*-hexane with H₃VO₄ and H₄V₂O₇ model catalysts, respectively. Both the models comprise the vanadyl O atoms that are associated with the RDSs, through β -H abstraction at the kinetically and thermodynamically favourable temperature of 573 K. The calculated relative energies were $\Delta E^\ddagger = +27.4$ and $+32.7$ kcal/mol, for H₃VO₄ and H₄V₂O₇, respectively. From the calculated value of $\Delta E^\ddagger = +43.9$ kcal/mol, the bridging O atom in H₄V₂O₇ is not likely to activate *n*-hexane molecules. The produced C₆H₁₃ radical intermediate may either generate the desired olefin through the second H-abstraction by another vanadyl O in close proximity to it, or it may chemisorb to any of the surface O atoms, thereby enabling side-reaction channels for producing undesired products, such as the oxygenates. For both the catalyst models, the calculations show that the chemisorption pathways are kinetically and thermodynamically more favourable by ~10 kcal/mol than the H-abstraction pathways. This may be the reason for low yields (< 20%) that were obtained in our laboratory experiments for this catalytic system. The H-abstraction pathways that may lead to olefins are also likely to lead to the accumulation of OH groups on the catalyst surface. Low energy barriers for H-transfer and migration between two adjacent OH groups were calculated, with related intermediates stabilizing as a result of the formation of H₂O. Barrier-less energies were also calculated for the reoxidation of the reduced V(III) by the O⁻ species, to produce V(V) in both H₃VO₄ and H₄V₂O₇. Finally, Chapter 5 discusses conclusions and the most likely mechanism for the combined non-catalytic and catalytic systems is proposed.

PREFACE

The theoretical work described in this thesis was carried out in the School of Chemistry, University of KwaZulu-Natal, Westville campus, from January 2010 to November 2016, under the supervision of Professor H.B. Friedrich and co-supervision of Professor H.G. Kruger and Dr D. Willock.

These studies represent original work by the author and have not otherwise been submitted in any form for any degree or diploma to any tertiary institution. Where use has been made of the work of others it is duly acknowledged in the text.

DECLARATION 1 - PLAGIARISM

I, NKULULEKO E. DAMOYI declare that,

1. The research reported in this thesis, except where otherwise indicated, is my original research.
2. This thesis has not been submitted for any degree or examination at any other university.
3. This thesis does not contain other persons' data, pictures, graphs or other information, unless specifically acknowledged as being sourced from other persons.
4. This thesis does not contain other persons' writing, unless specifically acknowledged as being sourced from other researchers. Where other written sources have been quoted, then:
 - (a) Their words have been re-written but the general information attributed to them has been referenced.
 - (b) Where their exact words have been used, then their writing has been placed in italics and inside quotation marks, and referenced.
5. This thesis does not contain text, graphics or tables copied and pasted from the Internet, unless specifically acknowledged, and the source being detailed in the thesis and in the References sections.

Signed:

DECLARATION 2 - PUBLICATIONS

1. One paper (Publication 1) has been published in a peer-reviewed journal:

N.E. Damoyi, H.B. Friedrich, H.G. Kruger and D. Willock, **Density Functional Theory Studies of the Uncatalysed Gas-Phase Oxidative Dehydrogenation Conversion of *n*-Hexane to Hexenes**, *Comput. Theor. Chem.* 1114 (2017) 153-164.

2. Two other papers are presently being finalized for publication successively from Publication 2, “A DFT Study of the ODH of *n*-hexane on isolated H_3VO_4 ” to Publication 3, “A Density Functional Theory Study of the Catalytic ODH of *n*-Hexane Over Isolated $\text{H}_4\text{V}_2\text{O}_7$ ”.

3. The details of the contributions from authors are,

N.E. Damoyi conducted the computational/theoretical work and prepared the three draft papers. The final publications are being supervised by Professors H.B. Friedrich and H.G. Kruger, and Dr D. Willock.

ACKNOWLEDGEMENTS

I would like to thank my supervisor Professor H.B. Friedrich and co-supervisors Professor H.G. Kruger and Dr D. Willock for their guidance, encouragement and assistance throughout the duration of this research project.

This work was financially supported by the NRF, SASOL and Johnsson Matthey.

I am grateful to the following:

My parents, brother and sisters for their continued support through difficult times.

My employer, Mangosuthu University of Technology (MUT) for support.

My MUT and UKZN-CRG colleagues for encouragement.

The Centre for High Performance Computing (CHPC) in Cape Town, South Africa, for providing the computational resources.

My absolute praise to the Almighty God who has always been with me all my life.

LIST OF CONTENTS

TITLE	ii
ABSTRACT.....	iii
PREFACE.....	iv
DECLARATION 1 – PLAGIARISM	v
DECLARATION 2 – PUBLICATIONS	vi
ACKNOWLEDGEMENTS	vii
LIST OF CONTENTS	viii
CHAPTER 1	1
1.1 THE PETROCHEMICAL INDUSTRY	1
1.2 THERMAL AND STEAM CRACKING	1
1.3 OXIDATION METHODS	2
1.4 METHODS AND MODELLING STUDIES	4
1.5 OUTLINE OF THESIS.....	7
REFERENCES	8
CHAPTER 2	15
DENSITY FUNCTIONAL THEORY STUDIES OF THE NONCATALYTIC GAS PHASE OXIDATIVE DEHYDROGENATION CONVERSION OF <i>n</i>-HEXANE TO HEXENES	15
ABSTRACT	15
INTRODUCTION	16
THEORETICAL METHODOLOGY	18
RESULTS AND DISCUSSION	20
CONCLUSIONS	31
ACKNOWLEDGEMENTS	32
REFERENCES	32

CHAPTER 3	36
A DFT STUDY OF THE ODH OF <i>n</i>-HEXANE OVER ISOLATED H₃VO₄ IN GAS PHASE	36
ABSTRACT	36
INTRODUCTION	37
THEORETICAL METHODOLOGY	38
RESULTS AND DISCUSSION	40
CONCLUSIONS	50
ACKNOWLEDGEMENTS	51
REFERENCES	51
CHAPTER 4	56
A DFT STUDY OF THE GAS PHASE ACTIVATION OF <i>n</i>-HEXANE OVER ISOLATED H₄V₂O₇	56
ABSTRACT	56
INTRODUCTION	57
THEORETICAL METHODOLOGY	58
RESULTS AND DISCUSSION	60
CONCLUSIONS	70
ACKNOWLEDGEMENTS	71
REFERENCES	71
CHAPTER 5	74
SUMMARY AND PROPOSED MECHANISM	74

CHAPTER 1

1.1 The Petrochemical Industry

The development of South Africa's petrochemical industry started in the 1950s with Sasol's coal-to-liquid (CTL) plant in Sasolburg, and presently approximately 40% of the country's liquid fuels are derived from coal through Sasol's Fischer-Tropsch technology [1]. The production of South Africa's chemicals is well diversified and contributes ~5% to gross domestic product and ~25% of manufacturing sales. The production of liquid fuels and plastic products accounts for >50%, and nine other chemicals, for example pharmaceuticals and organic chemicals, accounting for >40% [2]. Figure 1 below shows the global production of organic chemicals in 1993. Although alkenes are important raw materials in the petrochemical industry due to their low cost and ability to be functionalised easily, it has been envisaged that the future of the petrochemical industry leans towards the direct use of alkanes as starting materials, since they are a much more economical raw material and can be easily sourced from petroleum by-products [3].

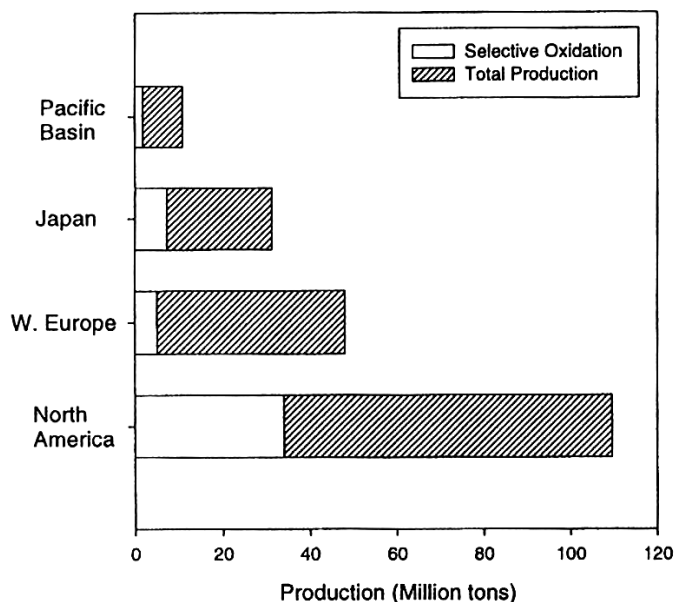
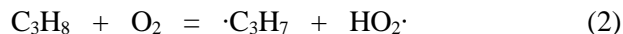


Figure 1 World organic chemical production in 1993 [4]

1.2 Thermal and Steam Cracking

Natural gas and mainly petroleum are the natural sources of saturated hydrocarbons. Cracking of hydrocarbon feedstock, for example, ethane, LPG, or naphtha, has been the major source of light olefins, accounting for ~70% of global olefin production, and fluidized catalytic cracking (FCC) accounting for ~28% of total gasoline production [5]. Thermal decomposition of saturated hydrocarbons proceeds stepwise by loss of hydrogen or hydrocarbon fragments with concomitant formation of industrially useful unsaturated cracked products such as acetylene, olefins and aromatic hydrocarbons [6]. In both thermal and steam cracking, high temperatures in the range of 450 to 750 °C and pressures of up to 70 bar are used to break the large hydrocarbons into smaller ones with, however, large amounts of unwanted solid coke also produced [7]. Choudhary *et al.* [8] reported that in the absence of oxygen, propane is thermally activated only at temperatures above 700 °C, and its reaction is initiated through the homolytic scission of

a C-C bond (equation 1), while in the presence of oxygen, propane is activated at lower temperatures (~635 °C) and the chain initiation reaction is expected to occur through an abstraction of H from propane molecules by oxygen to form the propyl radicals (equation 2):



Other disadvantages of the thermal and steam cracking methods include, the endothermic nature of the reaction, deactivation of the catalyst and formation of undesired products when heavier feedstock is used [9]. The increasing demand for ethylene and propylene has reinforced research for alternative technologies for their production. A number of alternative technologies, including oxidative dehydrogenation (ODH) have been investigated for olefin production [10–18].

1.3 Oxidation Methods

Oxidation methods do not suffer from the drawbacks of thermal and steam cracking. The presence of oxygen in the process renders the production of a variety of products thermodynamically favourable through the formation of water and carbon oxides. The partial oxidation of hydrocarbons in the gas phase occurs at moderate temperatures, from ~300 to ~1200 °C, i.e. below the characteristic temperature of the gas phase combustion of hydrocarbons (above 1200 °C) [19]. The distinction between partial oxidation and combustion mechanisms is determined not only by the difference in the temperature of the process, but also by the mechanism itself. Figure 2 shows the oxidation of methane which has been thoroughly studied, with different parts of the indicated temperature range dominated by different products. The intermediate-temperature range can be divided into three sub-ranges, namely, (i) the formation of oxygenates (300-600 °C), (ii) oxidative coupling of methane (OCM) with predominant formation of C₂ hydrocarbons (600-900 °C), and (iii) the preferential formation of syngas (>900 °C).

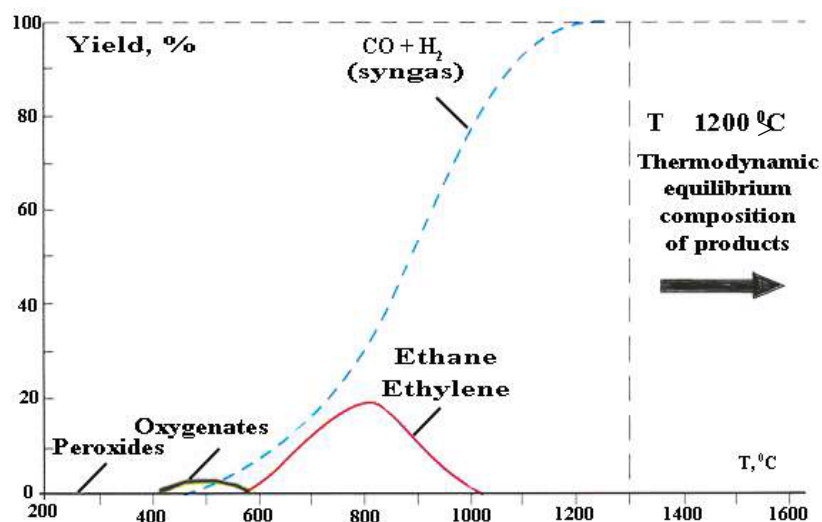
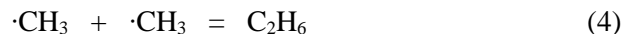


Figure 2 Temperature ranges of formation and the yields of the main products of methane partial oxidation [20].

At temperatures below 600 °C, the dominant reaction is the formation of the methylperoxy radical, CH₃OO·, through reversible reaction (equation 3) which leads to the formation of the oxygenates,



At temperatures of 600 °C to 900 °C, the oxidation of the methyl radicals is too slow, as a result they combine to form C₂H₆,



Above 900 °C, the rates of these reactions (equations 3 and 4) are high enough, resulting in the deep oxidation of methane, forming syngas,



ODH of low chain hydrocarbons can also be operated at lower temperatures than either the thermal or the non-oxidative catalytic processes. However, given that the formation of combustion products, for example carbon oxides, is also thermodynamically favourable, selectivity control is a major challenge [21]. The undesired carbon oxides can be formed either by direct alkane combustion, or by deep oxidation of the produced olefins. Thus, a catalyst for such a reaction should be designed to prevent the undesirable reactions leading to carbon oxides [22-24]. Supported vanadium oxide catalysts comprise high thermal stabilities, large surface areas and are one of the best catalysts for the ODH of alkanes [25-29]. Several research groups have studied the mechanisms of ODH reactions on vanadium-based catalysts [30-32], and all support a radical mechanism for alkane activation. There is limited literature on oxidative conversion of *n*-hexane or longer paraffins over catalysts made up of vanadium oxides as active species and magnesium oxides as supports (VMgO). Some of the publications include, (i) Centi *et al.* [33] who reported on the conversion of cyclohexane to cyclohexanol and cyclohexanone; (ii) Schmidt *et al.* [34] also reported on the partial oxidation of iso-octane, *n*-hexane, cyclohexane and *n*-butane on Rh-coated alumina monolith; (iii) Centi *et al.* [35] reported on the oxidation of *n*-hexane over a VPO catalyst yielding maleic anhydride, phthalic anhydride, benzoic acid, cracked products and carbon oxides (a 23 % selectivity to maleic anhydride at a conversion of 50 % was observed); (iv) Michalakos *et al.* [36] reported benzene, cyclohexene and carbon oxide production from cyclohexane oxidation over a VMgO catalyst; (v) Skotak *et al.* [37] reported on the conversion of *n*-hexane in excess hydrogen in air over Pd/Al₂O₃ and Pt/Al₂O₃ catalysts (the main products obtained were methylpentane and methylcyclopentane, while benzene and cyclohexane were obtained as minor products); and (vi) Mikovsky *et al.* [38] reported the oxidation of *n*-hexane over tellurium loaded NaX and KX zeolites to produce benzene (conversions of greater than 80 % with selectivities to benzene greater than 90 % were obtained via a dehydrocyclisation process, with the other by-products being C₁-C₅ cracked compounds and coke).

Our research group (CRG) at the University of KwaZulu Natal (UKZN) under the leadership of Professor Friedrich has also published a number of papers involving ODH of *n*-hexane and higher alkanes over VMgO catalysts [39-42]. The low yields of olefins and aromatics that were obtained in laboratory experiments necessitated this theoretical study. Generally, it is accepted that at low V loadings, the VMgO catalyst is characterised as comprising mainly tetrahedral and isolated VO_x species, with dimeric V-O-V and long-chain species featuring at high V loadings [43]. The vanadyl bond (V=O) has been proposed by many investigators to contain a critical oxygen involved in hydrocarbon oxidation reactions [44-48], while some others have mentioned the bridging O sites in V-O-V species [31], [49]. One of the aims of this work was to determine the most active O site, as either the vanadyl O or the bridging O, in *n*-hexane elementary oxidation reactions to hexenes. The merits of the oxidative dehydrogenation (ODH) of the inexpensive alkanes to produce the synthetically more valuable products, such as olefins and aromatics, represents a driving force that motivates the research for developing active and selective catalysts for this purpose [50].

1.4 Methods and Modelling Studies

Although heterogeneous catalysis is largely an experimental field, computational modelling and simulation, as a complementary and supplementary tool, is an exploding field that is increasingly being recognized as important and essential in the study and development of catalytic systems [51-53]. A good model not only helps experimentalists to rationalize their results, but also helps make predictions that challenges the capability of available experimental techniques in terms of the spatial, time and energy resolutions, and guide experimentalists to design new experiments [54].

Theoretical modelling plays a key role in the study of the mechanism of the target reaction. This includes the determination of the geometry, stability and electronic properties of reactant and intermediate species interacting with different active sites present on the catalyst, as well as determination of transition states and activation energy barriers for all elementary steps constituting the global process [55].

Computational modelling is either molecular mechanics or quantum mechanics-based. Common methods include semi-empirical, density functional theory (DFT) and *ab initio* methods. The least computationally demanding methods are molecular mechanics and *ab initio* methods are the most accurate and are therefore more demanding computationally [56]. Quantum mechanics was developed mainly by Bohr, Schrödinger, Heisenberg, Born and Pauli, and the understanding of chemical bonding, spectral phenomena, molecular reactivity and other fundamental chemical problems rests heavily on a knowledge of the detailed behaviour of electrons in atoms and molecules [57].

Density functional theory (DFT) modelling methods are the most popular in terms of computational time and the quality of results, as *ab initio* methods, is based on quantum mechanics [58], [59]. DFT methods are of particular value for transition metal complexes where electron correlation can be large, and for systems of similar complexity like metals, solid-state compounds, and surfaces [60-62]. Since the fundamental work of Hohenberg and Kohn [63], and Kohn and Sham [64], DFT has undergone significant theoretical and computational advances in recent years. The basis of DFT involves determining the properties of a molecule from its electron density. In the Kohn-Sham DFT formalism [65], the electron density is decomposed into a set of orbitals, leading to a set of one electron Schrodinger-like equations to be solved self-consistently.

DFT simulation of solid surfaces and surface complexes are nowadays performed with the help of two types of models, namely, (i) representation of surfaces in terms of a unit cell periodically repeated in two- (slabs) or three-dimensions [65], [66], and (ii) cluster models that treat complexes on solid surfaces in terms of localized states, using the conventional chemical language of molecular orbitals (MO), exactly as if one were simply considering a molecule formed by two fragments, and this model is particularly useful for clarification of the surface reactivity [67], [68]. Fortunately, the current accessibility of high-performance computers and efficient software makes such an increased computational demand affordable and slab models are becoming very popular in theoretical studies in catalysis [69], [70].

In studies of molecular interactions, basis set superposition errors (BSSEs) are encountered as a result of artificial shortening of intermolecular distances and concomitant artificial strengthening of the intermolecular interaction [71], [72]. Such errors are more pronounced for small basis sets. The dimer, AB, can be artificially stabilized as monomer A utilizes the extra basis functions from monomer B to describe its electron distribution, and vice versa. This inconsistent treatment of the basis set for each monomer as the intermolecular distance is varied is the source of the BSSE [73]. The common method that is utilised to remove BSSE is the counterpoise correction [74]. This correction was not included in this work because of the use of a relatively larger basis set.

In this study we opted for gas-phase cluster, and such modelling has proven to be a powerful tool in the comprehension of reaction mechanisms in a variety of fields [75]. There is a vast amount of quantum chemical codes that are readily available and applicable for cluster modelling studies [67], [76-79]. Figure 3 illustrate the hierarchical approach to modelling catalytic systems.

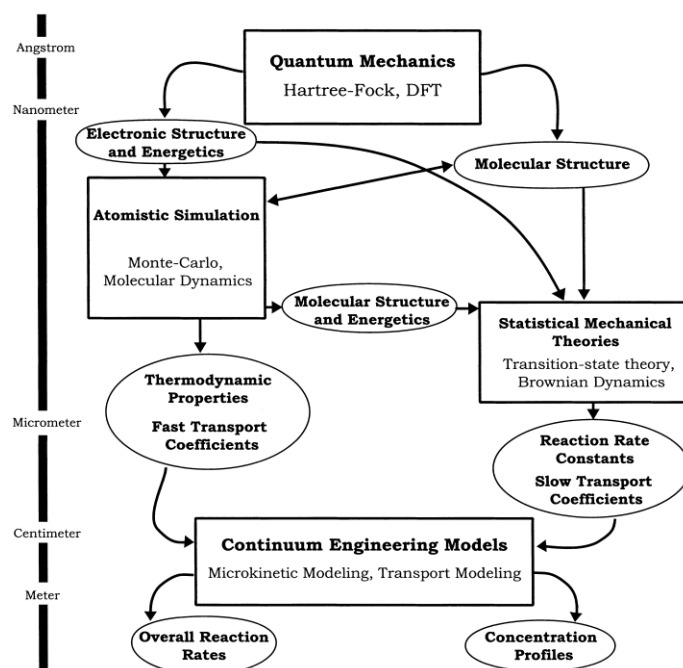


Figure 3 Hierarchical approach to modelling catalytic systems. Computational methods are shown in rectangles, with inputs and outputs in circles. General categories of computational methods are in bold (e.g. Quantum Mechanics), and specific examples are in regular lettering (e.g. Hartree-Fock). The hierarchical approach integrates together information from computational techniques at various length and time scales. Feedback between different levels of the hierarchy is important in directing and refining the modelling performed at each level [80].

DFT gas-phase cluster modelling was followed because of reasonable computational costs compared to DFT periodic systems, and as a result quick insight that pertains to reaction mechanisms was established. The Gaussian 09W code [76] incorporating the Gausview 5.0 graphics interface was utilised and all the calculations were run through the Centre for High Performance Computing (CHPC) in Cape Town, South Africa. All optimizations of the reactant, intermediate, transition state (TS) and product structures were performed without constraints under laboratory experimental conditions of 573, 673 and 773 K. The frequency calculations were performed in order to calculate the zero-point energy and to confirm the optimised reactant, intermediate and product structures (no negative frequencies) and transition state structures (one negative frequency along the reaction coordinate). The B3LYP hybrid functional, which combines Becke's three-parameter nonlocal hybrid exchange potential and the nonlocal correlation functional of Lee, Yang and Parr [81], [82] together with the 6-311+g(d,p) basis set for C, O and H atoms and the relativistic Stuttgart effective core potentials (ECPs) [83], [84] for the V atom, were utilised for the calculations. The transition state optimizations were determined through "relaxed" potential energy surface (PES) scans and were confirmed by the intrinsic reaction coordinate (IRC) calculations from the algorithm developed by González and Schlegel [85], [86]. The B3LYP functional is quite popular and

known to provide good description of the PESs of many cluster systems including transition metal-containing compounds [87-89]. There is also a vast number of publications with DFT cluster modelling utilising the B3LYP functional [75], [90-98]. The qualitative description of bonding was performed through the presently most accurate and popular Natural Bonding Orbital (NBO) procedure [99], [100]. NBO is based on a method for optimally transforming a given wavefunction into localized form, corresponding to the one-center ("lone pair") and two-center ("bond") elements of the chemist's Lewis structure picture. The NBOs are obtained as local block eigenfunctions of the one-electron density matrix, having optimal convergence properties for describing the electron density. The set of high-occupancy NBOs, each taken doubly occupied, is said to represent the "natural Lewis structure" of the molecule. Delocalization effects appear as weak departures from this idealized localized picture. Some of the properties that may be calculated include atomic charges, highest occupied and lowest unoccupied molecular orbitals (HOMO and LUMO), hybrid orbitals and donor-acceptor stabilization energies.

The quantitative description of results is through the calculation of kinetic and thermodynamic properties, such as activation energies (ΔE^\ddagger , ΔH^\ddagger or ΔG^\ddagger), electronic energy changes (ΔE), enthalpy changes (ΔH), Gibbs free energy changes (ΔG) and entropy changes (ΔS) and rate constants (k), from elementary reaction steps under laboratory experimental conditions. These properties assist in the elucidation of mechanisms for overall reactions and are calculated thus [76],

$$\Delta E^\ddagger = E_{(TS)} - \Sigma E_{(R)} \quad (6)$$

$$\Delta E = \Sigma E_{(P)} - \Sigma E_{(R)} \quad (7)$$

$$\Delta H = \Sigma H_{(P)} - \Sigma H_{(R)} \quad (8)$$

$$\Delta G = \Sigma G_{(P)} - \Sigma G_{(R)} \quad (9)$$

$$\Delta S = \Sigma S_{(P)} - \Sigma S_{(R)} \quad (10)$$

$$k(T) = \frac{K_b T}{hc} e^{-\frac{\Delta G^\ddagger}{RT}} \quad (11)$$

Where: ΔE^\ddagger is the electronic energy of activation,

$E_{(TS)}$ is the electronic energy of the transition state,

$\Sigma E_{(P)}$ is the sum of the electronic energies of the products,

$\Sigma E_{(R)}$ is the sum of the electronic energies of the reactants,

$\Sigma H_{(P)}$ is the sum of the enthalpies of the products,

$\Sigma H_{(R)}$ is the sum of the enthalpies of the reactants,

$\Sigma G_{(P)}$ is the sum of the Gibbs free energies of the products,

$\Sigma G_{(R)}$ is the sum of the Gibbs free energies of the reactants,

$\Sigma S_{(P)}$ is the sum of the entropies of the products,

$\Sigma S_{(R)}$ is the sum of the entropies of the reactants,

$k(T)$ is the rate at temperature T,

K_b is the Boltzmann constant,

ΔG^\ddagger is Gibbs free energy of activation,

h is Planck's constant,

R is the gas constant,

c is the concentration (for these calculations, c is taken to be 1).

The contribution of computational modelling in chemistry research has been highlighted by the conferment of the Nobel Prizes in Chemistry to Pople and Kohn in 1998 for their work on laying the foundations and to Ahmed Zewail in 1999 for his work in femtosecond spectroscopy of chemical reactions.

1.5 Outline of Thesis

The aim of this project was to calculate and compare the kinetic and thermodynamic properties for the activation of *n*-hexane by gas-phase molecular O₂, catalytic H₃VO₄ and catalytic H₄V₂O₇, in order to determine the most likely mechanism for the formation of 1- and 2-hexene. The UKZN Catalysis Research Group (CRG) under the leadership of Professor H.B. Friedrich has been involved in a number of experimental research projects that include catalytic (VMgO) ODH of long chain alkanes. Low yields of olefins and aromatics obtained from experiments necessitated the development of this DFT modelling project, with the belief that understanding the reaction mechanism would facilitate the improvement of experiments and reaction yields.

Chapter 2 of the thesis deals with the activation of *n*-hexane by gas-phase molecular O₂ and the most likely reaction mechanism is proposed from calculated kinetic and thermodynamic properties. The paper for this research work is in its final stages of preparation for publication. Chapters 3 and 4 relate to activation of *n*-hexane by catalytic H₃VO₄ and catalytic H₄V₂O₇, respectively. Again the mechanisms, albeit similar to some extent, are also proposed based on calculated kinetic and thermodynamic properties. The two related papers are presently being prepared for publication early next year, 2017. Finally, Chapter 5 discusses conclusions and the most likely mechanism for the combined non-catalytic and catalytic systems is proposed.

All supplementary material, namely, optimised structures of reactants, intermediates, products and transition states are attached on a CD, and can be accessed through the Gausview 5.0 graphics interface as implemented in the Gaussian 09W code.

References

- [1] G.C. Gerrans, **Historical Overview of the South African Chemical Industry: 1896-1998**, Chem. Int. 21 (1999) 71-77.
- [2] E. Mahembe, **Underhill Corporate Solutions, Research study to identify needs, opportunities and challenges of small and medium enterprises in the plastics and chemical sector**, Pretoria, South Africa, 2013.
- [3] F. Cavani, F. Trifiro, **Some innovative aspects in the production of monomers via catalyzed oxidation processes**, Appl. Catal., A 88 (1992) 115–135.
- [4] S.T. Oyama, A.N. Desikan, J.W. Hightower, **Catalytic selective oxidation**, ACS Symp. Ser. 523, Washington DC, 1993.
- [5] D. Dharia, W. Letzsch, H. Kim, D. McCue, L. Chapin, **Increasing light olefins production**, Hydrocarbon Process., Int. Ed. 83 (2004) 61-66.
- [6] F.D. Rossini, **Selected Values of Properties of Hydrocarbons**, Printing Office, U.S. Govt., 1947.
- [7] H. Zimmermann, R. Walzl, **Ethylene**, in: **Ullmann's encyclopedia of industrial chemistry**, 6th rev. ed., vol. 12, Wiley VCH, 2003.
- [8] V.R. Choudhary, V.H. Rane, A.M. Rajput, **Simultaneous thermal cracking and oxidation of propane to propylene and ethylene**, AIChE J. 44 (1998) 2293-2301.
- [9] H. Cai, A. Krzywicki, M.C. Oballa, **Coke formation in steam crackers for ethylene production**, Chem. Eng. Process. 41 (2002) 199–214.
- [10] V.D. Dasireddy, S. Singh, H.B.Friedrich, **Effect of the support on the oxidation of heptane using vanadium supported on alkaline earth metal hydroxyapatites**, Catal. Lett. 145 (2015) 668–678.
- [11] H. Kung, M. Kung, **Oxidative dehydrogenation of alkanes over vanadium-magnesium-oxides**, Appl. Catal., A 157 (1997) 105-116.
- [12] J. Dobler, M. Pritzsche, J. Sauer, **Oxidation of methanol to formaldehyde on supported vanadium oxide catalysts compared to gas phase molecules**, J. Am. Chem. Soc. 127 (2005) 10861–10868.
- [13] Z. Shen, J. Liu, H. Xu, Y. Yue, W. Hua, W. Shen, **Dehydrogenation of ethane to ethylene over a highly efficient Ga₂O₃/HZSM-5 catalyst in the presence of CO₂**, Appl. Catal., A 356 (2009) 148–153.
- [14] X. Shi, S. Ji, K. Wang, **Oxidative dehydrogenation of ethane to ethylene with carbon dioxide over Cr-Ce/SBA-15 catalysts**, Catal. Lett. 125 (2008) 331–339.
- [15] D. Brzic, D. Ahchieva, M. Peglow, S. Heinrich, **An experimental study of the partial oxidation of ethane to ethylene in a shallow fluidized bed reactor**, J. Serb. Chem. Soc. 72 (2007) 183–192.

- [16] B. Tope, Y. Zhu, J.A. Lercher, **Oxidative dehydrogenation of ethane over Dy₂O₃/MgO supported LiCl containing eutectic chloride catalysts**, Catal. Today 123 (2007) 113–121.
- [17] A.A. Lemonidou, E. Heracleous, **Reaction pathways of ethane oxidative and non-oxidative dehydrogenation on γ -Al₂O₃ studied by temperature-programmed reaction (TP-reaction)**, Catal. Today 112 (2006) 23–27.
- [18] E. Heracleous, A.A. Lemonidou, **Ni–Nb–O mixed oxides as highly active and selective catalysts for ethene production via ethane oxidative dehydrogenation. Part II: Mechanistic aspects and kinetic modeling**, J. Catal. 237 (2006) 175–189.
- [19] P. Arpentinier, F. Cavani, F. Trifiro, **The contribution of homogeneous reactions in catalytic oxidation processes: Safety and selectivity aspects**, Catal. Today 99 (2005) 15–22.
- [20] V.S. Arutyunov, L.N. Strekova, A.V. Nikitin, **Partial oxidation of light alkanes as a base of new generation of gas chemical processes**, Eurasian Chem. Technol. J. 15 (2013) 265–273.
- [21] E.A. Mamedov, V.C. Corberán, **Oxidative dehydrogenation of lower alkanes on vanadium oxide-based catalysts. The present state of the art and outlooks**, Appl. Catal., A 127 (1995) 1–40.
- [22] K. Chen, **Alkali effects on molybdenum oxide catalysts for the oxidative dehydrogenation of propane**, J. Catal. 195 (2000) 244–252.
- [23] H. Kung, **Oxidative dehydrogenation of light (C₂ to C₄) alkanes**, Adv. Catal. 40 (1994) 1–38.
- [24] K. Chen, A. Khodakov, J. Yang, A.T. Bell, E. Iglesia, **Isotopic Tracer and Kinetic Studies of Oxidative Dehydrogenation Pathways on Vanadium Oxide Catalysts**, J. Catal. 186 (1999) 325–333.
- [25] V.D. Dasireddy, S. Singh, H.B. Friedrich, **Activation of *n*-octane using vanadium oxide supported on alkaline earth hydroxyapatites**, Appl. Catal., A 456 (2013) 105–117.
- [26] M.D. Argyle, K. Chen, E. Iglesia, A.T. Bell, **Effect of catalyst structure on oxidative dehydrogenation of ethane and propane on alumina-supported vanadia**, J. Catal. 208 (2002) 139–149.
- [27] E.V. Kondratenko, M. Baerns, **Catalytic oxidative dehydrogenation of propane in the presence of O₂ and N₂O - the role of vanadia distribution and oxidant activation**, Appl. Catal., A 222 (2001) 133–143.
- [28] A. Khodakov, J. Yang, S. Su, E. Iglesia, A.T. Bell, **Structure and properties of vanadium oxide-zirconia catalysts for propane oxidative dehydrogenation**, J. Catal. 177 (1998) 343–351.
- [29] A. Khodakov, B. Olthof, A.T. Bell, E. Iglesia, **Structure and catalytic properties of supported vanadium oxides: Support effects on oxidative dehydrogenation reactions**, J. Catal. 181 (1999) 205–216.
- [30] I.E. Wachs, B.M. Wechuysen, **Structure and reactivity of surface vanadium oxide species on oxide support**, Appl. Catal. A 157 (1997) 67–90.

- [31] J.G. Eon, R. Olier, J.C. Volta, **Oxidative dehydrogenation of propane on γ -Al₂O₃ supported vanadium oxides**, *J. Catal.* 145 (1994) 318-326.
- [32] T. Balsko, J.M. Lopez-Nieto, **Oxidative dehydrogenation of short chain alkanes on supported vanadium oxide catalysts**, *Appl. Catal., A* 157 (1997) 117-142.
- [33] G. Centi, F. Cavani, F. Trifirò, **Selective oxidation by heterogeneous catalysis**, *Fundam. Appl. Catal.*, Springer, US, 2001.
- [34] L.D. Schmidt, E.J. Klein, C.A. Leclerc, J.J. Krummenacher, K.N. West, **Syngas in millisecond reactors: higher alkanes and fast lightoff**, *Chem. Eng. Sci.* 58 (2003) 1037-1041.
- [35] G. Centi, F. Trifirò, **Functionalization of paraffinic hydrocarbons by heterogeneous vapour-phase oxidation. III. Conversion of the C₁-C₇ alkane**, *Catal. Today* 3 (1988) 151-162.
- [36] P.M. Michalakos, M.C. Kung, I. Jahan, H.H. Kung, **Selectivity patterns in alkane oxidation over Mg₃(VO₄)₂, Mg₂V₂O₇, and (VO)₂P₂O₇**, *J. Catal.* 140 (1993) 226-242.
- [37] M. Skotak, Z. Karpiński, **C₆-alkane conversion over γ -alumina supported palladium and platinum catalysts**, *Chem. Eng. J.* 90 (2002) 89-96.
- [38] R.J. Mikovsky, A.J. Silvestri, E. Dempsey, D.H. Olson, **Tellurium-loaded zeolites: II. The nature of the dehydrocyclization site**, *J. Catal.* 22 (1971) 371-378.
- [39] H.B. Friedrich, N. Govender, M.R. Mathebula, **The effect of voids and dilution on *n*-hexane oxidation over a VMgO catalyst**, *Appl. Catal. A* 297 (2006) 81-89.
- [40] B. Pillay, M.R. Mathebula, H.B. Friedrich, **The oxidative dehydrogenation of *n*-hexane over Ni-Mo-O catalysts**, *Appl. Catal. A* 361 (2009) 57-64.
- [41] V.D.B.C. Dasireddy, S. Singh, H.B. Friedrich, **Activation of *n*-octane using vanadium oxide supported on alkaline earth hydroxyapatites**, *Appl. Catal. A* 456 (2013) 105-117.
- [42] E.A. Elkhailifa, H.B. Friedrich, **Oxidative dehydrogenation of *n*-octane using vanadium-magnesium oxide catalysts with different vanadium loadings**, *Appl. Catal. A* 373 (2010) 122-131.
- [43] B. Grzybowska-Świerkosz, **Active centres on vanadia-based catalysts for selective oxidation of hydrocarbons**, *Appl. Catal. A* 157 (1997) 409-420.
- [44] L. Burcham, L. Briand, I. Wachs, **Quantification of active sites for the determination of methanol oxidation turn-over frequencies using methanol chemisorption and in situ infrared techniques. 1. Supported metal oxide catalysts**, *Langmuir* 17 (2001) 6164-6174.
- [45] X. Rozanska, R. Fortrie, J. Sauer, **Size-dependent catalytic activity of supported vanadium oxide species: Oxidative dehydrogenation of propane**, *J. Am. Chem. Soc.* 136 (2014) 7751-7761.
- [46] X. Rozanska, E.V. Kondratenko, J. Sauer, **Oxidative dehydrogenation of propane: Differences between N₂O and O₂ in the reoxidation of reduced vanadia sites and consequences for selectivity**, *J. Catal.* 256 (2008) 84-94.

- [47] M.M. Islam, D. Costa, M. Calatayud, F. Tielens, **Characterization of supported vanadium oxide species on silica: A periodic DFT investigation**, *J. Phys. Chem. C* 113 (2009) 10740–10746.
- [48] K. Tamara, S. Yoshida, S. Ishida, H. Kakioka, **Spectroscopic studies of catalysis by vanadium pentoxide**, *Bull. Chem. Soc. Jpn.* 41 (1968) 2840-2845.
- [49] R. Ramirez, B. Casal, L. Utrera, E. Ruiz-Hitzky, **Oxygen reactivity in vanadium pentoxide: Electronic structure and infrared spectroscopy studies**, *J. Phys. Chem.* 94 (1990) 8960-8965.
- [50] E.A. Elkhalfi, H.B. Friedrich, **Oxidative dehydrogenation and aromatization of *n*-octane over VMgO catalysts obtained by using different MgO precursors and different precursor treatments**, *J. Mol. Catal. A: Chem.* 392 (2014) 22–30.
- [51] M. Witko, **Oxidation of hydrocarbons on transition metal oxide catalysts - quantum chemical studies**, *J. Mol. Catal.* 70 (1991) 277-333.
- [52] F. Ruetter, **Quantum chemistry approaches to chemisorption and heterogeneous catalysis**, Kluwer Academic Publishers, Boston, 1992.
- [53] R.A. van Santen, M. Neurock, **Concepts in theoretical heterogeneous catalytic reactivity**, *Catal. Rev. Sci. Eng.* 37 (1995) 557-698.
- [54] G.A. Somorjai, Y.M. Li, **Major successes of theory and experiment-combined studies in surface chemistry and heterogeneous catalysis**, *Top. Catal.* 53 (2010) 311–325.
- [55] M. Boronat, P. Concepción, **Combined theoretical and spectroscopic mechanistic studies for improving activity and selectivity in heterogeneous catalysis**, *Catal. Today* 285 (2017) 166–178.
- [56] T. Clark, **A handbook of computational chemistry**, Wiley-Interscience, New York, 1985.
- [57] J.P. Lowe, **Quantum chemistry**, Academic Press, New York, 1978.
- [58] R.G. Parr and W. Wang, **Density functional theory for atoms and molecules**, Oxford University Press, Oxford, (1989).
- [59] J.C. Slater, **The self-consistent field for molecules and solids: Quantum theory of molecules and solids**, vol. 4, McGraw-Hill, N.Y., 1974.
- [60] T. Lovell, F. Himmo, W.G. Han, L. Noodleman, **Density functional methods applied to metalloenzymes**, *Coord. Chem. Rev.* 238 (2003) 211-232.
- [61] P.E.M. Siegbahn, M.R.A. Blomberg, **Density functional theory of biologically relevant metal centers**, *Annu. Rev. Phys. Chem.* 50 (1999) 221-249.
- [62] M. Springborg, **DFT in chemistry and material science**, Wiley, NY, 1997.
- [63] P. Hohenberg, W. Kohn, **Inhomogeneous electron gas**, *Phys. Rev. B: Condens. Matter* 136 (1964) 864-871.

- [64] W. Kohn, L.J. Sham, **Self-consistent equations including exchange and correlation effects**, Phys. Rev. A: At. Mol. Opt. Phys. 140 (1965) 1133-1138.
- [65] M. Payne, M.P. Teter, D.C. Allan, T.A. Arias, J.D. Joannopoulos, **Iterative minimization techniques for ab initio total-energy calculations: Molecular dynamics and conjugate gradients**, Rev. Mod. Phys. 64 (1992) 1045-1097.
- [66] J. Sauer, **Molecular models in ab initio studies of solids and surfaces: from ionic crystals and semiconductors to catalysts**, Chem. Rev. 89 (1989) 199-255.
- [67] K. Judai, S. Abbet, A.S. Wörz, A.M. Ferrari, L. Giordano, G. Pacchioni, U. Heiz, **Acetylene polymerization on supported transition metal clusters**, J. Mol. Catal. A: Chem. 199 (2003) 103-113.
- [68] H. Häkkinen, W. Abbet, A. Sanchez, U. Heiz, U. Landman, **Structural, electronic, and impurity-doping effects in nanoscale chemistry: Supported gold nanoclusters**, Angew. Chem. Int. Ed. 42 (2003) 1297-1300.
- [69] B. Hammer, **Theoretical surface science and catalysis - calculations and concepts**, Adv. Catal. 45 (2000) 71-129.
- [70] J. Greeley, J.K. Nørskov, M. Mavrikakis, **Electronic structure and catalysis on metal surfaces**, Annu. Rev. Phys. Chem. 53 (2002) 319-348.
- [71] H.B. Jansen, P. Ros, **Non-empirical molecular orbital calculations on the protonation of carbon monoxide**, Chem. Phys. Lett. 3 (1969) 140-143.
- [72] B. Liu, A.D. McLean, **Accurate calculation of the attractive interaction of two ground-state helium atoms**, J. Chem. Phys. 59 (1973) 4557-4558.
- [73] F.B. van Duijneveldt, J.G.C.M. van Duijneveldt-van de Rijdt, J.H. van Lenthe, **State of the art in counterpoise theory**, Chem. Rev. 94 (1994) 1873-1885.
- [74] S.F. Boys, F. Bernardi, **The calculation of small molecular interactions by the differences of separate total energies. Some procedures with reduced errors**, Mol. Phys. 19 (1970) 553-566.
- [75] F. Tielens, M. Calatayud, **The synergistic power of theory and experiment in the field of catalysis**, Catal. Today 177 (2011) 1-2.
- [76] M.J. Frisch, G.W. Trucks, H.B. Schlegel, G.E. Scuseria, M.A. Robb, J.R. Cheeseman, G. Scalmani, V. Barone, B. Mennucci, G.A. Petersson, H. Nakatsuji, M. Caricato, X. Li, H.P. Hratchian, A.F. Izmaylov, J. Bloino, G. Zheng, J.L. Sonnenberg, M. Hada, M. Ehara, K. Toyota, R. Fukuda, J. Hasegawa, M. Ishida, T. Nakajima, Y. Honda, O. Kitao, H. Nakai, T. Vreven, J. Montgomery, J. A., J.E. Peralta, F. Ogliaro, M. Bearpark, J.J. Heyd, E. Brothers, K.N. Kudin, V.N. Staroverov, R. Kobayashi, J. Normand, K. Raghavachari, A. Rendell, J.C. Burant, S.S. Iyengar, J. Tomasi, M. Cossi, N. Rega, N.J. Millam, M. Klene, J.E. Knox, J.B. Cross, V. Bakken, C. Adamo, J. Jaramillo, R. Gomperts, R.E. Stratmann, O. Yazyev, A.J. Austin, R. Cammi, C. Pomelli, J.W. Ochterski, R.L. Martin, K. Morokuma, V.G. Zakrzewski, G.A. Voth, P. Salvador, J.J. Dannenberg, S. Dapprich, A.D. Daniels, Ö. Farkas, J.B. Foresman, J.V. Ortiz, J. Cioslowski, D.J. Fox, **Gaussian 09, Revision B.01**, Gaussian, Inc., Wallingford, 2010.

- [77] C. Pisani, **Software for the quantum-mechanical simulation of the properties of crystalline materials: state of the art and prospects**, J. Mol. Struct. THEOCHEM 463 (1999) 125-137.
- [78] P. Blaha, K. Schwarz, P. Dufek, R. Augustyn, **WIEN95: A full potential linearized augmented plane wave package for calculating crystal properties**, Technical University, Vienna, 1995.
- [79] F. Illas, C. Sousa, J.R.B. Gomes, A. Clotet, J.M. Ricart, **Theoretical Aspects of Heterogeneous Catalysis**, in: M.A.C. Nascimento (Ed.), Kluwer, Dordrecht, 2001, pp. 149-181.
- [80] L.J. Broadbelt, R.Q. Snurr, **Applications of molecular modeling in heterogeneous catalysis research**, Appl. Catal., A 200 (2000) 23-46.
- [81] A.D. Becke, **Density functional thermochemistry III - The role of exact exchange**, J. Chem. Phys. 98 (1993) 5648-5652.
- [82] C. Lee, W. Yang, R.G. Parr, **Development of the Colle-Salvetti correlation energy formula into a functional of the electron density**, Phys. Rev. B: Condens. Matter 37 (1988) 785-789.
- [83] M. Dolg, U. Wedig, H. Stoll, H. Preuss, **Energy-adjusted ab initio pseudopotentials for the first row transition elements**, J. Chem. Phys. 86 (1987) 866-872.
- [84] J.M.L. Martin and A. Sundermann, **Correlation consistent valence basis sets for use with the Stuttgart-Dresden-Bonn relativistic effective core potentials: The atoms Ga-Kr and In-Xe**, J. Chem. Phys. 114 (2001) 3408-3420.
- [85] C. Gonzales, H.B. Schlegel, **An improved algorithm for reaction path following**, J. Chem. Phys. 90 (1989) 2154-2161.
- [86] C. Gonzales, H.B. Schlegel, **Reaction path-following in mass-weighted internal coordinates**, J. Phys. Chem. 94 (1990) 5523-5527.
- [87] J. Oxgaard, R.A. Periana, W.A. Goddard, **Mechanistic analysis of hydroarylation catalysts**, J. Am. Chem. Soc. 126 (2004) 11658-11665.
- [88] D. Benitez, D. W.A. Goddard, **The isomerization equilibrium between cis and trans chloride ruthenium olefin metathesis catalysts from quantum mechanics calculations**, J. Am. Chem. Soc. 127 (2005) 12218-12219.
- [89] J.A. Keith, J. Oxgaard, W.A. Goddard, **Inaccessibility of beta-hydride elimination from -OH functional groups in Wacker-type oxidation**, J. Am. Chem. Soc. 128 (2006) 3132-3133.
- [90] K.M. Neyman, F. Illas, **Theoretical aspects of heterogeneous catalysis: Applications of density functional methods**, Catal. Today 105 (2005) 2-16.
- [91] L. Gracia, J. R. Sambrano, V. S. Safont, M. Calatayud, A. Beltràn, J. Andrés, **Theoretical study on the molecular mechanism for the reaction of VO₂⁺ with C₂H₄**, J. Phys. Chem. A 107 (2003) 3107-3120.
- [92] J. Sauer, J. Döbler, **Structure and reactivity of V₂O₅: Bulk solid, nanosized clusters, species supported on silica and alumina, cluster cations and anions**, Dalton Trans. (2004) 3116-3121.

- [93] X.X. Chen, B. Xie, Y.C. Wang, **A theoretical study of C–H bond of CH₄ activation catalyzed by VO₂⁺ in gas phase**, *Comput. Theor. Chem.* 1054 (2015) 63-70.
- [94] L. Cheng, G.A. Ferguson, S.A. Zygmunt, L.A. Curtiss, **Structure-activity relationships for propane oxidative dehydrogenation by anatase-supported vanadium oxide monomers and dimers**, *J. Catal.* 302 (2013) 31-36.
- [95] E. Kurnaz, M.F. Fellah, I. Onal, **A density functional theory study of C-H bond activation of methane on a bridge site of M-O-M-ZSM-5 Clusters (M = Au, Ag, Fe and Cu)**, *Microporous Mesoporous Mater.* 138 (2011) 68-74.
- [96] I. Ascoop, V.V. Galvita, K. Alexopoulos, M.F. Reyniers, P. Van Der Voort, V. Bliznuk, G.B. Marin, **The role of CO₂ in the dehydrogenation of propane over WO_x-VO_x/SiO₂**, *J. Catal.* 335 (2016) 1-10.
- [97] X. Gao, X. Du, Y. Fu, J. Mao, Z. Luo, M. Ni, K. Cen, **Theoretical and experimental study on the deactivation of V₂O₅ based catalyst by lead for selective catalytic reduction of nitric oxides**, *Catal. Today* 175 (2011) 625-630.
- [98] A. Beste, A.C. Buchanan, P.F. Britt, B.C. Hathorn, R.J. Harrison, **Ab initio study of hydrogen abstraction reactions on toluene and tetralin**, *J. Mol. Struct. THEOCHEM* 851 (2008) 232-241.
- [99] J.E. Carpenter, F. Weinhold, **Analysis of the geometry of the hydroxymethyl radical by the “different hybrids for different spins” natural bond orbital procedure**, *J. Mol. Struct. THEOCHEM* 169 (1988) 41-62.
- [100] J.E. Carpenter, F. Weinhold, **The natural bond orbital Lewis structure concept for molecules, radicals, and radical ions**, in: R. Naaman, Z. Vager (Eds.), *The structure of small molecules and ions*, Plenum, N.Y., 1988, pp. 227-236.

CHAPTER 2

Density Functional Theory Studies of the Uncatalysed Gas-Phase Oxidative Dehydrogenation Conversion of *n*-Hexane to Hexenes

N.E. Damoyi^{a,*}, H.B. Friedrich^b, H.G. Kruger^c and D. Willock^d

^aDepartment of Chemistry, Mangosuthu University of Technology, Box 12363, Jacobs, 4026, South Africa, E-mail: damoyi@mut.ac.za

^bSchool of Chemistry, University of KwaZulu Natal, Westville Campus, Private Bag X 54001, Durban, 4000, South Africa

^cCatalysis and Peptide research unit, School of Pharmacy, University of KwaZulu Natal, Westville Campus, Private Bag X 54001, Durban, 4000, South Africa

^dSchool of Chemistry, Cardiff University, Park Place, Cardiff CF10 3AT, Wales, UK

Keywords: DFT, ODH, *n*-hexane, RDS, mechanism.

ABSTRACT

Density Functional Theory (DFT) modelling studies were conducted for the activation of *n*-hexane in the gas-phase under experimental conditions of 573, 673 and 773K.

The aim of the study was to establish the most favourable radical mechanism for the oxidative dehydrogenation (ODH) of *n*-hexane to 1- and 2-hexene. Modelling of the 3-hexene pathway was omitted due to absence of this product in laboratory experiments. Computations were performed using GAUSSIAN 09W and molecular structures were drawn using the GaussView 5.0 graphics interface. The B3LYP hybrid functional and the 6-311+g(d,p) basis set were utilized for all the atoms. The most kinetically and thermodynamically favourable pathways are proposed based on the determination of the relative total energies (ΔE^\ddagger , ΔE , ΔG^\ddagger and ΔG) for the different reaction pathways. The initial C-H activation step is β -H abstraction from *n*-hexane (C₆H₁₄) by molecular oxygen (O₂) to form the alkoxy (C₆H₁₃O·) and hydroxyl (·OH) radicals. This is proposed as the rate-determining step (RDS) with the calculated $\Delta E^\ddagger = +42.4$ kcal/mol. Two propagation pathways that involve, separately, the C₆H₁₃O· and ·OH radicals may lead to the formation of 2-hexene. In both the propagation pathways, the C₆H₁₃O· and ·OH radicals activate further C₆H₁₄ molecules to produce C₆H₁₃OH and H₂O, respectively, and the alkyl radicals (·C₆H₁₃). Thereafter, one pathway involves the interaction of the ·C₆H₁₃ radical with further molecular O₂, and leads to a second C-H activation step that yields 2-hexene and the peroxy radical (·OOH). The other pathway is associated with hydrogen transfer from the ·OOH radical to C₆H₁₃OH that is produced earlier, leading to water and the alkyl peroxy radical (C₆H₁₃OO·). The C₆H₁₃OO· radical undergoes intramolecular H-abstraction to yield 2-hexene and the ·OOH radical, and the latter disproportionate through intermediate ·OH radicals to produce O₂ and H₂O in the termination step.

* Corresponding author e-mail address: damoyi@mut.ac.za

1 Introduction

The range of carbon resources used by the chemicals industry is set to diversify to include natural gas, heavy oils and tars, coal and biomass. It is attractive to use these various materials as the input to a single chemical processing infrastructure by first converting carbon source materials into syngas and then using a Fischer Tropsch (FT) approach to build the alkanes required for fuels. To use this approach for chemicals production requires low energy conversion of the hydrocarbon feedstocks into more valuable products, such as alkenes and aromatics, making this a critical area of research [1-3]. Reactions of long chain alkanes are limited mainly to combustion and cracking because the C-H bond is non-polar, and the formation of radicals through cracking facilitates propagation steps such as hydrogen abstraction and substitution reactions [4].

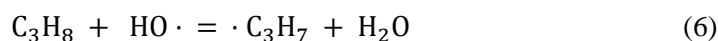
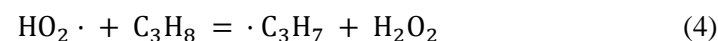
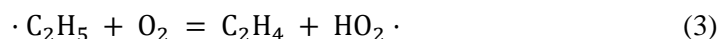
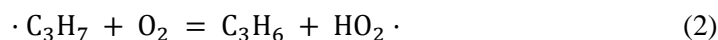
Presently large amounts of ethene and propene are produced by thermal cracking of a variety of hydrocarbon feedstocks in the presence of steam at high temperatures [5-7]. Since thermal cracking is an endothermic and energy-intensive process, the most common alternatives include the less energy-intensive non-catalytic and catalytic oxidative dehydrogenation (ODH) routes. The use of gaseous oxygen as oxidant yields water as a by-product and provides the thermodynamic driving force which permits the reaction to be conducted at a lower temperature than a simple dehydrogenation without oxygen [8]. Non-catalytic ODH of propane and butane has been reported before [9], [10] and there are significant publications on catalytic ODH of propane and butane [11-14]. There are, however, limited publications on non-catalytic and catalytic ODH of long chain alkanes, including *n*-hexane.

Thermal cracking in the absence and presence of molecular oxygen is known to proceed by a radical mechanism [15-17]. The non-catalytic ODH of propane is believed to proceed in the same way as thermal cracking [18]. Choudhary *et al.* [9] suggested that, in the absence of oxygen, the initiation step in the thermal cracking of propane occurs through the homolysis of a C-C bond at temperatures above 700°C,

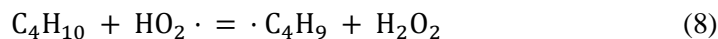


Formation of the propyl radical ($\cdot\text{C}_3\text{H}_7$) through C-H bond scission is less likely because the C-H bond energy (+23.8 kcal/mol) is higher than the C-C bond energy (+21.1 kcal/mol). The mechanism of the formation of propyl radicals may involve the attack of other propane molecules by the methyl and ethyl radicals formed in reaction (1). The authors supported Dente and Ranzi [19], that after the initiation step, the majority of the alkane molecules are activated by such radical species and the reactions proceed through complex free-radical chain propagation and termination reactions, leading to the formation of different products, namely, hydrogen, methane, higher alkanes, alkenes, and coke.

Burch and Crabb [20] observed that the same reaction in the presence of oxygen began at a temperature about 75°C lower than in the absence of oxygen. They further suggested that the presence of oxygen in the gas phase allows additional reaction pathways involving oxygen centred radicals, for example,



The contribution of molecular oxygen was also discussed in the study of the non-catalytic ODH of butane by Toledo et al. [16]. They proposed that one possible initiation step, besides cracking, is the abstraction of a hydrogen atom from a butane molecule by molecular oxygen to form the butyl ($\cdot\text{C}_4\text{H}_9$) and hydroperoxy ($\text{HO}_2\cdot$) radicals. The biradical character of the triplet molecular oxygen facilitates the initiation of a free-radical chain mechanism as follows,



The participation of molecular oxygen was further reported by Pitz and Westbrook [21]. Their kinetic data showed that the activation energy of reaction (7) (+49 kcal/mol) is lower than that of reactions (9) (+85 kcal/mol) and (10) (+81 kcal/mol). Other authors, Liu et al. [22], Lemonidou et al. [10] and Vislovskiy et al. [23], have also reported the homogeneous activation of *n*-hexane via hydrogen abstraction by gas phase diatomic oxygen.

Hunter et al. [24] proposed that the initiation step for thermal cracking of *n*-hexane in the absence of oxygen was the C-C bond fission to form two radicals, with C-C rupturing occurring between the most highly substituted carbons atoms. We believe that the presence of oxygen in the same reaction would provide for the possibility of the initiation step being the hydrogen abstraction by molecular oxygen as observed with shorter chain alkanes [21].

The work presented in this publication seeks to establish the overall likely mechanistic pathways in the reaction of *n*-hexane and related intermediates with O_2 , $\cdot\text{OH}$ and $\text{HO}_2\cdot$ radicals to form 1- and 2-hexene under experimental conditions. Note that 3-hexene is not observed in our laboratory experiments nor reported in literature. Most similar reported work in modelling involves catalytic systems and shorter chain hydrocarbons [25-27]. As a result there are limited publications on DFT modelling of gas-phase hydrogen abstraction reactions of long chain alkanes. We, however, focussed on the DFT gas-phase non-catalytic radical mechanisms in order to gain insight and acquire a theoretical baseline for modelling the heterogeneous catalytic (VMgO) ODH reaction of *n*-hexane to benzene at a later stage. This is necessary because in certain catalytic experimental conditions, gas-phase ODH mechanisms may compete with the catalytic ODH mechanisms. We believe that the DFT calculations and comparisons of some kinetic and thermodynamic properties for this reaction will be insightful for better understanding of the reaction mechanisms of the indicated radicals with *n*-hexane and related intermediates.

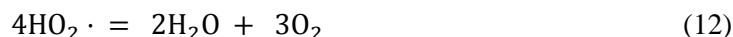
The proposed reaction scheme shown in Figure 1 indicates the formation of 2-hexene from gas-phase ODH of *n*-hexane. Hoog *et al.* [28] investigated this reaction and concluded that an equilibrium exists between 1- and 2-hexene in the reactor. Nevertheless, for clarity purposes we only show the formation of 2-hexene.

Initiation of the reaction involves H-abstraction from the central carbons of the *n*-hexane chain by molecular oxygen which then undergoes O-O scission in the RDS. This follows the formation of a new C-O bond at the activated carbon to give an alkoxy radical species and a hydroxyl radical. The hydroxyl radical may then activate further *n*-hexane molecules to give carbon centred radicals following the formation of water. The alkoxy radical can also activate *n*-hexane to give a secondary alcohol and a carbon centred radical. Interaction of the carbon centred radicals with molecular oxygen can then lead directly to 2-hexene via a second C-H activation event with the production of a hydroperoxyl radical species. The hydroperoxyl radical itself is also capable of additional reaction steps, most notably combining with the alcohol produced earlier in the mechanism to give water and an alkyl peroxy radical which can internally decompose to 2-hexene, reforming the peroxy radical for further reaction. Eventually termination of the radical processes may occur through disproportionation of the hydroperoxyl radicals into water and oxygen.

The overall reaction is,



The intermediate $\text{HO}_2\cdot$ radicals produced in reaction (11) may combine as presented in reaction (12),



The relative hydrogen abstraction abilities of molecular O_2 , the $\cdot\text{OH}$ and $\text{HO}_2\cdot$ radicals were examined for activation of *n*-hexane through likely intermediates to 1- and 2-hexene. The activation energies (E_a), total energy changes (ΔE) and Gibbs free energy changes (ΔG) at different temperatures were calculated and compared.

2.2 Computational Details

The geometries of all stationary points were optimized using the restricted and unrestricted B3LYP/6-311+G(d,p) level of theory. The B3LYP is a hybrid functional that is made up of Becke's three-parameter nonlocal hybrid exchange potential [29] and the nonlocal correlation functional of Lee, Yang and Parr [30]. All the calculations were performed using the Gaussian09 code [31] incorporating the Gausview5.0 graphics interface. The conditions chosen were those used by our group in laboratory experiments, namely 573, 673 and 773 K. Geometry optimizations were carried out without symmetry constraints. The harmonic vibrational frequencies of all the stationary points in potential energy surfaces were calculated at the same level of theory used for their geometry optimizations in order to confirm local minima and transition states, and also determine the corresponding zero-point vibrational energy (ZPVE). The intrinsic reaction coordinate (IRC) [32], [33] calculations were conducted in order to confirm that all transition states connect the relative minima. Stability calculations were performed for all reactants and products so as to determine whether the lowest energy is a restricted or unrestricted wavefunction and natural bond orbital (NBO) [34], [35] analyses were conducted in order to gain insight into the bonding properties of all the stationary points.

3 Results

3.1 Activation of *n*-hexane

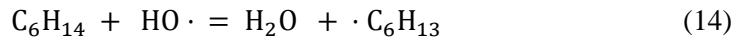
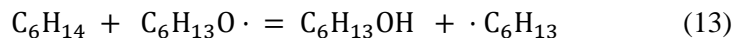
The activation of *n*-hexane by O₂ and the two radicals, ·OH and HO₂· was investigated over the three temperatures 573, 673 and 773K in order to contrast the relative energetics involved. All the Gaussian optimised structures of reactants, intermediates, transition states and products/intermediates are included as supplementary material.

Figure 2A displays the relative energy-reaction coordinate pathways for the reaction involving molecular O₂ on a triplet potential energy surface (PES). All the values of the calculated energetics, E_a , ΔE and ΔG are recorded in Table 1.

The initiation step for the reaction is the interaction of the only two precursors, *n*-hexane and triplet O₂. The highest calculated barrier (the rate-determining step) corresponds to a β -hydrogen abstraction by O₂ with a barrier height of +42.4 kcal/mol (TS₁), relative to separate reactants, utilizing the B3LYP functional. We compared this activation energy with the one calculated using the M06-2X functional [36] in order to investigate the degree of underestimation due to self-interaction errors when utilizing the B3LYP functional [37]. We calculated a barrier of +44.3 kcal/mol for the rate-determining step using the M06-2X functional, indicating an underestimation of 1.9 kcal/mol. Nevertheless, we decided to continue with utilizing the B3LYP functional for this non-catalytic reaction in order to compare the same reaction under catalytic conditions with this recommended functional. These results are in agreement with our expectations from the discussion of the mechanism in Figure 1. The calculated C-H activation by O₂ is accompanied by a decrease in the O--H interaction distance from 3.40Å in the pre-reaction complex to 1.06Å in the TS. The calculated activation energy is comparable to a barrier of +49 kcal/mol that was reported by Pitz and Westbrook [21] for the reaction of O₂ and *n*-butane. Three possible intermediates resulting from this C-H activation process were considered: Int₁ corresponds to the formation of an alkoxy hydroxyl radical pair, Int₂ an alcohol and free oxygen atom and Int₃ a carbon centred radical species with a peroxy radical. The relative thermodynamic energies of these triplet intermediates were calculated (Figure 2A). Although none of the intermediates are thermodynamically stable, relative to reactants, Int₁ is the most stable of the three, with $\Delta E = +20.5$ kcal/mol followed by Int₂ with $\Delta E = +28.9$ kcal/mol, relative to separate reactants. As expected on a triplet PES, the O--O bond distance in Int₁ is 2.23Å, reflecting a weak interaction between the two oxygen-containing radicals, C₆H₁₃O· and ·OH. Therefore, the ·OH radicals that may be produced in the pathway through Int₁ are expected to dominate in reactions involving the propagation steps.

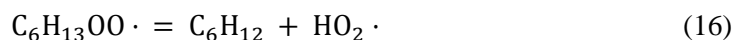
The highly energetic Int₃ with $\Delta E = +44.8$ kcal/mol is the most thermodynamically unstable indicating that the reverse reaction for the formation of reactants O₂ and *n*-hexane is kinetically and thermodynamically more favourable (Figure 2A). This is expected because the O-H bond dissociation energy in the HO₂· radical is +47 kcal/mol, which is lower than that in the ·OH radical, namely +103 kcal/mol, and typical C-H bond energies that are *ca.* +100 kcal/mol, [38],[39]. This observation indicates that H-transfer reactions may occur from the HO₂· radical to other electron-deficient species, as also suggested by Anglada *et al.* [40] and Clifford *et al.* [41]. However, the direct formation of a carbon centred radical based solely on the reaction with dioxygen is unlikely to be important in the pathway to alkene formation.

From Figure 2A we conclude that the propagation pathways to the formation of 1- and 2-hexene are likely to proceed through the lowest energy intermediate Int₁, comprising C₆H₁₃O· + ·OH radicals. The two radicals may participate in β -hydrogen abstraction reactions from further *n*-hexane molecules through the following steps,



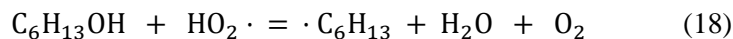
Reaction (13) involves the formation of a stable alcohol and hexyl radical. It is necessary to mention that no alcoholic products are observed in our laboratory experiments for this reaction. This means that the alcohol that may form is likely to be the intermediate for the production of olefins. As illustrated in the energy diagram in Figure 2B, the calculated barrier for this step is +8.7 kcal/mol (TS₂), and the indicated intermediate (Int₄) stabilizes to $\Delta E = -1.8$ kcal/mol, relative to reactants. The O--H interaction distance in the TS is 1.29Å and this decreases in the intermediate to 0.97Å, indicating the formation of an alcohol. In the case of reaction (14) we calculated a barrier of +14.6 kcal/mol (TS₅) and the energy difference, $\Delta E = -18.0$ kcal/mol, relative to reactants, as illustrated in Figure 2C. The thermodynamic stability of the reaction is as a result of water being produced as a product.

The formation of 1- and 2-hexene by the reaction of the radical intermediate produced in reactions (13) and (14), with molecular O₂ may proceed either through consecutive reaction steps (15) and (16), or step (17), namely,



In studies involving ethylene and oxygen, Gutman *et al.* [42], [43] found that reacting oxygen with ethyl radicals leads predominantly to the alkene at higher temperatures, and the mechanism involves intramolecular H-abstraction followed by elimination of the hydroperoxyl radical. Similarly, reaction (15) and (16) are, consecutively, chemisorption of O₂ on to the $\cdot\text{C}_6\text{H}_{13}$ radical to produce the alkyl peroxy radical, C₆H₁₃OO \cdot , which undergoes 1,4 intramolecular H-abstraction on α - (1-hexene) and γ - (2-hexene) carbon atoms followed by elimination of the hydroperoxyl radical to produce 1- and 2-hexene. For the two reactions we calculated barriers of +2.6 kcal/mol and +24.4 kcal/mol and energy differences of $\Delta E = -30.2$ kcal/mol and -10.5 kcal/mol for the formation of 2-hexene, respectively (Table 1 – TS₉ and TS₁₀). However, our calculations show a barrierless pathway that is similar to TS₃ (-4.5 kcal/mol) for reaction (17), which is a direct H-abstraction in C3 to produce 2-hexene and the hydroperoxyl radical, as indicated in both Figures 2B and 2C. This pathway produces the required 2-hexene (P₁ and P₃) with $\Delta E = -11.5$ kcal/mol. This is accompanied by a decrease in C-C bond length from 1.39Å in the TSs to 1.34Å in the products, which is comparable to experimental C-C bond lengths of alkenes, namely 1.33 +/- 0.01Å. Therefore the formation of alkenes is likely to proceed by the elementary propagation step (17) rather than the two consecutive propagation steps (15) and (16). Thus, this barrier-less, kinetically and thermodynamically favourable mechanistic pathway is one of the key propagation steps that is likely to dominate in the production of the alkenes and also simultaneously increase the concentration of the HO₂ \cdot radicals.

Since no alcoholic products are obtained in our experiments, we then investigated the likely conversion of C₆H₁₃OH obtained in reaction (13) to C₆H₁₂. The pathway investigated is H-transfer from HO₂ \cdot obtained in reaction (17) to produce the hexyl radical, water and oxygen,



As illustrated in Figure 2D, we calculated an energy barrier of +29.4 kcal/mol (TS₈) for this step, however, the intermediate obtained was C₆H₁₃OO· rather than ·C₆H₁₃, with ΔE = -8.6 kcal/mol (Int₆). Other studies [44], [45] also confirm the higher thermodynamic stability of C₆H₁₃OO· compared to that of ·C₆H₁₃. The formation of the stable H₂O is facilitated by advanced scission of the CO (2.17Å) and OH (1.53Å) bonds in the TS for C₆H₁₃OH and HO₂·, respectively. As discussed above in reaction (16), the alkyl peroxy radical, C₆H₁₃OO· may undergo intramolecular H-abstraction, and we calculated a barrier (TS₉) of +24.4 kcal/mol for this step. This is followed by a 1,5 elimination to produce 2-hexene and the hydroperoxyl radical, with ΔE = -10.5 kcal/mol (P₅).

The prominent feature of the ·C₆H₁₃ radical in our calculations obligated the examination of the intramolecular H-elimination pathway to produce 2-hexene, namely,

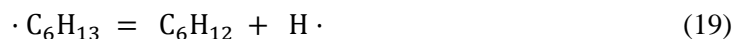


Table 2 shows the calculated ΔE[#] value of +36.3 kcal/mol (TS₁₁) and the corresponding ΔE value of +36.5 kcal/mol (Int₇) for the 2-hexene pathway, suggesting that such a reaction is unlikely to occur under the specified conditions.

Finally, the remaining hydroperoxyl radicals may combine to produce the intermediate hydroxyl radicals,



The activation barrier for reaction (20) has ΔE[#] = -2.3 kcal/mol (TS₁₂) and the products, 2·OH + O₂ stabilize to ΔE = -18.8 kcal/mol (Int₈ in Table 1), relative to TS. This suggests that this reaction pathway may be one of those that generate the more reactive ·OH radicals, with the reformation of O₂ also contributing to the stabilization of the products. Moreover, the ·OH and HO₂· radicals that are likely to be produced may also participate in the activation of more *n*-hexane molecules and also the produced 1- and 2-hexenes.

The termination step involves the hydroxyl radicals that combine kinetically and thermodynamically favourably to produce water and oxygen,



The first step is H-transfer between the two ·OH radicals to produce H₂O and O diradical with ΔE[#] = -4.7 kcal/mol (TS₁₃) and ΔE = -8.3 kcal/mol (Int₉), relative to TS. The second step is the combination of two O diradicals with ΔE[#] = -2.1 kcal/mol (TS₁₄) and ΔE = -115.7 kcal/mol (P₇) relative to TS, for the formation of O₂ (Table 1).

3.2 Temperature Effects

Trends are observed with respect to the Gibbs free energies of activation (ΔG[#]) and the Gibbs free energies (ΔG) for all the steps at the indicated temperatures of 573K, 673K and 773K (Table 1).

As expected, the activation of *n*-hexane by O₂ (TS₁) and the H-transfer from HO₂· radical to C₆H₁₃OH (TS₈) pathways have the largest ΔG[#] values as a result of the low reactivity of the triplet O₂ molecule in the first case and the breaking and creation of many bonds in the H-transfer case. The lowest ΔG[#] values are generally observed in reaction pathways that include propagation by O₂ (TS₃, TS₄, TS₆ and TS₇). Similarly the ΔG values, relative to separate reactants in each case, become less negative (more positive)

as the temperature increases from 573 to 773K, suggesting that the reaction steps become less thermodynamically favourable with increase in temperature. Again, as predictable, our calculations reflect small changes in entropy factors, ΔS^\ddagger and ΔS , as the temperature changes for all the steps, suggesting that all the thermodynamically favourable reactions are driven by negative enthalpy changes, ΔH . Of note is the conversion of $2\text{HO}_2\cdot$ radicals to $2\cdot\text{OH}$ radicals and O_2 (TS₁₁), where the reaction becomes slightly more thermodynamically favourable from 573 to 773K. Clearly, for this reaction pathway ΔS is positive at any temperature and our calculations show that the former remains constant with increase in temperature. Therefore, ΔG becomes slightly more negative with increase in temperature because ΔH follows the same trend.

Clearly, the most kinetically and thermodynamically favourable pathways are for the propagation steps associated with the O_2 molecule.

3.3 Natural Bond Orbital Analyses

Natural bond orbital (NBO) analysis provides an efficient method for studying intra- and intermolecular bonding, interaction among bonds and also provides a convenient basis for investigating charge transfer or conjugative interaction in molecular systems [46]. NBO analyses were performed on the stationary points (TS) of the most likely mechanistic pathways at the B3LYP/6-311+G(d,p) level. The TSs and the corresponding highest occupied NBOs (HONBOs), representing donor orbitals, and lowest unoccupied NBOs (LUNBOs), representing acceptor orbitals, are displayed in Figure 3. Only the TSs and NBOs associated with 2-hexene (TS₃) and 1-hexene (TS₄) in the earlier pathways are illustrated and those in later pathways (TS₆ for 2-hexene) and (TS₇ and 1-hexene) are omitted because of similarities. However, Table 2 lists all the TSs, NBOs, atomic charges and largest orbital energies for each TS.

For the initiation step (TS₁), the abstraction of H by O_2 corresponds to the largest interaction that comprises the Lewis-type highest occupied NBO (HONBO) that comprises a C *s*(7.1%) *p*(92.9%) nonbonding-type hybrid as the donor orbital. The numbers in % indicate the contribution of each orbital to the NBO hybrid. The acceptor orbital is the non-Lewis-type lowest unoccupied NBO (LUNBO) that is the H *s*(76.3%) and O *s*(6.9%) *p*(16.8%) antibonding hybrid. The HONBO donates electron density to the LUNBO with orbital stabilization energy of +38.2 kcal/mol, thereby facilitating the formation of a new HO bond. The largest negative charge among the three interacting atoms is on the O atom (-0.277) and the positive charge on the H atom (+0.423), indicating qualitatively, a relatively stronger interaction between the two atoms. The interaction is between the O *s*(28.0%) *p*(72.0%) nonbonding hybrid orbital (HONBO) that donates electron density to the H *s*(71.9%) and C *s*(5.5%) *p*(22.6%) antibonding hybrid (LUNBO), phases of the lobes. For TS₂, the largest orbital energy is +45.6 kcal/mol. The corresponding atomic charges on the three interacting atoms are C = -0.275, H = +0.312 and O = -0.567. We calculated the orbital energy of +42.1 kcal/mol for the formation of 2-hexene (TS₃ and TS₆) through the O_2 propagation pathways. The flow of electron density is from the O *s*(13.1%) *p*(86.9%) nonbonding hybrid to the H *s*(71.1%) and C *s*(3.4%) *p*(25.5%) antibonding hybrid. Similarly, for 1-hexene (TS₄ and TS₇) electron density flows from the O *s*(13.3%) *p*(86.7%) nonbonding hybrid to the H *s*(71.4%) and C *s*(3.7%) *p*(24.9%) antibonding hybrid. The distribution of atomic charges in interacting atoms follows the same trend with negative charges on C and O atoms and positive charges on the H atoms. In all these cases, further electron density directional flow is a result of the LUNBOs delocalizing principally to vicinal CC antibonding orbitals to facilitate π -bond formation. The donor-acceptor orbitals for TS₅ are the O *s*(27.3%) *p*(72.7%) nonbonding hybrid and the H *s*(66.6%) and C *s*(7.7%) *p*(25.7%) antibonding hybrid with atomic charges on involved atoms being C = -0.478, H = +0.0257 and O = -0.613. For TS₈ two HONBOs and LUNBOs were identified corresponding to H-transfer from (HO₂) the O *s*(15.1%) *p*(84.9%) nonbonding hybrid to (C₆H₁₃OH) H *s*(78.9%) and O *s*(4.9%) *p*(16.2%) antibonding hybrid, and the OH scission from C₆H₁₃OH with the O *s*(35.6%) *p*(64.4%) nonbonding hybrid transferring electron

density to (C_6H_{13}) the C *s*(1.0%) *p*(99.0%) antibonding hybrid. The associated orbital energies are +21.3 and +22.0 kcal/mol, respectively. Examination of the TS reveals that this step follows a concerted mechanistic pathway that involves OH scission from $C_6H_{13}OH$ accompanied by H_2O formation. Lastly, TS_9 and TS_{10} represent the formation of 2- and 1-hexene from intramolecular H-abstraction in $C_6H_{13}OO\cdot$, respectively, and in both cases the donor orbitals are the O *s*(13.1%) *p*(86.9%) and the O *s*(13.4%) *p*(86.6%) nonbonding hybrids and the acceptor orbitals are the H *s*(70.8%) and C *s*(3.5%) *p*(25.7%), and the H *s*(70.2%) and C *s*(4.0%) *p*(25.8%) with orbital interaction energies of +39.3 and +43.5 kcal/mol.

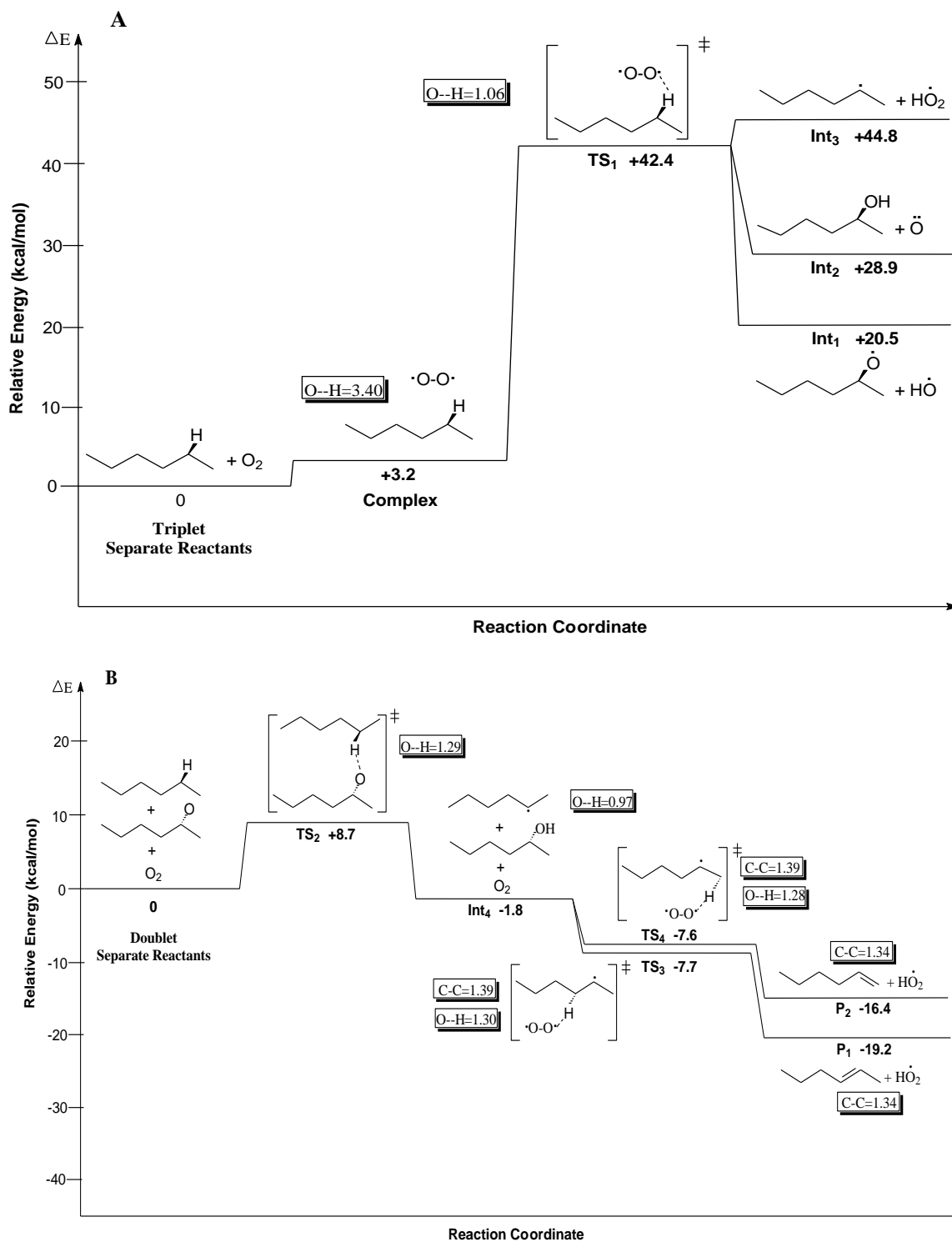


Figure 2 Zero-point corrected relative electronic energy (ΔE) diagrams for the reaction of *n*-hexane to 1- and 2-hexene. Scheme A is the activation of *n*-hexane to intermediates. Scheme B is the propagation pathway involving the $C_6H_{13}O\cdot$ radical from Int₁, viz. Reaction (13) and (17). The indicated bond distances are in Å. B3LYP/6-311+g(d,p) for the C, O and H atoms. Cartesian coordinates of all TSs are provided as supplementary material.

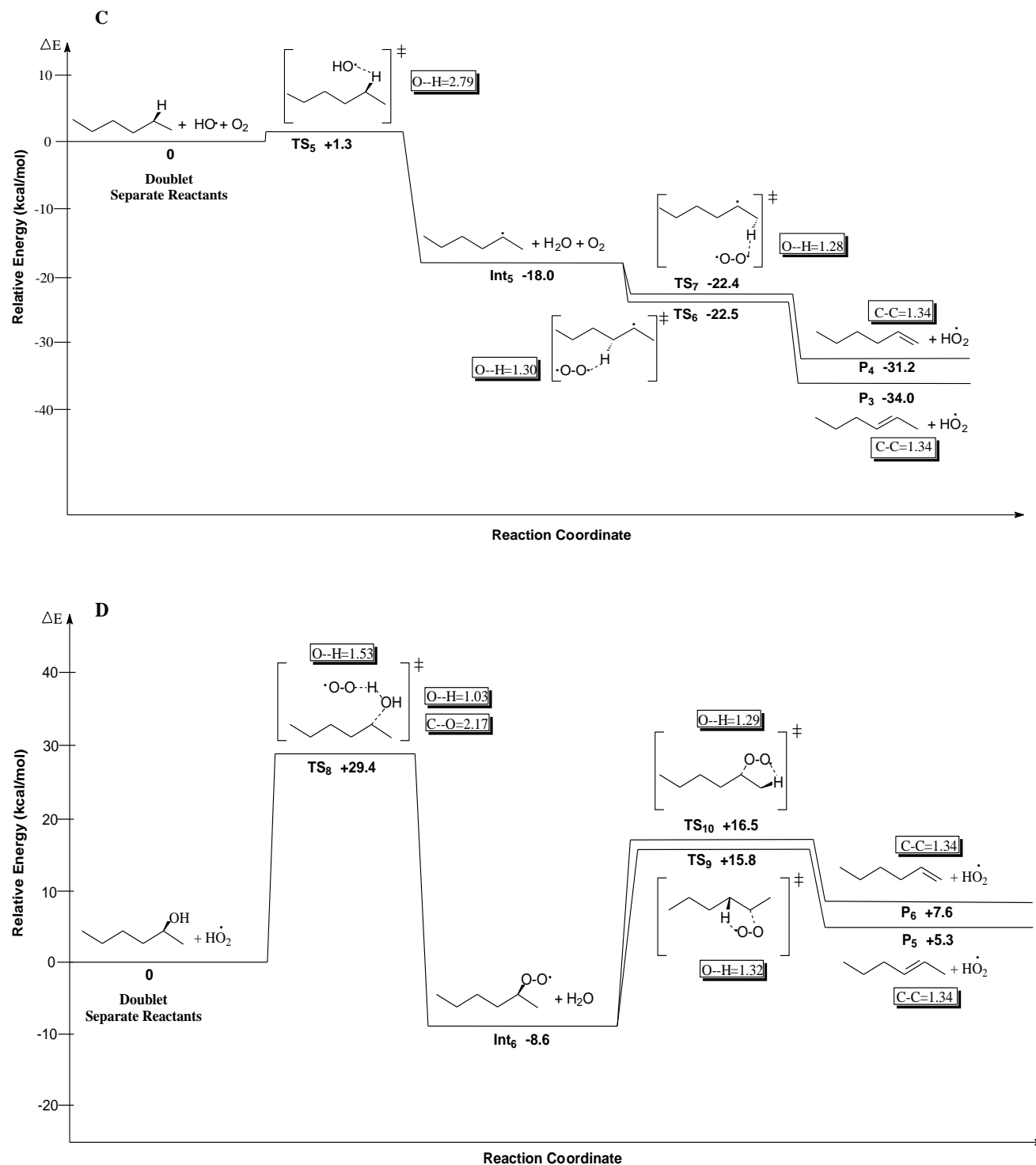


Table 1: Relative Energies (ΔE) and Gibbs Free Energies (ΔG) for the reaction of *n*-hexane with molecular O₂^a. B3LYP/6-311+g(d,p) for the C, O and H atoms. Cartesian coordinates of all TSs are provided as supplementary material.

Reaction Pathway	ΔE	ΔG		
		573	673	773
Initiation				
<i>t</i> -O ₂ + <i>n</i> -C ₆ H ₁₄	0	0	0	0
<i>t</i> -O ₂ -- <i>n</i> -C ₆ H ₁₄ (TS ₁)	+42.4	+53.6	+55.8	+57.9
<i>t</i> -TS ₁ →HO+C ₆ H ₁₃ O (Int ₁)	+20.5 (-21.9)	+31.8 (-21.8)	+34.0 (-21.8)	+36.2 (-21.7)
<i>t</i> -TS ₁ →O+C ₆ H ₁₃ OH (Int ₂)	+28.9 (-13.5)	+35.7 (-17.9)	+38.0 (-17.8)	+40.3 (-17.6)
<i>t</i> -TS ₁ →HO ₂ +C ₆ H ₁₃ (Int ₃)	+44.8 (+2.4)	+51.9 (-1.7)	+53.4 (-2.4)	+54.8 (-3.1)
Propagation from Int₁ (C₆H₁₃O)				
<i>d</i> -C ₆ H ₁₃ O+ <i>n</i> -C ₆ H ₁₄	0	0	0	0
<i>d</i> -C ₆ H ₁₃ O-- <i>n</i> -C ₆ H ₁₄ (TS ₂)	+8.7	+25.6	+28.3	+31.9
<i>d</i> -TS ₂ →C ₆ H ₁₃ OH+C ₆ H ₁₃ (Int ₄)	-1.8 (-10.5)	+6.7 (-18.9)	+8.5 (-19.8)	+10.2 (-21.7)
<i>d</i> -Int ₄ →O ₂ --C ₆ H ₁₃ (TS ₃)	-7.7 (-5.9)	+10.5 (+3.8)	+13.9 (+5.4)	+17.3 (+7.1)
<i>d</i> -TS ₃ →HO ₂ +C ₆ H ₁₂ (P ₁): 2-hexene	-19.2 (-11.5)	-9.8 (-20.3)	-7.9 (-21.8)	-6.1 (-23.4)
<i>d</i> -Int ₄ →O ₂ --C ₆ H ₁₃ (TS ₄)	-7.6 (-5.8)	+10.7 (+4.0)	+14.2 (+5.7)	+17.6 (+7.4)
<i>d</i> -TS ₄ →HO ₂ +C ₆ H ₁₂ (P ₂): 1-hexene	-16.4 (-8.8)	-6.9 (-17.6)	-5.0 (-19.2)	-3.1 (-20.7)
Propagation from Int₁ (HO)				
<i>d</i> -HO+ <i>n</i> -C ₆ H ₁₄	0	0	0	0
<i>d</i> -HO-- <i>n</i> -C ₆ H ₁₄ (TS ₅)	+14.6	+28.1	+30.5	+32.7
<i>d</i> -TS ₅ →H ₂ O+C ₆ H ₁₃ (Int ₅)	-18.0 (-32.6)	-13.1 (-41.3)	-12.0 (-42.5)	-10.9 (-43.6)
<i>d</i> -Int ₅ →O ₂ --C ₆ H ₁₃ (TS ₆)	-22.5 (-4.5)	-5.7 (+7.4)	-2.6 (+9.4)	+0.6 (+11.5)
<i>d</i> -TS ₆ →HO ₂ +C ₆ H ₁₂ (P ₃): 2-hexene	-34.0 (-11.5)	-26.0 (-20.3)	-24.3 (-21.7)	-22.7 (-23.3)
<i>d</i> -Int ₅ →O ₂ --C ₆ H ₁₃ (TS ₇)	-22.4 (-4.4)	-5.4 (+7.7)	-2.2 (+9.8)	+1.0 (+11.9)
<i>d</i> -TS ₇ →HO ₂ +C ₆ H ₁₂ (P ₄): 1-hexene	-31.2 (-8.8)	-23.1 (-17.7)	-21.4 (-19.2)	-19.8 (-20.8)
Propagation – H-transfer				
<i>d</i> -HO ₂ +C ₆ H ₁₃ OH	0	0	0	0
<i>d</i> -HO ₂ --C ₆ H ₁₃ OH (TS ₈)	+29.4	+44.9	+47.9	+50.8
<i>d</i> -TS ₈ →H ₂ O+C ₆ H ₁₃ OO (Int ₆)	-8.6 (-38.0)	+1.7 (-43.2)	+3.8 (-44.1)	+5.8 (-45.0)
<i>d</i> -C ₆ H ₁₃ OO (TS ₉) Intra H-abstraction	+15.8 (+24.4)	+26.7 (+25.0)	+28.8 (+25.0)	+30.8 (+25.0)
<i>d</i> -TS ₉ →HO ₂ +C ₆ H ₁₂ (P ₅): 2-hexene	+5.3 (-10.5)	+7.8 (-18.9)	+8.5 (-20.3)	+9.2 (-21.6)
<i>d</i> -C ₆ H ₁₃ OO (TS ₁₀) Intra H-abstraction	+16.5 (+25.1)	+26.9 (+25.2)	+29.1 (+25.3)	+31.2 (+25.4)
<i>d</i> -TS ₁₀ →HO ₂ +C ₆ H ₁₂ (P ₆): 1-hexene	+7.6 (-8.9)	+12.3 (-14.6)	+9.3 (-19.8)	+15.0 (-16.2)
Intra H-elimination				
<i>d</i> ·C ₆ H ₁₃	0	0	0	0
<i>d</i> ·C ₆ H ₁₃ (TS ₁₁)	+36.3	+37.4	+37.6	+37.8
<i>d</i> -TS ₁₁ →C ₆ H ₁₂ +H· (Int ₇): 2-hexene	+36.5 (+0.2)	+30.6 (-6.8)	+29.5 (-8.1)	+28.5 (-9.3)
Termination				
<i>s</i> -HO ₂ +HO ₂	0	0	0	0
<i>s</i> -HO ₂ --HO ₂ (TS ₁₂)	-2.3	+4.9	+5.8	+6.7
<i>s</i> -TS ₁₂ →2HO+O ₂ (Int ₈)	-21.1 (-18.8)	-23.4 (-28.3)	-24.1 (-29.9)	-24.9 (-31.6)
<i>t</i> -HO--HO (TS ₁₂)	-4.7	+8.5	+11.0	+13.6
<i>t</i> -TS ₁₃ →H ₂ O+O (Int ₉)	-13.0 (-8.3)	-3.2 (-11.7)	-1.3 (-12.3)	+0.7 (-12.9)
<i>t</i> -O--O (TS ₁₄)	-2.1	+10.7	+13.1	+15.6
<i>t</i> -TS ₁₄ →O ₂ (P ₇)	-117.8 (-115.7)	-104.2 (-114.9)	-101.6 (-114.7)	-99.0 (-114.6)

^a ΔE and ΔG are zero-point corrected electronic energy and Gibbs free energy at standard pressure, relative to separate reactants respectively, in kcal/mol. The energies in parentheses are for the indicated reaction pathways. The temperature is in K and ΔE values are at 673K. Prefixes *t*-, *d*- and *s*- indicate triplet, doublet and singlet states, respectively.

Table 2: NBO atomic charges, HONBO and LUNBO orbital types, and largest orbital energies for the TSs of the *n*-hexane to 1- and 2-hexene pathways. B3LYP/6-311+g(d,p) for all the atoms. Cartesian coordinates of all TSs are provided as supplementary material.

Transition state	Atomic charges on interacting atoms	HONBO type	LUNBO type	Orbital Stabilization Energy (kcal/mol)
1	C = -0.191	C <i>s</i> (7.1%) <i>p</i> (92.9%)	H <i>s</i> (76.3%) O <i>s</i> (6.9%)	+38.2
	H = +0.423	nonbonding	<i>p</i> (16.8%) antibonding	
	O = -0.277	hybrid	hybrid	
2	C = -0.275	O <i>s</i> (28.0%) <i>p</i> (72.0%)	H <i>s</i> (71.9%) C <i>s</i> (5.5%)	+45.6
	H = +0.312	nonbonding	<i>p</i> (22.6%) antibonding	
	O = -0.567	hybrid	hybrid	
3 and 6	C = -0.478	O <i>s</i> (13.1%) <i>p</i> (86.9%)	H <i>s</i> (71.1%) C <i>s</i> (3.4%)	+42.1
	H = +0.360	nonbonding	<i>p</i> (25.5%) antibonding	
	O = -0.225	hybrid	hybrid	
4 and 7	C = -0.387	O <i>s</i> (13.3%) <i>p</i> (86.7%)	H <i>s</i> (71.4%) C <i>s</i> (3.7%)	+45.9
	H = +0.192	nonbonding	<i>p</i> (24.9%) antibonding	
	O = -0.408	hybrid	hybrid	
5	C = -0.478	O <i>s</i> (27.3%) <i>p</i> (72.7%)	H <i>s</i> (66.6%) C <i>s</i> (7.7%)	+23.6
	H = +0.257	nonbonding	<i>p</i> (25.7%) antibonding	
	O = -0.613	hybrid	hybrid	
8	C = -0.170	O <i>s</i> (35.6%) <i>p</i> (64.4%) and O	H <i>s</i> (78.9%) O <i>s</i> (4.9%)	+21.3 and +22.0
	O (O ₂) = -0.888	<i>s</i> (15.1%) <i>p</i> (84.9%)	<i>p</i> (16.2%) and	
	H = +0.480	nonbonding	C <i>s</i> (1.0%) <i>p</i> (99.0%)	
	O (OH) = -0.277	hybrids	antibonding hybrid	
9	C = -0.486	O <i>s</i> (13.1%) <i>p</i> (86.9%)	H <i>s</i> (70.8%) C <i>s</i> (3.5%)	+39.3
	H = +0.363	nonbonding	<i>p</i> (25.7%) antibonding	
	O = -0.218	hybrid	hybrid	
10	C = -0.667	O <i>s</i> (13.4%) <i>p</i> (86.6%)	H <i>s</i> (70.2%) C <i>s</i> (4.0%)	+43.5
	H = +0.361	nonbonding	<i>p</i> (25.8%) antibonding	
	O = -0.215	hybrid	hybrid	

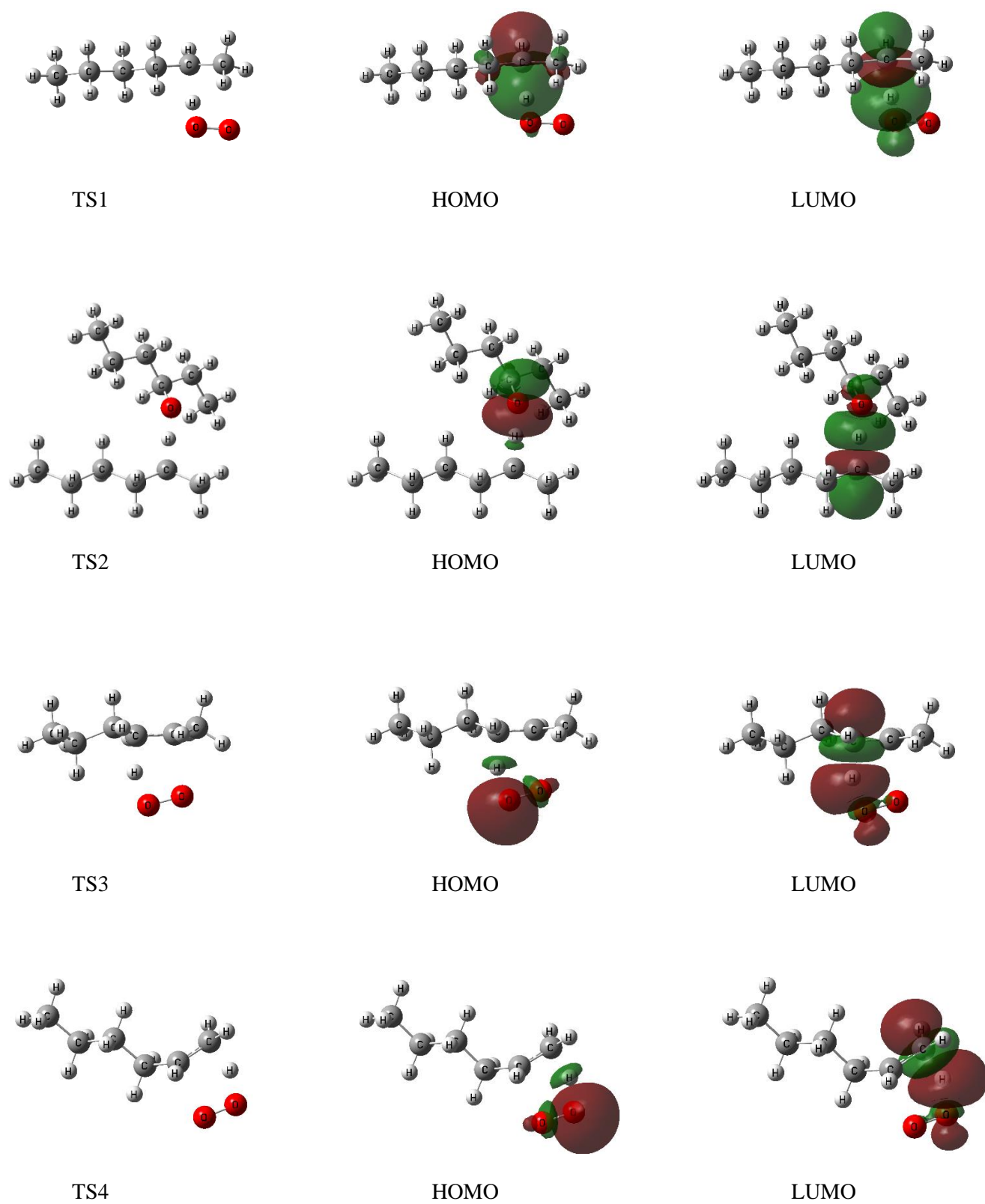


Figure 3A Transition state structures and frontier orbitals for the likely mechanistic scheme. The orbital lobes are oriented for better clarity in each case and correspond to the reaction coordinate.

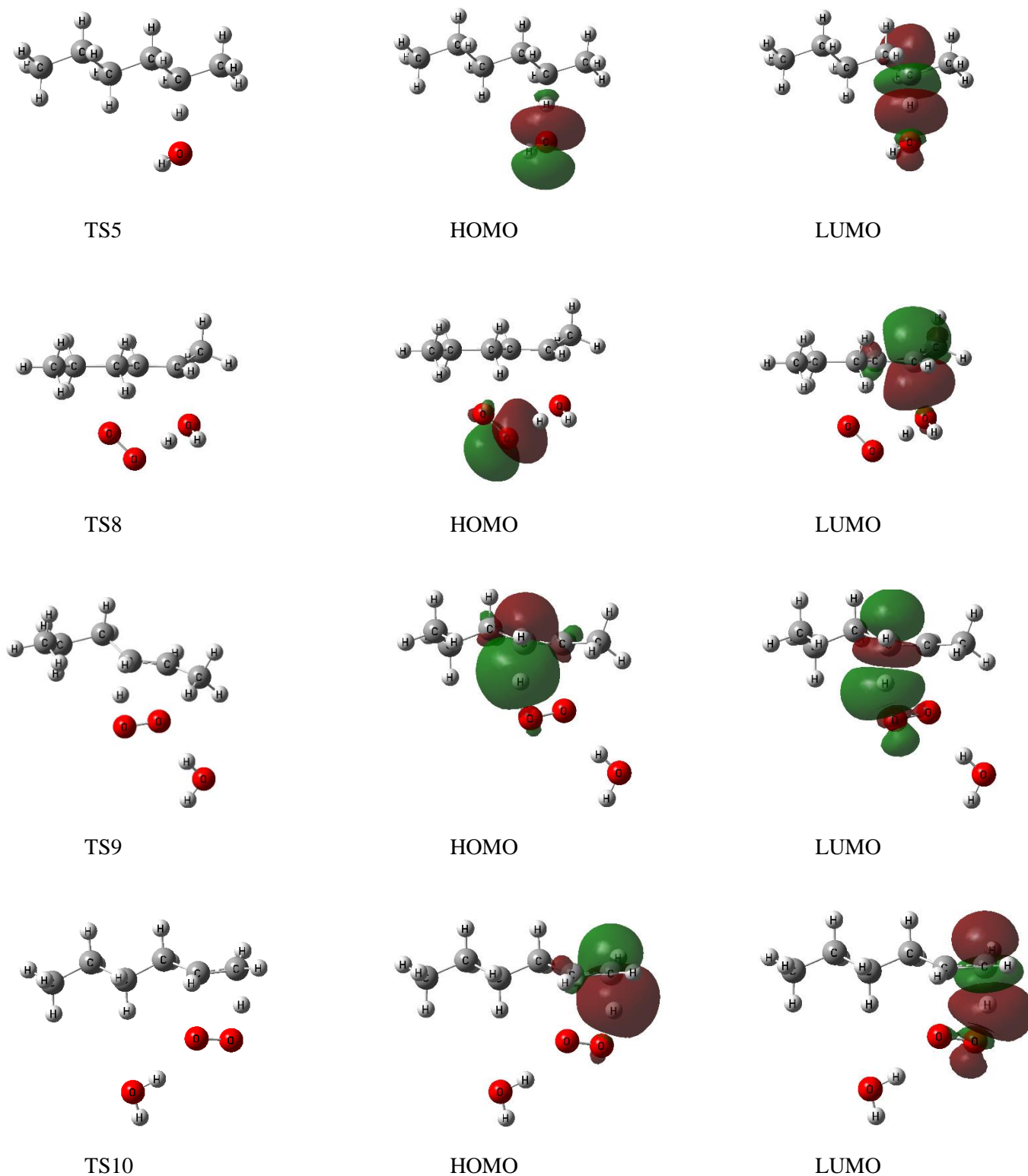


Figure 3B Transition state structures and frontier orbitals for the likely mechanistic scheme. The orbital lobes are oriented for better clarity in each case and correspond to the reaction coordinate.

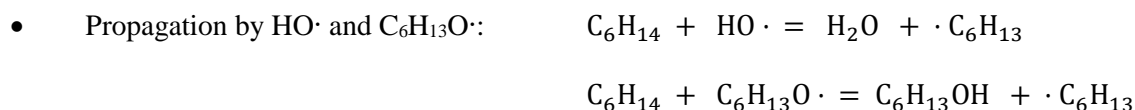
4 Conclusions

The mechanism for activation of *n*-hexane by molecular oxygen and subsequent propagation pathways is proposed based on DFT modelling using experimental conditions of 573, 673 and 773K. All the pathways are recorded in Table 1.

The formation of CO_x was not considered for this study. The most kinetically and thermodynamically favourable mechanistic pathways that are likely to drive the reaction are the following,



Since O₂ and *n*-hexane are the only species present at the initial stages of the reaction, the rate-determining step is the abstraction of H from *n*-hexane by triplet O₂ with a barrier height of +42.4 kcal/mol. The pathway stabilizes to produce the intermediate (Int₁) that comprises the alkoxy (C₆H₁₃O·) and hydroxyl (HO·) radicals. This intermediate is thermodynamically more stable ($\Delta E = +20.5$ kcal/mol) than that composed of the alkyl (C₆H₁₃·) and hydroperoxy radicals (HO₂·), with $\Delta E = +44.8$ kcal/mol, relative to separate reactants. (Figure 2A).



H-abstraction from further *n*-hexane molecules by ·OH and C₆H₁₃O· radicals. The indicated first step has a barrier of +14.6 kcal/mol and the second step +8.7 kcal/mol. The intermediates stabilize with associated ΔE values of -18.0 and -1.8 kcal/mol, respectively (Figures 2B and 2C).



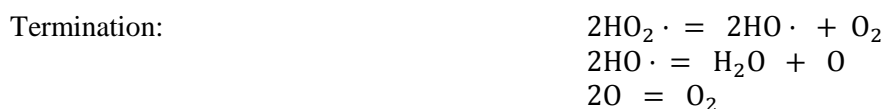
H-abstraction from the generated ·C₆H₁₃ radicals by molecular O₂. This step is barrierless (-5.9 kcal/mol) and also thermodynamically favourable by -17.4 kcal/mol for the formation of 2-hexene (Figure 2B).



A concerted mechanistic pathway that involves H-transfer from HO₂· radical to C₆H₁₃OH that is accompanied by H₂O formation has a barrier height of +29.4 kcal/mol and the reaction step is thermodynamically favourable and produces C₆H₁₃OO· and H₂O with $\Delta E = -8.6$ kcal/mol (Figure 2D).



Intramolecular H-abstraction and HO₂· elimination to produce 2-hexene with a barrier height of +24.4 kcal/mol and ΔE value of +5.3 kcal/mol from the initial reactants of HO₂· and C₆H₁₃OH (Figure 2D).



The remaining HO₂· radicals combine to produce H₂O and O₂ through a series of three steps. For the three steps we calculated barrier-less energies of -2.3, -4.7 and -2.1 kcal/mol, and the corresponding ΔE values of -21.1, -13.0 and -117.8 kcal/mol, relative to separate reactants, respectively (Table 1).

Acknowledgments

This work was supported by the NRF, SASOL and Johnson Matthey. We would like to thank the Centre for High Performance Computing (CHPC) in Cape Town, South Africa, for providing the computational resources necessary to conduct this work.

References

- [1] P. Viparellia, P. Ciambellib, L. Lisic, G. Ruoppoloa, G. Russoa, J. C. Volta, **Oxidative dehydrogenation of propane over vanadium and niobium oxides supported catalysts**, Appl. Catal., A 184 (1999) 291-301.
- [2] A.T. Bell, S. Chempath, **A DFT study of the mechanism and kinetics of methane oxidation to formaldehyde occurring on silica-supported molybdena**, J. Catal. 247 (2007) 119-126.
- [3] E.A. Elkhalfa, H.B. Friedrich, **Oxidative dehydrogenation of n-octane using vanadium-magnesium oxide catalysts with different vanadium loadings**, Appl. Catal., A 373 (2010) 122-131.
- [4] C. Boyadjian, L. Lefferts, K. Seshan, **Catalytic oxidative cracking of hexane as a route to olefins**, Appl. Catal., A 372 (2010) 167-174.
- [5] A. Chauvel, G. Lefebvre, **Petrochemical processes: Technical and economic characteristics**, Editions Technip, Paris, 1989.
- [6] J.A. Moulijn, M. Makkee, A. van Diepen, **Chemical process technology**, Wiley, Chichester, 2001.
- [7] D. Dharia, W. Letzsch, H. Kim, D. McCue, L. Chapin, **Increase light olefins production**, Hydrocarbon Process., Int. Ed. 83 (2004) 61.
- [8] H.H. Kung, **Transition metal oxides: Surface chemistry and catalysis**, Stud. Surf. Sci. Catal. 45, Elsevier, Amsterdam, 1989.
- [9] V.R. Choudhary, V.H. Rane, A.M. Rajput, **Simultaneous thermal cracking and oxidation of propane to propylene and ethylene**, AIChE J. 44 (1998) 2293-2301.
- [10] A.A. Lemonidou, A.E. Stambouli, **Catalytic and non-catalytic oxidative dehydrogenation of n-butane**, Appl. Catal., A 171 (1998) 325-332.
- [11] J. Park, C. Shin, **Influence of the catalyst composition in the oxidative dehydrogenation of 1-butene over BiV_xMo_{1-x} oxide catalysts**, Appl. Catal., A 495 (2015) 1-7.
- [12] F. Cavani, N. Ballarini, A. Cericola, **Oxidative dehydrogenation of ethane and propane: How far from commercial implementation**, Catal. Today 127 (2007) 113-131.
- [13] R. Grabowski, **Kinetics of the oxidative dehydrogenation of propane on vanadia/titania catalysts, pure and doped with rubidium**, Appl. Catal., A 270 (2004) 37-47.
- [14] D. Creaser, B. Andersson, R.R. Hudgins, P.L. Silveston, **Transient study of oxidative dehydrogenation of propane**, Appl. Catal., A 187 (1999) 147-160.

- [15] R.R. Baker, R.R. Baldwin, R.W. Walker, **Alkene formation in hydrocarbon oxidation**, Elsevier, Amsterdam, 1977.
- [16] J.A. Toledo, H. Armendariz, E. L'opez-Salinas, **Oxidative dehydrogenation of n-butane: a comparative study of thermal and catalytic reaction using Fe–Zn mixed oxides**, Catal. Lett. 66 (2000) 19-24.
- [17] V.S. Arutyunov, L.N. Strekova, A.V. Nikitin, **Partial oxidation of light alkanes as a base of new generation of gas chemical processes**, Eurasian Chem. Technol. J. 15 (2013) 265-273.
- [18] J.E. Taylor, D.M. Kulich, **Industrial and laboratory pyrolysis**, in: L.F. Albright, B.L. Crynes (Eds.), ACS Symposium Series 32, Washington, 1976, pp. 72-83.
- [19] M.E. Dente, E. M. Ranzi, **Mathematical modelling of hydrocarbon pyrolysis reactions**, in: L. F. Albright, B. L. Crynes, W. H. Corcoran (Eds.), **Pyrolysis: Theory and industrial practice**, Academic Press, New York, 1983, pp. 133-175.
- [20] R. Burch, E.M. Crabb, **Homogeneous and heterogeneous contributions to the oxidative dehydrogenation of propane on oxide catalysts**, Appl. Catal., A 100 (1993) 111-130.
- [21] W.J. Pitz, C.K. Westbrook, **Chemical kinetics of the high pressure oxidation of n-butane and its relation to engine knock**, Combust. Flame 63 (1986) 113-133.
- [22] X. Liu, W. Li, H. Xu, Y. Chen, **Production of light alkenes with low CO₂ emission from gas phase oxidative cracking (GOC) of hexane**, React. Kinet. Catal. Lett. 81 (2) (2004) 203-209.
- [23] V.P. Vislovskiy, T.E. Suleimanov, M.Yu. Sinev, Yu.P. Tulenin, L.Ya. Margolis, V. Cortés Corberán, **On the role of heterogeneous and homogeneous processes in oxidative dehydrogenation of C₃-C₄ alkanes**, Catal. Today 61 (2000) 287-293.
- [24] K.C. Hunter, A.L.L. East, **Properties of C-C bonds in n-alkanes: Relevance to cracking mechanisms**, J. Phys. Chem. A 106 (2002) 1346-1356.
- [25] Y. Liu, Z. Geng, Y. Wang, J. Liu, X. Hou, **DFT studies for activation of C-H bond in methane by gas-phase Rh_n⁺ (n = 1 – 3)**, Comput. Theor. Chem. 1015 (2013) 52-63.
- [26] K. Alexopoulos, M. Reyniers, G.B. Marin, **Reaction path analysis of propane selective oxidation over V₂O₅ and V₂O₅/TiO₂**, J. Catal. 289 (2012) 127-139.
- [27] E. Kurnaz, M.F. Fellah, I. Onal, **A density functional theory study of C-H bond activation of methane on a bridge site of M-O-M-ZSM-5 cluster (M = Au, Ag, Fe and Cu)**, Microporous Mesoporous Mater. 138 (2011) 68-74.
- [28] H. Hoog, J. Herheus, F.J. Zuiderweg, **Investigations into the cyclisation (aromatisation) of aliphatic hydrocarbons**, Trans. Faraday Soc. 35 (1939) 993.
- [29] A.D. Becke, **Density functional thermochemistry III. The role of exact exchange**, J. Chem. Phys. 98 (1993) 5648.
- [30] C. Lee, W. Yang, R.G. Parr, **Development of the Colle-Salvetti correlation energy formula into a functional of the electron density**, Phys. Rev. B 37 (1988) 785.
- [31] M.J. Frisch, G.W. Trucks, H.B. Schlegel, G.E. Scuseria, M.A. Robb, J.R. Cheeseman, G. Scalmani, V. Barone, B. Mennucci, G.A. Petersson, H. Nakatsuji, M. Caricato, X. Li, H.P. Hratchian, A.F. Izmaylov, J. Bloino, G. Zheng, J.L. Sonnenberg, M. Hada, M. Ehara, K.

- Toyota, R. Fukuda, J. Hasegawa, M. Ishida, T. Nakajima, Y. Honda, O. Kitao, H. Nakai, T. Vreven, J. Montgomery, J. A., J.E. Peralta, F. Ogliaro, M. Bearpark, J.J. Heyd, E. Brothers, K.N. Kudin, V.N. Staroverov, R. Kobayashi, J. Normand, K. Raghavachari, A. Rendell, J.C. Burant, S.S. Iyengar, J. Tomasi, M. Cossi, N. Rega, N.J. Millam, M. Klene, J.E. Knox, J.B. Cross, V. Bakken, C. Adamo, J. Jaramillo, R. Gomperts, R.E. Stratmann, O. Yazyev, A.J. Austin, R. Cammi, C. Pomelli, J.W. Ochterski, R.L. Martin, K. Morokuma, V.G. Zakrzewski, G.A. Voth, P. Salvador, J.J. Dannenberg, S. Dapprich, A.D. Daniels, Ö. Farkas, J.B. Foresman, J.V. Ortiz, J. Cioslowski, D.J. Fox, **Gaussian 09, Revision B.01**, Gaussian, Inc., Wallingford, 2010.
- [32] C. Gonzales, H.B. Schlegel, **An improved algorithm for reaction path following**, J. Chem. Phys. 90 (1989) 2154.
- [33] C. Gonzales, H.B. Schlegel, **Reaction path following in mass-weighted internal coordinates**, J. Phys. Chem. 94 (1990) 5523-5527.
- [34] J.E. Carpenter, F. Weinhold, **Analysis of the geometry of the hydroxymethyl radical by the “different hybrids for different spins” natural bond orbital procedure**, J. Mol. Struct. THEOCHEM 169 (1988) 41-62.
- [35] F. Weinhold, J. E. Carpenter, **The natural bond orbital Lewis structure concept for molecules, radicals, and radical ions**, in: R. Naaman, Z. Vager (Eds.), **The structure of small molecules and ions**, Plenum, New York, 1988, pp. 227-236.
- [36] Y. Zhao, D.G. Truhlar, **The M06 suite of density functionals for main group thermochemistry, thermochemical kinetics, noncovalent interactions, excited states, and transition elements: Two new functionals and systematic testing of four M06-class functionals and 12 other functionals**, Theor. Chem. Acc. 120 (2006) 215-241.
- [37] N. Chéron, D. Jacquemin, P. Fleurat-Lessard, **A qualitative failure of B3LYP for textbook organic reactions**, Phys. Chem. Chem. Phys. 14 (2012) 7170-7175.
- [38] K.P. Huber, G. Herzberg, **Molecular spectra and molecular structure. Constants of diatomic molecules**, Van Nostrand, New York, 1979.
- [39] D.F. McMillen, D.M. Golden, **Hydrocarbon bond dissociation energies**, Annu. Rev. Phys. Chem. 33 (1982) 493-532.
- [40] J.M. Anglada, V.M. Domingo, **Mechanism for the gas-phase reaction between formaldehyde and hydroperoxyl radical. A theoretical study**, J. Phys. Chem. A 109 (2005) 10786-10794.
- [41] E.P. Clifford, P.G. Wenthold, R. Gareyev, W.C. Lineberger, C.H. DePuy, V.M. Bierbaum, G.B. Ellison, **Photoelectron spectroscopy, gas phase acidity, and thermochemistry of tert-butyl hydroperoxide: Mechanisms for the rearrangement of peroxy radicals**, J. Chem. Phys. 109 (1998) 10293.
- [42] I.R. Slagle, Q. Feng, D. Gutman, **Kinetics of the reaction of ethyl radicals with molecular oxygen from 294 to 1002 K**, J. Phys. Chem. 88 (1984) 3648-3653.
- [43] A.F. Wagner, I.R. Slagle, D. Sarzynski, D. Gutman, **Experimental and theoretical studies of the ethyl + oxygen reaction kinetics**, J. Phys. Chem. 94 (1990) 1853-1868.
- [44] J.A. Howard, K.U. Ingold, **Self-reaction of sec-butylperoxy radicals. Confirmation of the Russell mechanism**, J. Am. Chem. Soc. 90 (1968) 1056-1058.

- [45] J.A. Howard, J.C. Scaiano, **Oxyl, peroxy and related radicals**, in: **H Fischer (Ed.), Landolt-Börnstein numerical data and functional relations in science and technology**, new series, vol. 13, Springer-Verlag, New York, 1984.
- [46] L. Jun-Na, C. Zhi-Rang, Y.J. Shen-Fang, **Study on the prediction of visible absorption maxima of azobenzene compounds**, Zhejiang Univ. Sci. B 6 (2005) 584-589.

CHAPTER 3

A DFT Study of the ODH of *n*-hexane over isolated H₃VO₄

N.E. Damoyi^{a,*}, H.B. Friedrich^b, H.G. Kruger^c and D. Willock^d

^aDepartment of Chemistry, Mangosuthu University of Technology, Box 12363, Jacobs, 4026, South Africa

^bSchool of Chemistry, University of KwaZulu Natal, Westville Campus, Private Bag X 54001, Durban, 4000, South Africa

^cCatalysis and Peptide Research Unit, School of Pharmacy, University of KwaZulu Natal, Westville Campus, Private Bag X 54001, Durban, 4000, South Africa

^dSchool of Chemistry, Cardiff University, Park Place, Cardiff CF10 3AT, Wales, UK

Keywords: DFT, ODH, *n*-hexane, RDS, mechanism, vanadia

ABSTRACT

Catalytic (VO₄) oxidative dehydrogenation (ODH) mechanistic studies of the activation of *n*-hexane have been conducted by means of Density Functional Theory (DFT).

The aim of this study was to determine the catalytic mechanism of the conversion of *n*-hexane to 1- and 2-hexene. The calculations were performed for only the 1- and 2-hexene radical pathways under laboratory experimental conditions of 573, 673 and 773K, since no 3-hexene was observed in our experiments, nor reported in literature. GAUSSIAN 09W and GaussView 5.0 codes were used for the study. The B3LYP hybrid functional and the 6-311+g(d,p) basis set for C, O and H atoms and effective core potentials (ECPs) for V atom were utilized. The stationary points on the potential energy surfaces have been characterized and the associated geometries and relative energies (ΔE^\ddagger , ΔE , ΔG^\ddagger and ΔG) have been determined. The relative energies allow for the development of thermodynamic and kinetic arguments about the mechanistic pathways for the reaction.

The catalyst model chosen for this study was the isolated, tetrahedral H₃VO₄ cluster comprising one vanadyl bond, V(V)=O. The calculated rate-limiting step is the C–H bond activation (β -hydrogen abstraction) from the C₆H₁₄ chain by the O atom of V(V)=O, with $\Delta E^\ddagger = +27.4$ kcal/mol, to produce the C₆H₁₃HOVO₃H₃ complex intermediate with V(IV) centre. The propagation step that leads to 2-hexene by the abstraction of the second γ -hydrogen on the radical intermediate fragment (\cdot C₆H₁₃) may proceed through two different pathways, one on a different active V(V)=O site and the other with gas-phase molecular O₂. The gas-phase pathway may dominate at lower *n*-hexane to oxygen molar ratios combined with low V(V)=O surface areas and be subdued at higher molar ratios in combination with high V(V)=O surface areas. However, chemisorption of the radical intermediate (\cdot C₆H₁₃) with either V(V)=O on a different site or with gas-phase O₂, rather than H-abstraction, may lead to more stable C₆H₁₃VO₄H₃ and C₆H₁₃O₂ intermediates, respectively. High reaction barriers to release 2-hexene from the more stable intermediates may be responsible for low experimental yields of 1- and 2-hexene, and this pathway may lead to oxygenates. The reoxidation to V(V) is achieved through the Mars-van Krevelen mechanism.

* Corresponding author e-mail address: damoyi@mut.ac.za

1 Introduction

Transition metal oxides are frequently used as heterogeneous catalysts for oxidation of hydrocarbons to produce a variety of products. Gas phase studies of metal oxide clusters and their reaction behaviour can help to understand the mechanism of elementary reactions in catalytic processes under isolated, controlled, and reproducible conditions [1-3].

Vanadium oxide-based catalytic systems are known to be active and selective in many oxidative dehydrogenation (ODH) reactions [4-8]. Studies [9], [10] have shown that depending on the method of preparation, vanadium oxide-based catalysts possess a variety of phases that include isolated VO_4 tetrahedral sites, comprising one vanadyl bond ($\text{V}=\text{O}$). The $\text{V}=\text{O}$ bond has been proposed by many investigators to contain a critical oxygen involved in hydrocarbon oxidation reactions [11-15]. Pieck et al. [16] studied the ODH of propane on $\text{V}_2\text{O}_5/\text{ZrO}_2$ catalysts and showed that monovanadates have both higher activities and better selectivities to propene than bulk V_2O_5 and polyvanadates. However, generally at high conversions of the alkane, non-selective combustion pathways limit the alkene selectivities, regardless of the good activity for the ODH of alkanes to their corresponding alkenes [17-19]. For example, it is well established that limited propene selectivity at higher propane conversions is related to propene adsorption on acid sites and their subsequent combustion to carbon oxides [20], [21]. Much effort has been spent over the last decades to develop suitable vanadium oxide-based catalysts for the oxidative dehydrogenation and selective oxidation of light hydrocarbons to valuable olefins and oxygenates [22], [23], however, these processes are still far from industrial application. Earlier experimental studies indicate that the selective oxidation of propane on vanadium oxides proceeds via a Mars–van Krevelen [24] (redox) mechanism that involves the reduction of the metal oxide surface by the alkane with the formation of the alkene and water, followed by reoxidation of the surface through gas-phase oxygen.

Reactions comprising isolated vanadate species with a variety of support materials including silica, titania and zirconia have been modelled previously with a variety of computational methods [25-28]. Reported work on Density Functional Theory (DFT) modelling of catalytic systems and shorter chain hydrocarbons is extensive [29-31], albeit that on long chain alkanes over vanadium oxide-based catalysts is limited. The chosen model for this study is the isolated monomeric H_3VO_4 unit with tetrahedral coordination [32], [33]. Our recent work on the gas-phase ODH of *n*-hexane show that the rate-determining step is the abstraction of β -hydrogen by molecular O_2 [34].

We proposed that molecular O_2 plays an important role in the radical propagation steps through the intermediates, to produce 1- and 2-hexene and the more reactive $\cdot\text{OH}$ and $\text{HO}_2\cdot$ radicals. Since our present studies include both molecular O_2 and isolated H_3VO_4 , we therefore seek to compare the contribution of H_3VO_4 and O_2 in the activation of *n*-hexane and radical propagation steps to produce 1- and 2-hexene. Although our modelling is an oversimplification of heterogeneous surface reactions because of the methodology followed, namely, gas-phase calculations on isolated active sites, we believe that the results will be essential in acquiring a theoretical baseline for future potential periodic-DFT calculations of this system. Furthermore, comparisons of the results with those obtained in our recent work [34] on gas-phase non-catalytic ODH of *n*-hexane would be useful, since under certain experimental conditions, gas-phase ODH mechanisms may compete with the catalytic ODH mechanisms.

The energetics calculated, namely, activation energies (ΔE^\ddagger), electronic (ΔE) and Gibbs energy (ΔG) changes facilitate in elucidating the likely intermediate species involved and the mechanistic pathways followed for the transformation of *n*-hexane to 1- and 2-hexene.

2 Theoretical Methodology

2.1 Computational Details

Gas-phase DFT calculations were performed using the Gaussian 09W package [35] incorporating the Gausview5.0 graphics interface. All calculations were performed on a cluster based at the Centre for High Performance Computing (CHPC) in Cape Town, South Africa. All the structures were optimized without constraints and the harmonic vibrational frequencies performed using the B3LYP hybrid functional, which combines Becke's three-parameter nonlocal hybrid exchange potential and the nonlocal correlation functional of Lee, Yang and Parr [36], [37]. This functional is known to provide a good description of the potential energy surface (PES) of transition metal-containing compounds [38-40]. The 6-311+g(d,p) basis set was employed for C, O and H atoms and the V atom described using the relativistic Stuttgart effective core potentials (ECPs) [41], [42]. The transition states (TS) were determined by using relaxed-PES scan techniques on the closed shell and open-shell singlet systems and the laboratory experimental conditions, namely 573, 673 and 773 K were utilized. The intrinsic reaction coordinate (IRC) calculations in the mass-weighted internal coordinate system, using the algorithm developed by González and Schlegel [43], [44], were conducted to confirm the connection of transition states to related minima. The natural bonding orbital (NBO) calculations were performed using the NBO 3.1 program as implemented in the Gaussian 09W package and the donor-acceptor interactions were analysed based on second order perturbation theory analysis of Fock matrix in NBO basis [45], [46].

2.2 Model System

Figure 1 displays the structure of the selected model of the proposed active site [33], namely the H_3VO_4 monomeric unit with vanadium in a tetrahedral coordination sphere. The structure has one $\text{V}=\text{O}$ bond with vanadium in its highest oxidation state (+5), and the three H atoms are added to balance the -3 charge on the three O atoms. In all calculations the atoms were allowed to relax. Comparisons of some calculated parameters and vibrational spectra of the model structure with experimental values show that the percentage errors in the calculated $\text{V}=\text{O}$ bond length is 1% and that of the $\text{V}-\text{O}$ bond length is 3%. The calculated percentage error for the $\text{V}=\text{O}$ stretching vibration is 6%. More information is included as supplementary material.

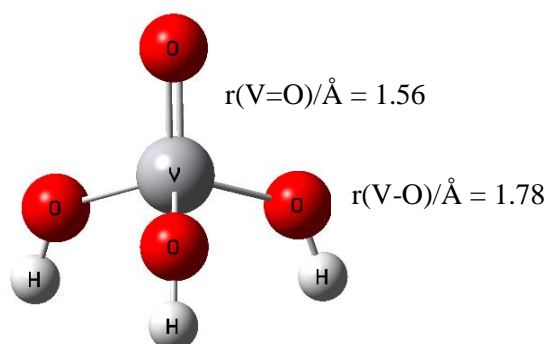


Figure 1 H_3VO_4 model. B3LYP/6-311+G(d,p) for the H and O atoms, and Stuttgart ECPs for the V atom.

2.3 Reaction Scheme for *n*-Hexane to 2-Hexene

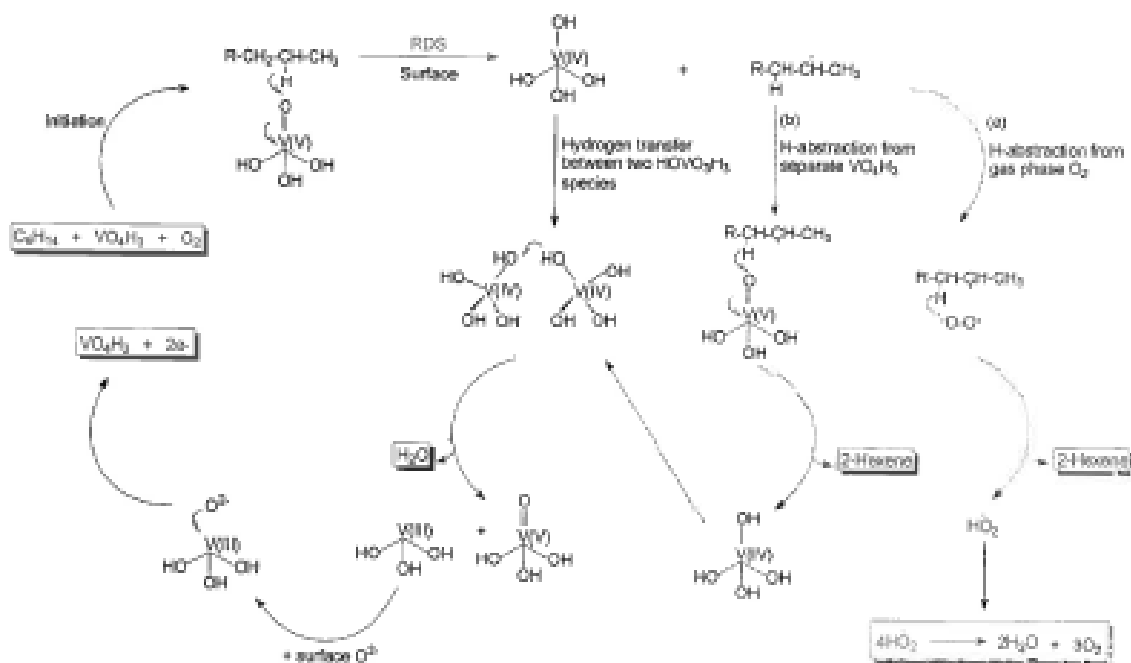


Figure 2 Proposed reaction scheme, $R = CH_2CH_2CH_3$.

The proposed reaction scheme for the catalytic (H_3VO_4) ODH reaction of *n*-hexane is shown in Figure 2. Observations from our recent experimental results [47], reflect that only 1- and 2-hexene (no 3-hexene) exist in equilibrium in the reactor over VMgO catalysts, as also suggested by Hoog *et al.* [48]. Figure 2 only indicates the pathway for formation of 2-hexene for clarity purposes.

The rate-determining step involves H-abstraction from the *n*-hexane chain by the vanadyl O atom in H_3VO_4 , leading to an alkyl radical and a new V-O-H bond in $HOVO_3H_3$. This is associated with the change in vanadium oxidation state from (V) in H_3VO_4 to (IV) in $HOVO_3H_3$. Two pathways that may lead to 2-hexene are (a) the green-coloured pathway, where the alkyl radical may interact with gas-phase O_2 through the second γ -H abstraction to produce 2-hexene and a hydroperoxyl radical species, and (b) the blue-coloured pathway, where a vanadyl O atom from a different H_3VO_4 species abstracts the second γ -H atom to form 2-hexene and another V-O-H bond in $HOVO_3H_3$. Interaction between the two formed V(IV) ($HOVO_3H_3$) species may involve disproportionation through H-transfer from one entity to another to produce H_2O and regenerate V(V) as H_3VO_4 and also V(III) as H_3VO_3 . The radical termination step may occur through disproportionation of the hydroperoxyl radicals, produced in pathway (a) above, into water and oxygen. Finally, the reoxidation of V(III) to V(V) may be achieved through the Mars–van Krevelen mechanism [24] with surface O species.

3 Results

3.1 Activation of *n*-hexane

The main aim of this study was to characterize the most likely mechanistic steps associated with the interaction of *n*-hexane and the related intermediates with the model catalyst (H_3VO_4) and O_2 under specific conditions in order to gain insight about the overall mechanism that is followed for the reaction.

The energy profile of the singlet PES for the interaction of *n*-hexane with H_3VO_4 at 673K is displayed in Figure 3 and all the energies are recorded in Table 1. The C-H bond activation through H-abstraction by the vanadyl O (V=O) has been identified as the rate-determining step (RDS) for alkanes ODH to alkenes on V_2O_5 and supported vanadium oxide in several mechanistic studies [49-52]. In our previous theoretical work on the gas-phase non-catalytic ODH of *n*-hexane we concluded that the RDS is H-abstraction by $^3\text{O}_2$, with a barrier height of $\Delta E^\ddagger = +42.4$ kcal/mol [34]. In our present work we calculated the RDS as β -hydrogen abstraction by the vanadyl O of H_3VO_4 to produce the intermediate 1 (Int₁ – Figure 3), $\text{C}_6\text{H}_{13}\text{HOVO}_3\text{H}_3$. We calculated the activation barrier (TS₁ – Figure 3) with $\Delta E^\ddagger = +27.4$ kcal/mol for this step. A number of authors have also reported on the formation of similar radical intermediates that eventually lead to the formation of olefins [53-55]. This reaction step is associated with the cleavage of the π -bond in V=O to form a new V-O-H bond and the V centre alters its state from V^{5+} to V^{4+} . The VO bond length simultaneously increases from 1.56 Å in the isolated unit to 1.71 Å in TS₁ and 1.78 Å in Int₁. The presence of V^{4+} sites on the partially reduced catalytic surface has been confirmed experimentally for both the unsupported and supported vanadia catalysts [56-58]. Our calculated barrier is comparable to experiments, reported by Argyle *et al.* [52], [59] who measured the activation barrier for both propane and ethane ODH on alumina-supported vanadia and found both to be +27.0 kcal/mol. Our results show that intermediate 2 (Int₂ – Figure 3), with the V-C bond, is unlikely to form because of its thermodynamic instability with $\Delta E = +4.8$ kcal/mol compared to Int₁ ($\Delta E = -3.4$ kcal/mol), relative to TS₁.

Figure 4 displays the propagation steps we explored that lead to 2-hexene. All the energies, including those for the 1-hexene pathway are recorded in Table 1. The pathway coloured in red indicates the second H-abstraction from the $\cdot\text{C}_6\text{H}_{13}$ radical by the OH group within Int₁ to produce 2-hexene, V(III) and H_2O . The calculated barriers are respectively, +34.4 (TS₂ – Figure 4) and +40.3 kcal/mol (TS₅) and the products stabilize to P₁ with $\Delta E = +5.0$ and P₄ = +24.3 kcal/mol for the formation of 2- and 1-hexene. In the ODH of *n*-propane, Hui *et al.* [54] reported reaction barriers (>30 kcal/mol) for a similar pathway, namely, abstraction of the second H from the same O site as that of the first H abstraction, leading to formation of propene. The authors suggested that this pathway is likely to be hindered by high reaction barriers and they proposed that the second H-abstraction occurs on a different O site. In light of this we explored the abstraction of the second H on a different vanadyl O site, to produce 2- and 1-hexene. The reaction equation for the pathway is: $\text{H}_3\text{VO}_4 + \cdot\text{C}_6\text{H}_{13} = \text{HOVO}_3\text{H}_3 + \text{C}_6\text{H}_{12}$. We calculated barriers of $\Delta E^\ddagger = +0.3$ (TS₃ – Figure 4) and +0.8 kcal/mol (TS₆) for this step and $\Delta E = -33.5$ (P₃) and -30.8 kcal/mol (P₆) for the formation of 2- and 1-hexene, respectively. Our results are in agreement with what was reported by Hui *et al.* Since gas phase O_2 is another species present in the reaction mixture, we calculated the propagation pathway that involves H-abstraction from $\cdot\text{C}_6\text{H}_{13}$ by O_2 . Barrier-less TS₄ (Figure 4) and TS₇ with the respective values of $\Delta E^\ddagger = -3.0$ and -2.9 kcal/mol and $\Delta E = -14.7$ (P₂) and -11.4 (P₅) kcal/mol were calculated for 2- and 1-hexene. In all the above pathways, the formation of the olefins is accompanied by decrease in π -bond-forming CC bond lengths from ~1.5 Å in $\cdot\text{C}_6\text{H}_{13}$ to ~1.4 Å in the TS and ~1.3 Å in the produced alkene.

Comparisons of energetics for the two likely steps for the second H-abstraction, namely, either from a different vanadyl O site ($\Delta E^\ddagger = +0.3$ kcal/mol and $\Delta E = -33.5$ kcal/mol) or from the gas-phase O_2 ($\Delta E^\ddagger = -3.0$ kcal/mol and $\Delta E = -14.7$ kcal/mol) for the formation of 2-hexene, indicate that gas phase H-abstraction is slightly more kinetically favourable (by -2.7 kcal/mol), albeit the products formed are less thermodynamically favourable by +18.8 kcal/mol. A relatively large amount of gas phase O_2 in

the experimental mixture coupled with low V(V)=O surface areas may lead to the domination of the gas-phase pathway, and the opposite may be true also. In our previous results on gas-phase ODH of *n*-hexane [34], we found that the $\cdot\text{C}_6\text{H}_{13}$ radical (Figure 4) is not likely to undergo intramolecular H-elimination to produce 1- or 2-hexene and the $\text{H}\cdot$ radical. This is because of the calculated barriers of $\Delta E^\ddagger = +38.2$ and $+36.3$ kcal/mol and values of $\Delta E = +39.5$ and $+36.5$ kcal/mol for the formation of 1- and 2-hexene, respectively, confirming that the pathways are kinetically and thermodynamically less feasible. However, chemisorption of the $\cdot\text{C}_6\text{H}_{13}$ radical on the H_3VO_4 or O_2 , rather than H-abstraction, may produce more stable intermediates, $\text{C}_6\text{H}_{13}\text{VO}_4\text{H}_3$ and $\text{C}_6\text{H}_{13}\text{O}_2\cdot$ respectively, with high barriers for releasing 2-hexene and thereby enabling side-reaction channels, such as complete oxidation to undesired carbon oxides and production of oxygenates [60]. Table 1 shows the calculated adsorption energies of the $\cdot\text{C}_6\text{H}_{13}$ radical on to the O atoms in H_3VO_4 and O_2 as $\Delta E^\ddagger = -4.9$ (TS₈) and $+1.9$ kcal/mol (TS₉), and $\Delta E = -46.0$ (Int₃) and -28.6 kcal/mol (Int₄), respectively. Clearly, low barriers for both adsorption and H-abstraction processes coupled with large differences in the stabilities of the intermediates suggest that the adsorption and H-abstraction pathways are likely to be driven by thermodynamic terms. This may be the reason why, amongst other products, low yields of less than 20% for 1- and 2-hexene are obtained in our laboratory experiments.

Since the Int₁ fragment, HOVO_3H_3 , is not likely to be involved in the second H-abstraction, an accumulation of the OH groups on the surface is likely. Therefore, another pathway for H_2O formation through the coupling of adjacent surface OH groups is feasible, as also suggested by Hui *et al.* [54] in the production of propene through ODH of propane. We therefore investigated the interaction energetics between two adjacent HOVO_3H_3 species. This reaction step pertains to H-transfer from one HOVO_3H_3 species to another to produce H_2O , H_3VO_4 and H_3VO_3 and represents a disproportionation pathway from two V(IV) centres to produce V(III) and V(V) species, followed by reoxidation of the V(III) to V(V). We calculated an activation barrier with $\Delta E^\ddagger = +3.6$ kcal/mol (TS₁₀ – Figure 5) and $\Delta E = -5.9$ kcal/mol (Int₅) for this pathway and the stabilities of H_2O and H_3VO_4 that are produced indicate that the pathway is kinetically and thermodynamically favourable. Termination and reoxidation of H_3VO_3 to H_3VO_4 is likely to proceed via a Mars–van Krevelen mechanism. We explored separately the adsorption of “surface O” and O_2 on to the V(III) centre and calculated a barrier-less energy of activation, $\Delta E^\ddagger = -119.4$ kcal/mol (TS₁₁ – Figure 5) for the $\text{O}\cdot$ species (NBO atomic charge = -0.860 – Table 2) and $\Delta E = -239.7$ kcal/mol (P₇) for the formation of H_3VO_4 . However, we could not determine the TS for reoxidation with molecular O_2 . If the formation of 2-hexene proceeds through gas-phase H-abstraction by O_2 , then the termination step (Figure 2) may involve disproportionation of the produced hydroperoxyl radical to produce H_2O and O_2 , as recorded in Table 1 (TS₁₂ – TS₁₄) and our previous calculations [34].

We believe that future periodic-DFT calculations that we will engage in for this system with a variety of oxide supports will assist in the modifications of the kinetic and thermodynamic terms and as a result reveal the best oxide support for the vanadium oxide catalyst. This is likely because the support may modify the activity of the vanadia monolayer by changing the activation energy of the potentially rate-determining step and affect the selectivity of the active vanadia phase by favouring the formation of the alkene compared to the formation of oxygenated products [30]. The increased/decreased activity of the vanadia monolayer in H-abstraction is well explained by the increase of the chemical hardness above the vanadyl oxygen (increased proton affinity) and of the Lewis acidity of vanadium (increased electron affinity) upon deposition of the vanadia monolayer on the support [61], [62].

3.2 Temperature Effects

The laboratory experimental conditions with a temperature range of 573 to 773 K were included in modelling the reaction. Gibbs free energies of activation (ΔG^\ddagger) and Gibbs free energies (ΔG) were calculated for all the reaction pathways over the temperature range as indicated in Table 1.

For the rate-determining step (TS₁), ΔG^\ddagger increases as the temperature increases from 573 to 673 and 773 K. From the ΔG^\ddagger values and transition state theory, we calculated the corresponding rates (k) over the three temperatures and obtained the following results, $k(573) = 6.18 \times 10^{-4} \text{ s}^{-1}$, $k(673) = 1.87 \times 10^{-}$

$^2 \text{ s}^{-1}$ and $k(773) = 2.73 \times 10^{-1} \text{ s}^{-1}$. The calculated rate at 773 K is approximately three orders of magnitude and one order of magnitude greater than the values at 573 and 673 K, respectively. This indicates that the rate-determining step is kinetically more favourable at 773 K. A similar trend is observed in ΔG^\ddagger values for all the propagation pathways where the reactions become more faster as the temperature increases.

The lowest calculated ΔG value for the rate-determining step is +32.5 kcal/mol for the formation of Int₁ at 573 K. The ΔG values at 673 and 773 K are +34.3 and +36.0 kcal/mol, respectively. Our calculations from the attached supplementary material show that the enthalpy ($\Delta H = +22.0$ kcal/mol) and entropy magnitude ($T\Delta S = -10.5$ kcal/mol) contributions are lowest at 573 K and highest at 773 K ($\Delta H = +23.2$ and $T\Delta S = -12.8$ kcal/mol). Furthermore, at all temperatures the ΔH contributions to the ΔG values are the dominant factors and are approximately two (2) times the magnitude values of $T\Delta S$. Therefore, the formation of Int₁ in the rate-determining step is thermodynamically more favourable at 573 K. A similar trend is also observed in ΔG values for all the propagation pathways where the reactions are thermodynamically more stable at 573 K.

Hence, the formation of 1- and 2-hexene from activation of *n*-hexane by H-abstraction with surface H₃VO₄, followed by the second H-abstraction from either a different surface H₃VO₄ or from gas-phase O₂, is likely to be more kinetically more favourable at 773 K and thermodynamically more favourable at 573 K.

3.3 Natural Bond Orbital Analyses

NBO calculations [45], [46] were conducted on the selected TS of the most likely pathways at the B3LYP/6-311+G(d,p) level. Figure 6 displays the TSs and the associated highest occupied NBOs (HONBOs) representing the donor orbitals, and the lowest unoccupied NBOs (LUNBOs) representing acceptor orbitals. For each TS, the atomic charges of the interacting atoms, the NBOs and the largest stabilization energies are recorded in Table 2.

The rate-determining step (TS₁) is associated with the H-abstraction by vanadyl O from the H₃VO₄ unit and the corresponding donor orbital is the Lewis-type highest occupied NBO (HONBO) that is a C *s*(7.2%) *p*(92.8%) hybrid-type character. The acceptor orbital is the non-Lewis-type lowest unoccupied NBO (LUNBO) that is H *s*-type character. The spatial orientation of the two interacting species facilitates maximum overlap of the orbitals. The stabilization energy involved with the transfer of electron density is +272.4 kcal/mol, indicating a strong interaction between the two orbitals. The calculated atomic charges indicate a stronger interaction between the O (-0.512) and H (+0.324) as compared to C (-0.336) and H (+0.324). The pathway for the second H-abstraction through a different V site to produce 2-hexene (TS₃) has donor-acceptor orbital characters that are O *s*(79.7%) *p*(20.3%) nonbonding and H *s* and C *s*(18.6%) *p*(81.4%) antibonding. The stabilization energy is +4.86 kcal/mol and the charges on the interacting atoms are H (+0.327), C (-0.505) and O (-0.492). The donor and acceptor orbitals describing the propagation pathway barriers for the formation of 2-hexene (TS₄) through H-abstraction by gas-phase O₂ are the O *s*(13.3%) *p*(86.7%) nonbonding hybrid to the H *s* and C *s*(11.6%) *p*(88.4%) antibonding hybrid. The calculated energy is +45.9 kcal/mol. The distribution of atomic charges on interacting atoms follows the same trend with negative charges on C (-0.387) and O (-0.408) atoms and a positive charge on the H (+0.192) atom. Similar orbitals, atomic charges and comparable orbital stabilization energies were obtained for the 1-hexene pathways, as shown in Table 2 (TS₃ for 2-hexene and TS₆ for 1-hexene, TS₄ for 2-hexene and TS₇ for 1-hexene).

The donor-acceptor orbitals for the disproportionation pathway (H-transfer) of two HOVO₃H₃ to produce H₂O, H₃VO₃ and H₃VO₄ (TS₁₀) are O *s*(16.3%) *p*(83.7%) nonbonding hybrid and H *s* and O *s*(8.5%) *p*(91.5%) antibonding hybrid, respectively, with an energy of +35.4 kcal/mol. The positive charge is on the H atom (+0.500) and the charge on the O atom that releases the H atom is -0.650 and that on the O atom that receives the H atom is -0.926. Lastly, the calculated orbital stabilization energy for reoxidation of V(III) to V(V) through TS₁₁ is +1.87 kcal/mol. Examination of the total

electron distribution shows that there is also shift of electron density from three other O atoms in H_3VO_3 to the V atom. This facilitates the formation of a vanadyl bond in H_3VO_4 . The atomic charges on O and V atoms are -0.860 and +0.619, respectively.

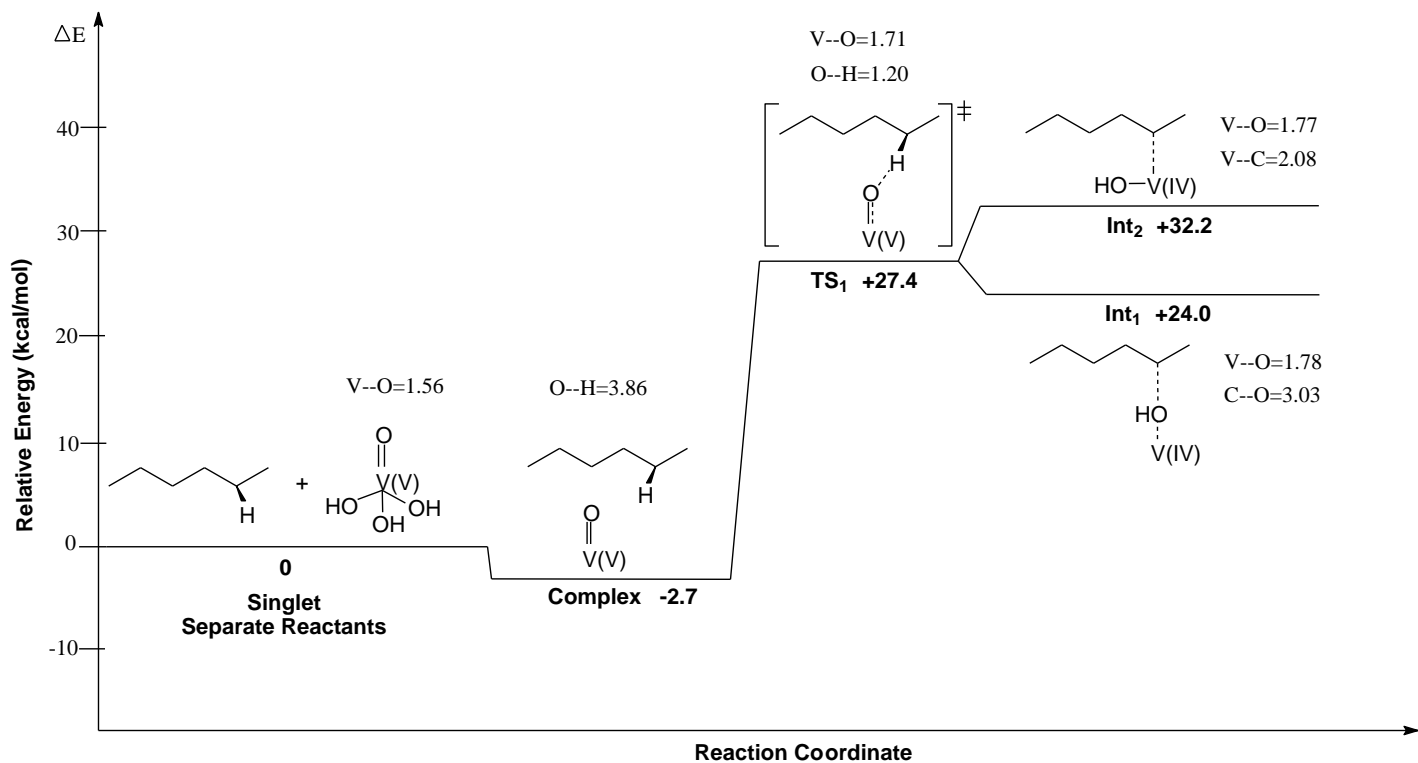


Figure 3 Zero-point corrected relative electronic energy (ΔE) diagram for activation of *n*-hexane over H_3VO_4 . B3LYP/6-311+g(d,p) for the C, O and H atoms, and Stuttgart ECPs for the V atom. The indicated bond distances are in Å. Cartesian coordinates of all TSs are provided as supplementary material.

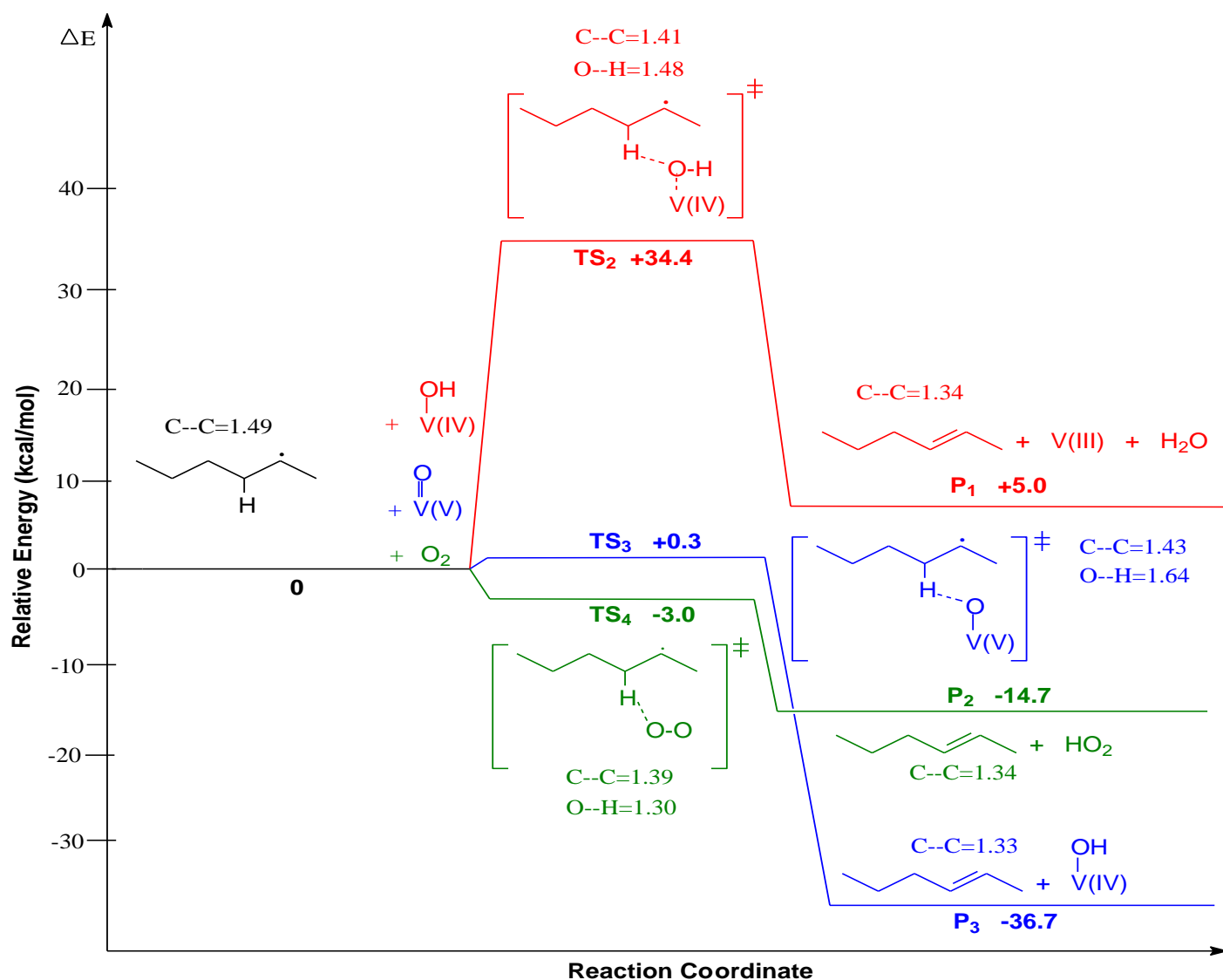


Figure 4 Zero-point corrected relative electronic energy (ΔE) diagram for propagation pathways for the formation of 2-hexene. The red colour indicate the kinetically unfavourable pathway for H-abstraction from $\cdot\text{C}_6\text{H}_{13}$ within Int_1 . The blue and green colours represent the kinetically and thermodynamically favourable pathways for H-abstraction from a different V(V) centre and gas-phase O_2 , respectively. B3LYP/6-311+g(d,p) for the C, O and H atoms, and Stuttgart ECPs for the V atom. The indicated bond distances are in Å. Cartesian coordinates of all TSs are provided as supplementary material.

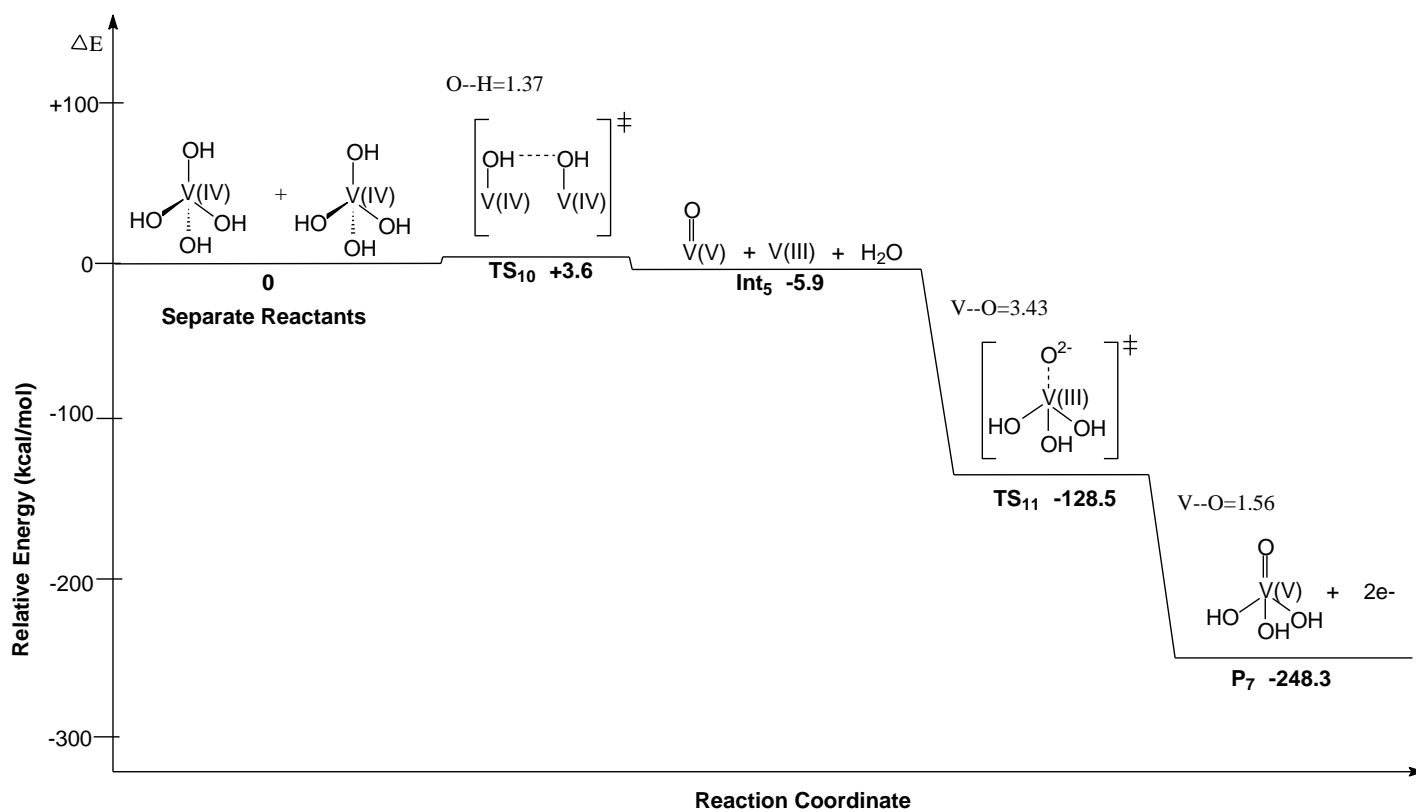


Figure 5 Zero-point corrected relative electronic energy (ΔE) diagram for disproportionation of two V(IV) centres to produce V(III) and V(V) centres, followed by reoxidation of V(III) to V(V) by O^{2-} . B3LYP/6-311+g(d,p) for the C, O and H atoms, and Stuttgart ECPs for the V atom. The indicated bond distances are in Å. Cartesian coordinates of all TSs are provided as supplementary material.

Table 1: Relative Energies (ΔE) and Gibbs Free Energies (ΔG) for the reaction of *n*-hexane with H_3VO_4 to produce 1- and 2-hexene^a. B3LYP/6-311+g(d,p) for the C, O and H atoms, and Stuttgart ECPs for the V atom. Cartesian coordinates of all TSs are provided as supplementary material.

Reaction Pathway	ΔE	ΔG		
		573	673	773
Initiation				
<i>s</i> -C ₆ H ₁₄ +H ₃ VO ₄	0	0	0	0
<i>s</i> -C ₆ H ₁₄ --H ₃ VO ₄ (TS ₁)	+27.4	+42.7	+45.8	+48.7
<i>s</i> -TS ₁ →C ₆ H ₁₃ -HO-VO ₃ H ₃ (Int ₁)	+24.0 (-3.4)	+32.5 (-10.2)	+34.3 (-11.5)	+31.0 (-17.7)
<i>s</i> -TS ₁ →C ₆ H ₁₃ -VO ₃ H ₃ -HO (Int ₂)	+32.2 (+4.8)	+51.9 (+9.2)	+55.7 (+9.9)	+59.4 (+10.7)
Propagation from Int₁				
<i>s</i> -C ₆ H ₁₃ -HO-VO ₃ H ₃	0	0	0	0
<i>s</i> -Int ₁ →C ₆ H ₁₃ -HO-VO ₃ H ₃ (TS ₂)	+34.4	+31.2	+30.8	+30.2
<i>s</i> -Int ₁ →C ₆ H ₁₃ -HO-VO ₃ H ₃ (TS ₅)	+40.3	+42.5	+42.9	+42.6
<i>s</i> -TS ₂ →C ₆ H ₁₂ +H ₃ VO ₃ +H ₂ O (P ₁)	+5.0 (-29.4)	-0.6 (-31.8)	-1.5 (-32.3)	-2.5 (-32.7)
<i>s</i> -TS ₅ →C ₆ H ₁₂ +H ₃ VO ₃ +H ₂ O (P ₄)	+24.3 (-16.0)	+17.2 (-25.3)	+16.2 (-26.7)	+14.7 (-27.9)
Propagation from separate H₃VO₄				
<i>d</i> -C ₆ H ₁₃ +H ₃ VO ₄	0	0	0	0
<i>d</i> -C ₆ H ₁₃ --H ₃ VO ₄ (TS ₃)	+0.3	+21.2	+25.2	+29.0
<i>d</i> -C ₆ H ₁₃ --H ₃ VO ₄ (TS ₆)	+0.8	+22.9	+25.9	+31.3
<i>d</i> -TS ₃ →C ₆ H ₁₂ +HOVO ₃ H ₃ (P ₃)	-36.7 (-37.0)	-20.2 (-41.4)	-17.1 (-42.3)	-13.8 (-42.8)
<i>d</i> -TS ₆ →C ₆ H ₁₂ +HOVO ₃ H ₃ (P ₆)	-30.8 (-31.6)	-17.2 (-40.1)	-14.5 (-40.4)	-11.8 (-43.1)
Propagation with O₂ – H abstraction				
<i>d</i> -C ₆ H ₁₃ +O ₂	0	0	0	0
<i>d</i> -C ₆ H ₁₃ --O ₂ (TS ₄)	-3.0	+19.7	+23.9	+28.1
<i>d</i> -C ₆ H ₁₃ --O ₂ (TS ₇)	-2.9	+20.0	+24.2	+28.4
<i>d</i> -TS ₄ →C ₆ H ₁₂ +HO ₂ (P ₂)	-14.7 (-11.7)	-0.6 (-20.3)	+0.7 (-23.2)	+4.8 (-23.3)
<i>d</i> -TS ₇ →C ₆ H ₁₂ +HO ₂ (P ₅)	-11.4 (-8.5)	+2.3 (-17.7)	+5.5 (-18.7)	+7.7 (-20.7)
C₆H₁₃ adsorption on H₃VO₄ and O₂				
<i>d</i> -C ₆ H ₁₃ +H ₃ VO ₄ or O ₂	0	0	0	0
<i>d</i> -C ₆ H ₁₃ --H ₃ VO ₄ (TS ₈)	-4.9	+15.5	+17.8	+19.5
<i>d</i> -TS ₈ →C ₆ H ₁₃ VO ₄ H ₃ (Int ₃)	-46.0 (-41.1)	-14.0 (-29.5)	-16.4 (-34.2)	-18.0 (-37.5)
<i>d</i> -C ₆ H ₁₃ --O ₂ (TS ₉)	+2.6	+37.9	+29.3	+48.0
<i>d</i> -TS ₉ →C ₆ H ₁₃ O ₂ (Int ₄)	-30.2 (-32.8)	-6.7 (-44.6)	-2.4 (-31.7)	+2.0 (-46.0)
Propagation involving 2HOVO₃H₃				
<i>s</i> -HOVO ₃ H ₃ +HOVO ₃ H ₃	0	0	0	0
<i>s</i> -HOVO ₃ H ₃ --HOVO ₃ H ₃ (TS ₁₀)	+3.6	+25.2	+29.2	+33.3
<i>s</i> -TS ₁₀ →H ₃ VO ₃ +H ₃ VO ₄ +H ₂ O (Int ₅)	-5.9 (-9.5)	+12.2 (-13.0)	+15.6 (-13.6)	+19.0 (-14.3)
Reoxidation of H₃VO₃ to H₃VO₄				
<i>t</i> -H ₃ VO ₃ +“surface O”	0	0	0	0
<i>t</i> -H ₃ VO ₃ --“surface O” (TS ₁₁)	-119.4	-96.1	-52.2	-109.1
<i>t</i> -TS ₁₁ →H ₃ VO ₄ (P ₇)	-239.7 (-120.3)	-220.2 (-124.1)	-216.5 (-164.3)	-213.0 (-103.9)
Termination				
<i>s</i> -HO ₂ +HO ₂	0	0	0	0
<i>s</i> -HO ₂ --HO ₂ (TS ₁₂)	-2.3	+4.9	+5.8	+6.7
<i>s</i> -TS ₁₂ →2HO+O ₂ (Int ₆)	-21.1 (-18.8)	-23.4 (-28.3)	-24.1 (-29.9)	-24.9 (-31.6)
<i>t</i> -HO--HO (TS ₁₃)	-4.7	+8.5	+11.0	+13.6
<i>t</i> -TS ₁₃ →H ₂ O+O (Int ₇)	-13.0 (-8.3)	-3.2 (-11.7)	-1.3 (-12.3)	+0.7 (-12.9)
<i>t</i> -O--O (TS ₁₄)	-2.1	+10.7	+13.1	+15.6
<i>t</i> -TS ₁₄ →O ₂ (P ₈)	-117.8 (-115.7)	-104.2 (-114.9)	-101.6 (-114.7)	-99.0 (-114.6)

^a ΔE and ΔG are zero-point corrected electronic energy and Gibbs free energy at standard pressure, relative to separate reactants respectively, in kcal/mol. The energies in parentheses are for the indicated reaction pathways. The temperature is in K and ΔE values are at 673K. Prefixes *s*-, *d*- and *t*- indicate singlet, doublet and triplet states, respectively.

Table 2: Selected NBO atomic charges, HONBO and LUNBO orbital types, and orbital energies for the TSs of the *n*-hexane to 1- and 2-hexene pathways. B3LYP/6-311+g(d,p) for all the atoms. Cartesian coordinates of all TSs are provided as supplementary material.

TS	Atomic charges on interacting atoms	HONBO type (donor)	LUNBO type (donor)	Stabilization Energy (kcal/mol)
1	C = -0.336 H = +0.324 O = -0.512	C <i>s</i> (7.2%) <i>p</i> (92.8%) nonbonding hybrid	H <i>s</i> -type antibonding	+272.4
3 (2-hexene)	C = -0.505 H = +0.327 O = -0.492	O <i>s</i> (79.9%) <i>p</i> (20.3%) nonbonding hybrid	H <i>s</i> and C <i>s</i> (18.6%) <i>p</i> (81.4%) antibonding hybrid	+4.86
4 (2-hexene)	C = -0.387 H = +0.192 O = -0.408	O <i>s</i> (13.3%) <i>p</i> (86.7%) nonbonding hybrid	H <i>s</i> and C <i>s</i> (13.0%) <i>p</i> (87.0%) antibonding hybrid	+45.9
6 (1-hexene)	C = -0.684 H = +0.324 O = -0.491	O <i>s</i> (80.0%) <i>p</i> (20.0%) nonbonding hybrid	H <i>s</i> and C <i>s</i> (20.7%) <i>p</i> (79.3%) antibonding hybrid	+7.86
7 (1-hexene)	C = -0.478 H = +0.360 O = -0.225	O <i>s</i> (13.1%) <i>p</i> (86.9%) nonbonding hybrid	H <i>s</i> and C <i>s</i> (11.6%) <i>p</i> (88.4%) antibonding hybrid	+42.1
10	O = -0.926 H = +0.500 O = -0.650	O <i>s</i> (16.3%) <i>p</i> (83.7%) nonbonding hybrid	H <i>s</i> and O <i>s</i> (8.5%) <i>p</i> (91.5%) antibonding hybrid	+35.4
11	O = -0.860 V = +0.619	O <i>s</i> (7.9%) <i>p</i> (92.1%) nonbonding	V <i>s</i> (12.1%) <i>p</i> (83.9%) <i>d</i> (4.0%) antibonding hybrid	+1.87

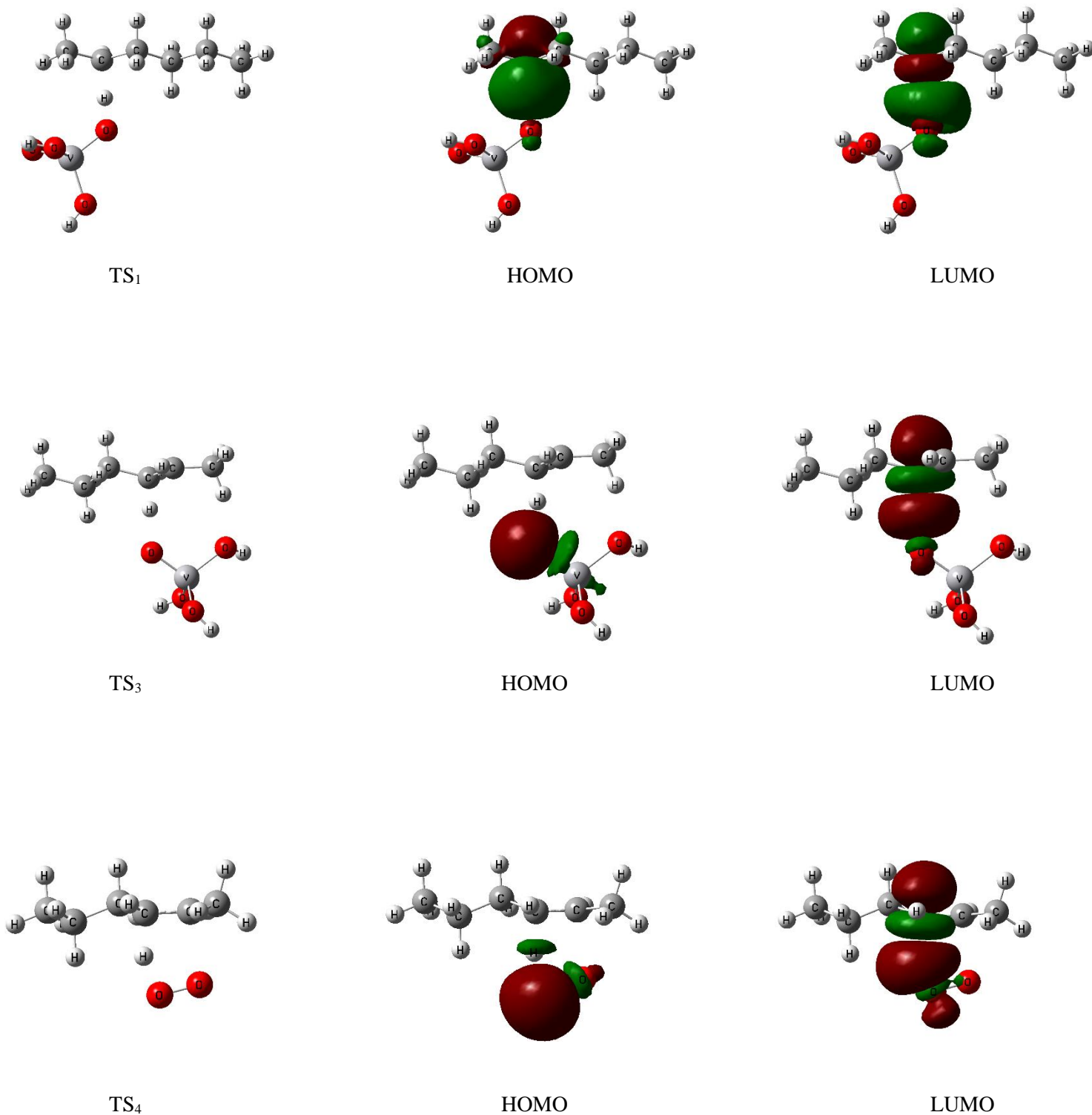


Figure 6 Selected TS structures and the NBO calculated frontier orbitals for the likely mechanistic pathway for the formation of 2-hexene. The orbital lobes are oriented for better clarity in each case and correspond to the reaction coordinate. B3LYP/6-311+g(d,p) for all the atoms. Cartesian coordinates of all TSs are provided as supplementary material.

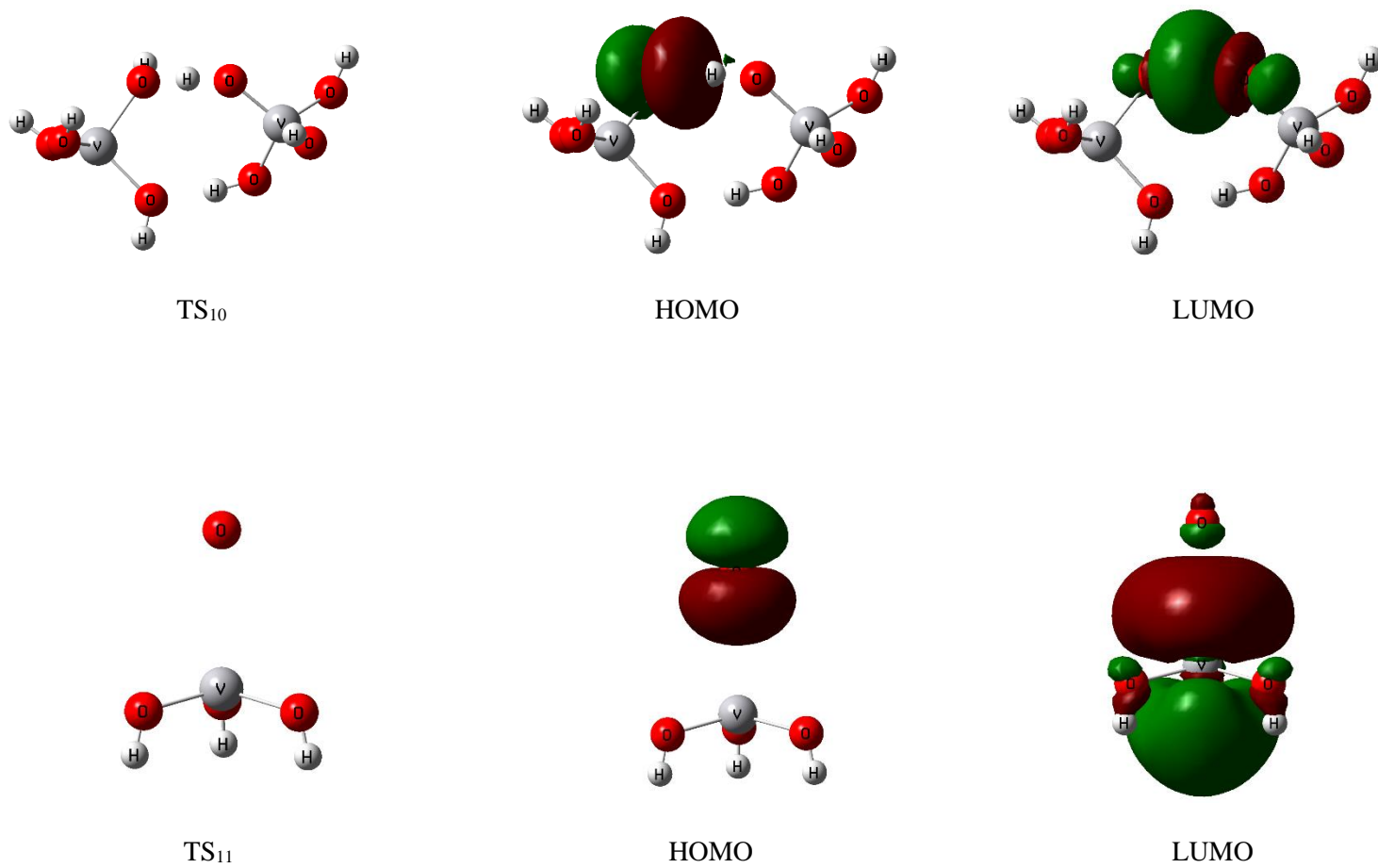


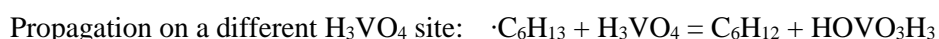
Figure 6 Continuing, Selected TS structures and the NBO calculated frontier orbitals for the likely mechanistic pathway for the formation of 2-hexene. The orbital lobes are oriented for better clarity in each case and correspond to the reaction coordinate. B3LYP/6-311+g(d,p) for all the atoms. Cartesian coordinates of all TSs are provided as supplementary material.

4 Conclusions

DFT methods have been used to investigate the activity of the tetrahedral monomeric H_3VO_4 structure for *n*-hexane ODH. We propose the following kinetically and thermodynamically favourable mechanistic pathways for the reaction,



n-hexane, H_3VO_4 and O_2 are the only species present initially. The rate-determining step is β -H abstraction from *n*-hexane by vanadyl O in H_3VO_4 to produce the $\cdot\text{C}_6\text{H}_{13} + \text{HOVO}_3\text{H}_3$ complex intermediate. This step has a barrier of $\Delta E^\ddagger = +27.4$ kcal/mol (TS₁). This activation energy is lower than β -H abstraction by O_2 ($\Delta E^\ddagger = +42.4$ kcal/mol) obtained in our previous work on gas-phase ODH. The intermediate stabilizes with $\Delta E = -3.4$ kcal/mol, relative to the transition state (Figure 3).



The second γ -H abstraction from the $\cdot\text{C}_6\text{H}_{13}$ radical produces 2-hexene and the second HOVO_3H_3 species. This step has $\Delta E^\ddagger = +0.3$ kcal/mol (TS₃) and the products stabilize to $\Delta E = -33.5$ kcal/mol, relative to separate reactants. The ΔE^\ddagger and ΔE values suggests that the formation of 2-hexene is likely to proceed on a different H_3VO_4 site. This is because we calculated higher activation barriers ($\Delta E^\ddagger > 30$ kcal/mol) for the abstraction of the second H atom on the same V site as abstraction of the first H atom (Figure 4).

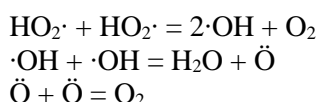


In competition with the previous pathway for the second γ -H abstraction from the $\cdot\text{C}_6\text{H}_{13}$ radical, is the likely involvement of gas-phase O_2 , with the products being 2-hexene and the $\text{HO}_2\cdot$ radical. This is a barrier-less step with $\Delta E^\ddagger = -3.0$ kcal/mol (TS₄) and $\Delta E = -14.7$ kcal/mol, relative to separate reactants (Figure 4).

Both the propagation pathways may lead to 2-hexene. The chosen pathway is likely to depend on the relative amount of gas-phase O_2 and the surface area of H_3VO_4 sites at any given time.



If the formation of 2-hexene is achieved through propagation on a different H_3VO_4 site, to also produce the HOVO_3H_3 species, then disproportionation of the two HOVO_3H_3 species would follow. This step has a barrier with $\Delta E^\ddagger = +3.6$ kcal/mol (TS₁₀) and a stabilization energy of $\Delta E = -9.5$ kcal/mol, relative to TS, for the formation of the products (Figure 5).



The reoxidation of V(III) to V(V) with “surface O” (NBO atomic charge = -0.860) is achieved through a barrier-less height with $\Delta E^\ddagger = -119.4$ kcal/mol (TS₁₁) and the produced H_3VO_4 stabilization energy of $\Delta E = -120.3$ kcal/mol, relative to TS. If the formation of 2-hexene is achieved through propagation by gas-phase O_2 , then the produced $\text{HO}_2\cdot$ radicals disproportionate stepwise to produce O_2 and H_2O with barrier-less energies of $\Delta E^\ddagger = -2.3$ (TS₁₂), -4.7 (TS₁₃) and -2.1 kcal/mol (TS₁₄). The associated values of ΔE are -21.1 , -13.0 and -117.8 kcal/mol, relative to separate reactants, respectively (Table 1).

Acknowledgments

This work was supported by the NRF, SASOL and Johnsson Matthey. We would like to thank the Centre for High Performance Computing (CHPC) in Cape Town, South Africa, for providing the computational resources necessary to conduct this work.

References

- [1] F. Ogliaro, N. Harris, S. Cohen, M. Filatov, S.P. De Visser, S. Shaik, **A model 'rebound' mechanism of hydroxylation by cytochrome P450: Stepwise and effectively concerted pathways, and their reactivity patterns**, *J. Am. Chem. Soc.* 122 (2000) 8977-8989.
- [2] D.K. Bohme, H. Schwarz, **Gas-phase catalysis by atomic and cluster metal ions: the ultimate single-site catalysts**, *Angew. Chem. Int. Ed.* 44 (2005) 2336-2354.
- [3] K.A. Zemski, D.R. Justes, R.C. Bell, A.W. Castleman, **Reactions of niobium and tantalum oxide cluster cations and anions with *n*-butane**, *J. Phys. Chem. A* 105 (2001) 4410-4417.
- [4] I.P. Belomestnykh, E.A. Skrigan, N.N. Rozhdestvenskaya, G.V. Isaguliants, **New preparation methods of multicomponent oxide vanadium systems for oxidative dehydrogenation of alkanes, alkylaromatic and alkylheterocyclic compounds**, *Stud. Surf. Sci. Catal.* 72 (1992) 453-460.
- [5] H. Kung, M. Kung, **Oxidative dehydrogenation of alkanes over vanadium-magnesium-oxides**, *Appl. Catal., A* 157 (1997) 105-116.
- [6] J. Dobler, M. Pritzsche, J. Sauer, **Oxidation of methanol to formaldehyde on supported vanadium oxide catalysts compared to gas phase molecules**, *J. Am. Chem. Soc.* 127 (2005) 10861-10868.
- [7] A. Goodrow, A.T. Bell, **A theoretical investigation of the selective oxidation of methanol to formaldehyde on isolated vanadate species supported on silica**, *J. Phys. Chem. C* 111 (2007) 14753-14761.
- [8] E.A. Elkhalfi, H.B. Friedrich, **Oxidative dehydrogenation of *n*-octane using vanadium-magnesium oxide catalysts with different vanadium loadings**, *Appl. Catal. A* 373 (2010) 122-131.
- [9] N.U. Zhanpeisov, **A density functional theory study of the oxidation of methanol to formaldehyde over vanadia supported on silica, titania and zirconia**, *Res. Chem. Intermed.* 30 (2004) 133-141.
- [10] J.L. Bronkema, D.C. Leo, A.T. Bell, **Mechanistic studies of methanol oxidation to formaldehyde on isolated vanadate sites supported on high surface area anatase**, *J. Phys. Chem. C* 111 (2007) 14530-14540.
- [11] L. Burcham, L. Briand, I. Wachs, **Quantification of active sites for the determination of methanol oxidation turn-over frequencies using methanol chemisorption and in situ infrared techniques. 1. Supported metal oxide catalysts**, *Langmuir* 17 (2001) 6164-6174.
- [12] X. Rozanska, R. Fortrie, J. Sauer, **Size-dependent catalytic activity of supported vanadium oxide species: Oxidative dehydrogenation of propane**, *J. Am. Chem. Soc.* 136 (2014) 7751-7761.

- [13] X. Rozanska, E.V. Kondratenko, J. Sauer, **Oxidative dehydrogenation of propane: Differences between N₂O and O₂ in the reoxidation of reduced vanadia sites and consequences for selectivity**, *J. Catal.* 256 (2008) 84-94.
- [14] M.M. Islam, D. Costa, M. Calatayud, F. Tielens, **Characterization of supported vanadium oxide species on silica: A periodic DFT investigation**, *J. Phys. Chem. C* 113 (2009) 10740–10746.
- [15] K. Tamara, S. Yoshida, S. Ishida, H. Kakioka, **Spectroscopic studies of catalysis by vanadium pentoxide**, *Bull. Chem. Soc. Jpn.* 41 (1968) 2840-2845.
- [16] C.L. Pieck, M.A. Bañares, J.L.G. Fierro, **Propane oxidative dehydrogenation on VO_x/ZrO₂ catalysts**, *J. Catal.* 224 (2004) 1-7.
- [17] H. Kung, **Oxidative dehydrogenation of light (C₂ to C₄) alkanes**, *Adv. Catal.* 40 (1994) 1-38.
- [18] T. Balsko, J.M. Lopez-Nieto, **Oxidative dehydrogenation of short chain alkanes on supported vanadium oxide catalysts**, *Appl. Catal., A* 157 (1997) 117-142.
- [19] S. Sugiyama, Y. Iozuka, E. Nitta, H. Hayashi, J.B. Moffat, **Role of tetrachloromethane as a gas-phase additive in the oxidative dehydrogenation of propane over cerium oxide**, *J. Catal.* 189 (2000) 233-237.
- [20] F. Arena, F. Frusteri, A. Parmaliana, G. Martra, S. Coluccia, **Oxidative dehydrogenation of propane on supported V₂O₅ catalysts: Role of redox and acid-base properties**, *Stud. Surf. Sci. Catal.* 119 (1998) 665-670.
- [21] Y.M. Liu, Y. Cao, N. Yi, W.L. Feng, W.L. Dai, S.R. Yan, H.Y. He, K.N. Fan, **Vanadium oxide supported on mesoporous SBA-15 as highly selective catalysts in the oxidative dehydrogenation of propane**, *J. Catal.* 224 (2004) 417-428.
- [22] E.A. Elkhalfifa, H.B. Friedrich, **On the effect of hydrocarbon/oxygen ratios during the dehydrogenation of n-octane over a VMgO catalyst**, *Catal. Lett.* 141 (2011) 554-564.
- [23] F. Cavani, F. Trifiro, **Selective oxidation of light alkanes: Interaction between the catalyst and the gas phase on different classes of catalytic materials**, *Catal. Today* 51 (1999) 561-580.
- [24] P. Mars, D.W. van Krevelen, **Oxidations carried out by means of vanadium oxide catalysts**, *Chem. Eng. Sci.* 3 (1954) 41-59.
- [25] A. Andersson, **An oxidized surface state model of vanadium oxides and its application to catalysis**, *J. Solid State Chem.* 42 (1982) 263-275.
- [26] K. Mori, A. Miyamoto, Y. Murakami, **Catalytic reactions on well-characterized vanadium oxide catalysts. 4. Oxidation of butane**, *J. Phys. Chem.* 89 (1985) 4265-4269.
- [27] S.T. Oyama, **Adsorbate bonding and the selection of partial and total oxidation pathways**, *J. Catal.* 128 (1991) 210-217.
- [28] K.D. Chen, A.T. Bell, E. Iglesia, **The Relationship between the electronic and redox properties of dispersed metal oxides and their turnover rates in oxidative dehydrogenation reactions**, *J. Catal.* 209 (2002) 35-42.

- [29] Y. Liu, Z. Geng, Y. Wang, J. Liu, X. Hou, **DFT studies for activation of C-H bond in methane by gas-phase Rh_n^+ ($n = 1-3$)**, *Comput. Theor. Chem.* 1015 (2013) 52-63.
- [30] K. Alexopoulos, M. Reyniers, G.B. Marin, **Reaction path analysis of propane selective oxidation over V_2O_5 and V_2O_5/TiO_2** , *J. Catal.* 289 (2012) 127-139.
- [31] E. Kurnaz, M.F. Fellah, I. Onal, **A density functional theory study of C-H bond activation of methane on a bridge site of M-O-M-ZSM-5 Clusters (M = Au, Ag, Fe and Cu)**, *Microporous Mesoporous Mater.* 138 (2011) 68-74.
- [32] L. Gracia, P. González-Navarrete, M. Calatayud, J. Andrés, **A DFT study of methanol dissociation on isolated vanadate groups**, *Catal. Today* 139 (2008) 214-220.
- [33] L. Cheng, G.A. Ferguson, S.A. Zygmunt, L.A. Curtiss, **Structure-activity relationships for propane oxidative dehydrogenation by anatase-supported vanadium oxide monomers and dimers**, *J. Catal.* 302 (2013) 31-36.
- [34] N.E. Damoyi, H.B. Friedrich, H.G. Kruger, D. Willock, **Density functional theory studies of the uncatalysed gas-phase oxidative dehydrogenation conversion of n -hexane to hexenes**, *Comput. Theor. Chem.* 1114 (2017) 153-164.
- [35] M.J. Frisch, G.W. Trucks, H.B. Schlegel, G.E. Scuseria, M.A. Robb, J.R. Cheeseman, G. Scalmani, V. Barone, B. Mennucci, G.A. Petersson, H. Nakatsuji, M. Caricato, X. Li, H.P. Hratchian, A.F. Izmaylov, J. Bloino, G. Zheng, J.L. Sonnenberg, M. Hada, M. Ehara, K. Toyota, R. Fukuda, J. Hasegawa, M. Ishida, T. Nakajima, Y. Honda, O. Kitao, H. Nakai, T. Vreven, J. Montgomery, J. A., J.E. Peralta, F. Ogliaro, M. Bearpark, J.J. Heyd, E. Brothers, K.N. Kudin, V.N. Staroverov, R. Kobayashi, J. Normand, K. Raghavachari, A. Rendell, J.C. Burant, S.S. Iyengar, J. Tomasi, M. Cossi, N. Rega, N.J. Millam, M. Klene, J.E. Knox, J.B. Cross, V. Bakken, C. Adamo, J. Jaramillo, R. Gomperts, R.E. Stratmann, O. Yazyev, A.J. Austin, R. Cammi, C. Pomelli, J.W. Ochterski, R.L. Martin, K. Morokuma, V.G. Zakrzewski, G.A. Voth, P. Salvador, J.J. Dannenberg, S. Dapprich, A.D. Daniels, Ö. Farkas, J.B. Foresman, J.V. Ortiz, J. Cioslowski, D.J. Fox, **Gaussian 09, Revision B.01**, Gaussian, Inc., Wallingford, 2010.
- [36] A.D. Becke, **Density functional thermochemistry III - The role of exact exchange**, *J. Chem. Phys.* 98 (1993) 5648-5652.
- [37] C. Lee, W. Yang, R.G. Parr, **Development of the Colle-Salvetti correlation energy formula into a functional of the electron density**, *Phys. Rev. B: Condens. Matter* 37 (1988) 785-789.
- [38] J. Oxgaard, R.A. Periana, W.A. Goddard, **Mechanistic analysis of hydroarylation catalysts**, *J. Am. Chem. Soc.* 126 (2004) 11658-11665.
- [39] D. Benitez, W.A. Goddard, **The isomerization equilibrium between cis and trans chloride ruthenium olefin metathesis catalysts from quantum mechanics calculations**, *J. Am. Chem. Soc.* 127 (2005) 12218-12219.
- [40] J.A. Keith, J. Oxgaard, W.A. Goddard, **Inaccessibility of beta-hydride elimination from -OH functional groups in Wacker-type oxidation**, *J. Am. Chem. Soc.* 128 (2006) 3132-3133.
- [41] M. Dolg, U. Wedig, H. Stoll, H. Preuss, **Energy-adjusted ab initio pseudopotentials for the first row transition elements**, *J. Chem. Phys.* 86 (1987) 866-872.

- [42] J.M.L. Martin, A. Sundermann, **Correlation consistent valence basis sets for use with the Stuttgart-Dresden-Bonn relativistic effective core potentials: The atoms Ga-Kr and In-Xe**, J. Chem. Phys. 114 (2001) 3408-3420.
- [43] C. Gonzales, H.B. Schlegel, **An improved algorithm for reaction path following**, J. Chem. Phys. 90 (1989) 2154-2161.
- [44] C. Gonzales, H.B. Schlegel, **Reaction path following in mass-weighted internal coordinates**, J. Phys. Chem. 94 (1990) 5523-5527.
- [45] J.E. Carpenter, F. Weinhold, **Analysis of the geometry of the hydroxymethyl radical by the "different hybrids for different spins" natural bond orbital procedure**, J. Mol. Struct. THEOCHEM 169 (1988) 41-62.
- [46] J.E. Carpenter, F. Weinhold, **The natural bond orbital Lewis structure concept for molecules, radicals, and radical ions**, in: R. Naaman, Z. Vager (Eds.), The structure of small molecules and ions, Plenum, N.Y., 1988, pp. 227-236.
- [47] J. Chetty, V.D.B.C. Dasireddy, S. Singh, H.B. Friedrich, **The oxidative aromatization of *n*-hexane over VMgO catalysts**, *Reac. Kinet. Mech. Catal.* 120 (2017) 307-321.
- [48] H. Hoog, J. Herheus, F.J. Zuiderweg, **Investigations into the cyclisation (aromatisation) of aliphatic hydrocarbons**, *Trans. Faraday Soc.* 35 (1939) 993-1006.
- [49] X. Rozanska, R. Fortrie, J. Sauer, **Oxidative dehydrogenation of propane by monomeric vanadium oxide sites on silica support**, *J. Phys. Chem. C* 111 (2007) 6041-6050.
- [50] M. Cheng, K. Chenoweth, J. Oxgaard, A. van Duin, W. Goddard, **Single-site vanadyl activation, functionalization, and reoxidation reaction mechanism for propane oxidative dehydrogenation on the cubic V₄O₁₀ cluster**, *J. Phys. Chem. C* 111 (2007) 5115-5127.
- [51] K.D. Chen, A.T. Bell, E. Iglesia, **Kinetic isotopic effects in oxidative dehydrogenation of propane on vanadium oxide catalysts**, *J. Catal.* 192 (2000) 197-203.
- [52] M.D. Argyle, K. Chen, E. Iglesia, A.T. Bell, **Effect of catalyst structure on oxidative dehydrogenation of ethane and propane on alumina-supported vanadia**, *J. Catal.* 208 (2002) 139-149.
- [53] L. Gracia, P. González-Navarrete, M. Calatayud, J. Andrés, **A DFT study of methanol dissociation on isolated vanadate groups**, *Catal. Today* 139 (2008) 214-220.
- [54] K. Tamara, S. Yoshida, S. Ishida, H. Kakioka, **Spectroscopic studies of catalysis by vanadium pentoxide**, *Bull. Chem. Soc. Jpn.* 41 (1968) 2840-2845.
- [55] J.G. Eon, R. Olier, J.C. Volta, **Oxidative dehydrogenation of propane on γ -Al₂O₃ supported vanadium oxides**, *J. Catal.* 145 (1994) 318-326.
- [56] K. Devriendt, H. Poelman, L. Fiermans, G. Creten, G.F. Froment, **Angular resolved XPS applied to V₂O₅-based catalysts**, *Surf. Sci.* 352-354 (1996) 750-754.
- [57] F. Hui, L. Zhi-Pan, L. Zhen-Hua, W. Wen-Ning, F. Kang-Nian, **Periodic density functional theory study of propane oxidative dehydrogenation over V₂O₅(001) surface**, *J. Am. Chem. Soc.* 128 (2006) 11114-11123.

- [58] J. Sauer, J. Döbler, **Structure and reactivity of V₂O₅: Bulk solid, nanosized clusters, species supported on silica and alumina, cluster cations and anions**, Dalton Trans. (2004) 3116-3121.
- [59] M.D. Argyle, K.D. Chen, A.T. Bell, E. Iglesia, **Ethane oxidative dehydrogenation pathways on vanadium oxide catalysts**, J. Phys. Chem. B 106 (2002) 5421-5427.
- [60] M. D. Argyle, K. Chen, C. Resini, C. Krebs, A. T. Bell, E. Iglesia, **Extent of reduction of vanadium oxides during catalytic oxidation of alkanes measured by in-situ UV-Visible spectroscopy**, J. Phys. Chem. B 108 (2004) 2345-2353.
- [61] K. Alexopoulos, P. Hejduk, M. Witko, M.-F. Reyniers, G.B. Marin, **Theoretical study of the effect of (001) TiO₂ anatase support on V₂O₅**, J. Phys. Chem. C 114 (2010) 3115-3130.
- [62] M. Calatayud, F. Tielens, F. De Proft, **Reactivity of gas-phase, crystal and supported V₂O₅ systems studied using density functional theory based reactivity indices**, Chem. Phys. Lett. 456 (2008) 59-63.

CHAPTER 4

A Density Functional Theory Study of the Catalytic ODH of *n*-Hexane Over Isolated H₄V₂O₇

N.E. Damoyi^{a,*}, H.B. Friedrich^b, H.G. Kruger^c and D. Willock^d

^aDepartment of Chemistry, Mangosuthu University of Technology, Box 12363, Jacobs, 4026, South Africa,

^bSchool of Chemistry, University of KwaZulu Natal, Westville Campus, Private Bag X 54001, Durban, 4000, South Africa

^cCatalysis and Peptide Research Unit, School of Pharmacy, University of KwaZulu Natal, Westville Campus, Private Bag X 54001, Durban, 4000, South Africa

^dSchool of Chemistry, Cardiff University, Park Place, Cardiff CF10 3AT, Wales, UK

Keywords: DFT, ODH, *n*-hexane, RDS, mechanism.

ABSTRACT

The catalytic oxidative dehydrogenation (ODH) of *n*-hexane over isolated H₄V₂O₇ clusters is analysed using density functional theory (DFT) methods. The ODH pathways that lead to 1- and 2-hexene were investigated. The 3-hexene pathway was omitted because it has not been reported in literature and was not characterised as one of the products in our laboratory experiments. All structures on the potential energy surfaces were optimized using the GAUSSIAN 09W program, at the B3LYP level, with the 6-311+g(d,p) basis set for C, O and H atoms and effective core potentials (ECPs) for the V atom. The laboratory experimental conditions of 573, 673 and 773K were included in computations. The chosen model for the study was the isolated H₄V₂O₇ cluster with two vanadyl bonds, V(V)=O, and the bridging O atom in the V(V)-O-V(V) unit. The rate-determining step (RDS) is preferentially associated with *n*-hexane interaction with H₄V₂O₇ through a secondary C-H bond activation via a direct H-abstraction by vanadyl O ($\Delta E^\ddagger = +32.7$ kcal/mol) rather than by the bridging O in the V(V)-O-V(V) unit ($\Delta E^\ddagger = +43.9$ kcal/mol). Both these values are higher than the one we calculated for the same reaction with the H₃VO₄ cluster ($\Delta E^\ddagger = +27.4$ kcal/mol) in our previous studies. The propagation pathways that lead to 2-hexene may involve the second γ -hydrogen abstraction by either the vanadyl O on a different active V(V)=O site or by gas-phase molecular O₂, depending on the relative V(V)=O active site surface area and *n*-hexane to oxygen ratios. The low yields of 1- and 2-hexene (< 20%) obtained in our laboratory experiments may be as a result of chemisorption properties of the radical intermediate ($\cdot\text{C}_6\text{H}_{13}$) on bridging or terminal O sites, leading to undesired products including oxygenates. The ODH process proceeds via a Mars–van Krevelen redox mechanism. The most energetically favourable pathways have been determined from the calculated ΔE^\ddagger , ΔE , ΔG^\ddagger and ΔG values and the catalytic mechanism that is likely to be followed has been proposed.

* Corresponding author e-mail address: damoyi@mut.ac.za

1 Introduction

The research studies of heterogeneous catalysis and surface science have long been producing qualitative and quantitative information from almost exclusively sophisticated experimental techniques [1-4]. However, quantum chemical calculations, including Density Functional Theory (DFT) methods, have emerged as key in the quest to understand catalytic processes and related mechanisms by determining the nature of the active sites and also link the atomic scale structure with the catalytic performance [5], [6].

Olefins are fundamental raw materials for many industrial processes such as the production of polypropylene, acrylonitrile and propylene oxide [7]. Since non-oxidative dehydrogenation of alkanes is an endothermic and therefore energy intensive process, it suffers from low alkene yields due to catalyst coking; whereas the alternative ODH is exothermic as a result of the formation of water, and does not lead to the formation of coke [8]. Presently, the main drawback in industrial processes for ODH of short alkanes is low selectivity to the desired alkenes, because the products are prone to total oxidation by the catalysts [9]. Therefore, a lot of present research in ODH of alkanes focuses on finding good catalysts with high selectivity to alkenes. Supported vanadium oxides are one of the best catalysts for the ODH of propane [10-13]. It is well known that, depending on the method of preparation, the vanadium surface may comprise three types of lattice oxygens, namely, (i) the singly coordinated vanadyl O, (ii) the two-coordinated bridging O, and (iii) the three-coordinated bridging O [14]. The location and structure of the reactive metal site is very important, in particular for understanding the mechanism of such active metal sites with reactants and intermediates on a molecular level [15]. A variety of authors [16-18] have proposed the involvement of vanadyl O as critical in hydrocarbon oxidation reactions, while others have mentioned the bridging O sites [19], [20]. However, the C-H bond activation on the three-coordinated bridging O site is the least possible, apparently because it is the most inert, as also reported in previous literature [21]. Hui *et al.* [14], also compared the reducibilities of the three differently coordinated O atoms, and found the largest reducibility on the singly coordinated vanadyl O. They concluded that the singly coordinated vanadyl O is the most active and it possesses the strongest electrophilic tendency, while the three-coordinated bridging O is the least active. The rate-determining step for C-H activation of propane has been proposed as the hydrogen abstraction by vanadyl O to form an isopropyl radical as an intermediate in the gas phase [22], [23]. In our previous studies of gas-phase activation of *n*-hexane by isolated H_3VO_4 species, we similarly proposed the rate-determining step as β -hydrogen abstraction by vanadyl O to form the hexyl radical and the reduced V(IV) species [24]. We will also show in this paper that the vanadyl O, rather than the two-coordinated bridging O, is key in C-H activation of *n*-hexane by isolated V_2O_7 species. Earlier experimental studies indicate that the selective oxidation of propane on vanadium oxides proceeds via a Mars-van Krevelen redox mechanism that involves the reduction of the metal oxide surface by the alkane with the formation of the alkene and water, followed by reoxidation of the surface through gas-phase oxygen [25].

The aim of this study was to investigate and compare C-H bond activation of *n*-hexane by vanadyl and bridging O atoms in isolated V_2O_7 species, and characterise the possible intermediates that may lead to 1- and 2-hexene, by means of DFT calculations as implemented in Gaussian 09. The relative energy changes (ΔE^\ddagger , ΔE , ΔG^\ddagger , ΔG) calculations were performed for determination of the likely mechanistic pathway for the reaction.

2 Theoretical Methodology

2.1 Computational Details

DFT calculations were carried out under laboratory experimental conditions of 573, 673 and 773 K using the GAUSSIAN 09W program [26] installed on a cluster based at the Centre for High Performance Computing (CHPC) in Cape Town, South Africa. The B3LYP hybrid correlation functional [27], [28] and 6-311+g(d,p) basis set were employed for C, O and H atoms and the V atom was described using the relativistic Stuttgart effective core potentials (ECPs) [29], [30]. The relaxed potential energy surface (PES) scans were utilised to get good initial structures for the transition states determinations. Intrinsic reaction coordinate (IRC) calculations, from the algorithm developed by Gonzàlez and Schlegel [31], [32], were performed to confirm that the transition states connect two appropriate local minima on the reaction pathways. The qualitative description of chemical bonding, namely the donor–acceptor interactions and atomic charges were analysed using the natural bonding orbital (NBO) [33], [34] calculations as implemented in the GAUSSIAN 09W package.

2.2 Model System

To represent the active site in this study, we have chosen the dimeric $\text{H}_4\text{V}_2\text{O}_7$ gas-phase model as illustrated in Figure 1 [9]. Although this model oversimplifies the catalytic surface, we believe the calculated relative energies will provide insight about the most likely mechanistic steps that are followed. The selected model structure comprises two vanadyl bonds, $\text{V}(\text{V})=\text{O}$, one two-coordinated bridging O atom, $\text{V}(\text{V})-\text{O}-\text{V}(\text{V})$, and the four H atoms are added to balance the -4 charge on the four O atoms that would be coordinated onto the support. Only the vanadyl O atom and the two-coordinated bridging O atom were considered for this study and all the atoms were allowed to relax in calculations. Our results show that there is reasonable agreement of the calculated model structure parameters and its vibrational spectrum when these are compared with the experimental values. More detail is included as supplementary material.

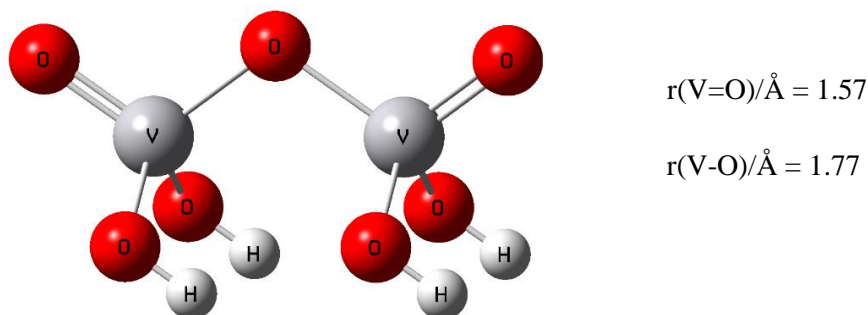


Figure 1 $\text{H}_4\text{V}_2\text{O}_7$ model. B3LYP/6-311+G(d,p) for H and O atoms, and ECPs for V atom.

2.3 Reaction Scheme for *n*-Hexane to 2-Hexene

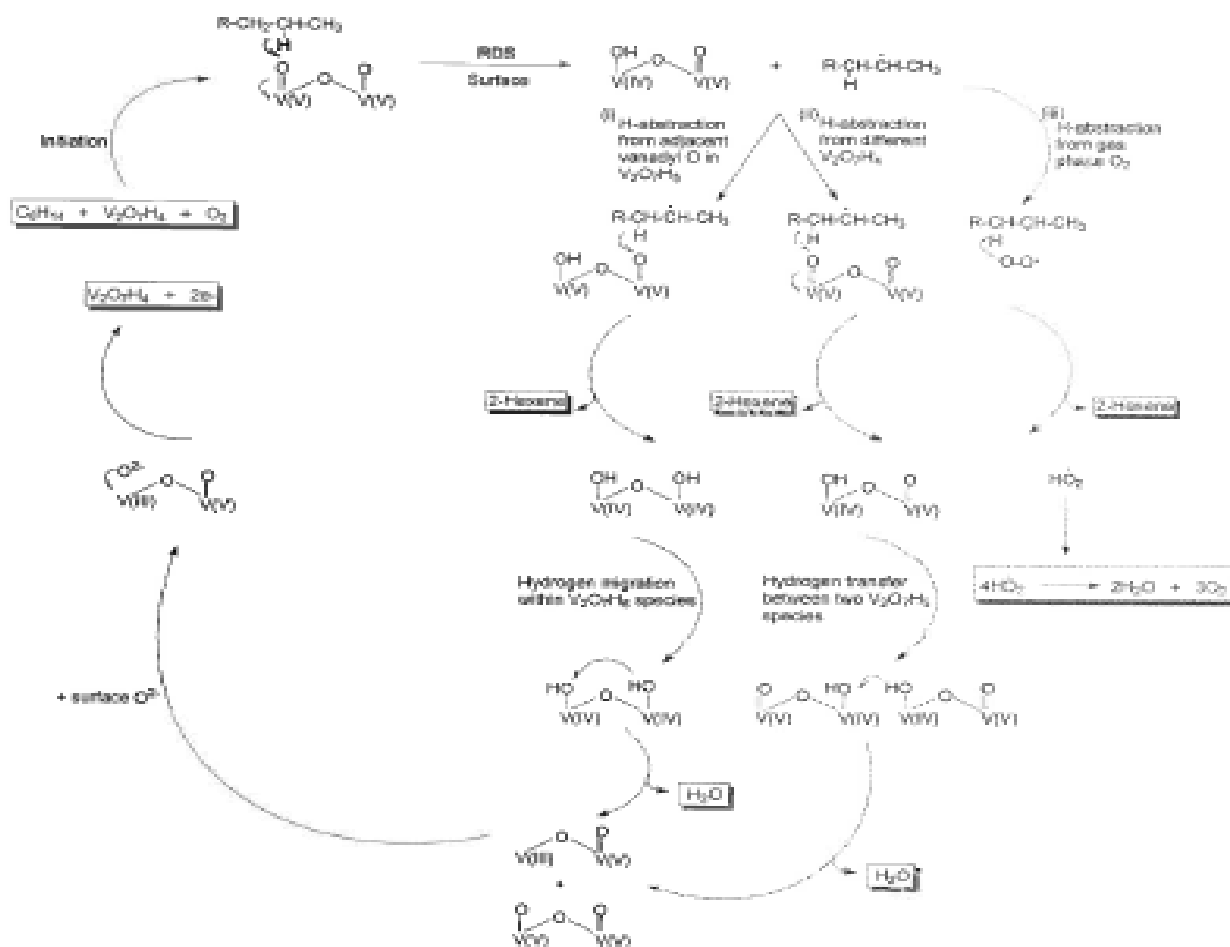


Figure 2 Proposed reaction scheme, $R = CH_2CH_2CH_3$.

Figure 2 depicts the proposed reaction scheme for catalytic ($H_4V_2O_7$) ODH reaction of *n*-hexane to 2-hexene. No literature has reported the formation of 3-hexene in the product mixture, and we have also not identified it in our experimental results. Therefore only the formation of 1- and 2-hexene is represented by the scheme above, with only the pathway for 2-hexene shown.

We propose that H-abstraction from the *n*-hexane chain by the vanadyl O atom in $H_4V_2O_7$ is the rate-determining step. The resulting intermediate stabilise to an alkyl radical and $V_2O_7H_5$. This reaction step is accompanied by reduction of one V(V) centre in $H_4V_2O_7$ to V(IV) in $V_2O_7H_5$. Three propagation pathways that may lead to 2-hexene are, (i) the blue-coloured pathway is γ -H abstraction by the adjacent vanadyl O in $V_2O_7H_5$ to produce 2-hexene and $V_2O_7H_6$ comprising two V(IV) centres, (ii) the green-coloured pathway is γ -H abstraction by a vanadyl O on a different $H_4V_2O_7$ active site to produce 2-hexene and $V_2O_7H_5$ containing one V(IV) centre, and (iii) the magenta-coloured pathway is the gas-phase γ -H abstraction by O_2 to produce 2-hexene and a hydroperoxyl radical (HO_2) species, which disproportionates in the termination step produce water and oxygen. One of the two pathways that may regenerate the V(V) centre include intramolecular H-migration in $V_2O_7H_6$ (with two V(IV) centres) that is formed in propagation pathway (i) above, to produce H_2O , V(III) and V(V) centres in $H_4V_2O_6$. The other pathway involves H-transfer between two $V_2O_7H_5$ (each with one V(IV) centre)

species to produce H₂O, V(V) centres, and H₄V₂O₆ comprising V(III) and V(V) centres. Lastly, the reoxidation of V(III) to V(V) centre may be achieved with interaction of surface O²⁻ species with H₄V₂O₆ to produce H₄V₂O₇.

3 Results

3.1 Activation of *n*-hexane

The radical mechanistic C-H bond activation of *n*-hexane by vanadyl and bridging O atoms in H₄V₂O₇ has been investigated. The energy profile for the two pathways is displayed in Figure 3 with energy values at 673 K, and all the other associated energies are recorded in Table 1.

Several studies [22], [23], [35], [36] have identified the C-H bond activation through H-abstraction by the O atom in V(V)=O as the rate-determining step (RDS). We calculated an activation barrier (TS₁ – Figure 3) of $\Delta E^\ddagger = +32.7$ kcal/mol at 673 K for a similar step, namely, the C-H bond activation in the interaction of C₆H₁₄ and vanadyl O in H₄V₂O₇, leading to the formation of the intermediate complex, $\cdot\text{C}_6\text{H}_{13} + \text{HOV}_2\text{O}_6\text{H}_4$ (Int₁), with $\Delta E = -1.1$ kcal/mol, relative to TS₁. In our previous studies [24], we calculated an activation barrier of $\Delta E^\ddagger = +42.4$ kcal/mol for H-abstraction by gas-phase O₂ and $\Delta E^\ddagger = +27.4$ kcal/mol for H-abstraction by the vanadyl O in H₃VO₄ at the same temperature. Clearly, the present value falls between the two previous values. The VO bond length in H₄V₂O₇ is elongated from 1.57 Å in the isolated unit to 1.70 Å in TS₁ and 1.76 Å in Int₁, and this is attributed to electron shift from a π bonding orbital in V(V)=O to a d-orbital of V, resulting in reduction of V(V) to V(IV). Different authors [19], [37], [38] have experimentally characterised reduced V(IV) sites in unsupported and supported vanadia catalysts. We also compared the above H-abstraction step with that involving the bridging O in H₄V₂O₇. We calculated a higher barrier of $\Delta E^\ddagger = +43.9$ kcal/mol (TS₂ – Figure 3) at 673 K, for C-H bond activation in C₆H₁₄ by the bridging O atom in H₄V₂O₇, and the pathway leads to the formation of Int₂, which comprises the $\cdot\text{C}_6\text{H}_{13}$ radical intermediate adsorbed on to the vanadyl O atom. Although Int₂ ($\Delta E = -40.8$ kcal/mol) is thermodynamically more stable than Int₁ ($\Delta E = -1.1$ kcal/mol), it is likely to lead to side-reaction channels with production of carbon oxides and oxygenates, as a result of the formation of stronger CO bonds [39]. Hui *et al.* [14] obtained similar results in their calculation of reaction barriers of the methylene C-H bond activation in ODH of propane over V₂O₅, with the vanadyl O and the bridging O being +27.3 and +30.4 kcal/mol, respectively. Our results show that the pathway for H-abstraction by the bridging O is more kinetically restricted and would require +11.2 kcal/mol more than that by vanadyl O, and therefore we can conclude that the vanadyl O is likely to be the one involved in C-H bond activation.

We then explored the pathways, through Int₁, that are likely to lead to the formation of 1- and 2-hexene. Figure 4 illustrates the energy diagram for the propagation steps to 2-hexene. All other results are presented in Table 1. The propagation step that involves γ -H abstraction in the $\cdot\text{C}_6\text{H}_{13}$ radical intermediate by the OH group in HOV₂O₆H₄ has an activation barrier of $\Delta E^\ddagger = +23.7$ kcal/mol (TS₃ – Figure 4, red-coloured pathway) at 673 K and leads to 2-hexene, H₂O and H₄V₂O₆ (P₁) with $\Delta E = -22.6$ kcal/mol, relative to TS₃. The involvement of the bridging O in the similar propagation step was also examined, and a slightly lower barrier of $\Delta E^\ddagger = +22.9$ kcal/mol was calculated. We then compared these energy barriers with that for γ -H abstraction in the $\cdot\text{C}_6\text{H}_{13}$ radical intermediate by the adjacent vanadyl O within Int₁ at 673 K, and obtained a lower value of $\Delta E^\ddagger = +9.1$ kcal/mol (TS₄ – Figure 4, blue-coloured pathway) and $\Delta E = -6.3$ kcal/mol, relative to TS₄. Moreover, we calculated an even lower energy barrier of $\Delta E^\ddagger = +6.7$ kcal/mol (TS₅ – Figure 4, green-coloured pathway) and $\Delta E = -35.2$ kcal/mol, relative to TS₅, for γ -H abstraction in the $\cdot\text{C}_6\text{H}_{13}$ radical intermediate by a vanadyl O on a different H₄V₂O₇ site. Examination of these results suggests that the propagation step that may lead to 2-hexene is less likely to involve γ -H abstraction by the OH group in HOV₂O₆H₄ and the bridging O, because these pathways are less kinetically favourable than the other two pathways, as also partly determined in our previous results of gas-phase activation of *n*-hexane over isolated H₃VO₄ species [24]. Therefore, either γ -H abstraction by the adjacent vanadyl O within Int₁ ($\Delta E^\ddagger = +9.1$ kcal/mol) or γ -H abstraction by a vanadyl O on a different H₄V₂O₇ site ($\Delta E^\ddagger = +6.7$ kcal/mol) is likely to be the pathway that produces 2-hexene. The preferred pathway is likely to depend on proximity of

the $\cdot\text{C}_6\text{H}_{13}$ radical intermediate to either the adjacent vanadyl O within Int_1 or the vanadyl O on a different $\text{H}_4\text{V}_2\text{O}_7$ site. However, as stated earlier, chemisorption of the $\cdot\text{C}_6\text{H}_{13}$ radical intermediate to surface O atoms may lead to sideways reactions, with high barriers for releasing 2-hexene and thereby enabling side-reaction channels, such as complete oxidation to undesired carbon oxides and production of oxygenates [39]. In our previous studies on gas-phase ODH of *n*-hexane over isolated H_3VO_4 [24], we calculated a barrier-less energy with $\Delta E^\ddagger = -4.2$ kcal/mol at 673 K, for chemisorption of the hexyl radical on to the vanadyl O. This observation may explain why low yields of less than 20% for 1- and 2-hexene are obtained in our laboratory experiments. Chemisorption of alkyl radicals has also been reported on selective oxidation of propane over V_2O_5 and $\text{V}_2\text{O}_5/\text{TiO}_2$ by Alexopoulos *et al.* [40], who concluded that propene formation via an adsorbed propoxide intermediate is less favourable than propene formation directly from the propyl radical without chemisorption.

Both the two propagation pathways (through TS_4 and TS_5) that are likely to produce the hexenes may lead to the accumulation of the OH groups on the surface. From the P_2 and P_5 fragment ($\text{HOHOV}_2\text{O}_5\text{H}_4$) that is likely to be produced through TS_4 , we then investigated the intramolecular H-migration pathway from one OH group to the other within the fragment. We calculated a barrier-less energy of $\Delta E^\ddagger = -21.5$ (TS_9 – Figure 4, pathway A) and $\Delta E = -1.8$ kcal/mol at 673 K, relative to TS_9 , for the formation of H_2O and $\text{H}_4\text{V}_2\text{O}_6$ (Int_3) that comprises the V(V)-O-V(III) fragment. Clearly, this concerted mechanistic step is associated with the formation of a new O-H bond to produce H_2O , and the scission of the two O-H and V-O bonds. Furthermore, from the P_3 and P_6 fragment ($\text{HOV}_2\text{O}_6\text{H}_4$), we calculated intermolecular H-transfer between two fragments that are likely to be produced through TS_5 . We obtained an energy barrier of $\Delta E^\ddagger = +3.3$ (TS_{10} – Figure 4, pathway B) and $\Delta E = -9.5$ kcal/mol at 673 K, relative to TS_{10} , for the formation of H_2O , regenerated $\text{H}_4\text{V}_2\text{O}_7$ and $\text{H}_4\text{V}_2\text{O}_6$ (Int_4) that also comprises the V(V)-O-V(III) fragment. From the calculated energies (ΔE^\ddagger and ΔE) of the two reaction steps through TS_9 and TS_{10} , we can conclude that both are kinetically and thermodynamically favourable, as also suggested by some authors [14] [41].

Reoxidation of V(V)-O-V(III) to V(V)-O-V(V) proceeds via a Mars–van Krevelen mechanism. We calculated a barrier-less energy of activation, $\Delta E^\ddagger = -177.3$ (TS_{11} – Table 1) and $\Delta E = -76.0$ kcal/mol at 673 K, relative to TS_{11} , for the adsorption of “surface O” species on to the V(III) centre. As reported in our previous studies [24], the involvement of gas-phase O_2 is likely to be limited to propagation steps that may lead to the hexenes, provided the $\cdot\text{C}_6\text{H}_{13}$ radical intermediate is released to the gas-phase rather than being chemisorbed onto the surface O sites. The resulting hydroperoxyl radicals ($\text{HO}_2\cdot$) from H-abstraction by O_2 , may disproportionate to produce H_2O and regenerate O_2 .

It is important to add that future periodic-DFT calculations on this system are likely to improve the quality of the calculated energetics because of better representation of the catalytic solid surface.

3.2 Temperature Effects

All the reaction pathways were modelled using the laboratory experimental conditions of 573, 673 and 773 K. Table 1 displays the calculated Gibbs free energies of activation (ΔG^\ddagger) and Gibbs free energies (ΔG) for all the reaction pathways at the three indicated temperatures.

The transition state theory was used to calculate the rates (k) over the three temperatures for the rate-determining step. The ΔG^\ddagger values increase as the temperature increases from 573 to 673 and 773 K. From the ΔG^\ddagger values we calculated the corresponding rates and obtained the following results, $k(573) = 1.87 \times 10^{-6} \text{ s}^{-1}$, $k(673) = 1.25 \times 10^{-4} \text{ s}^{-1}$ and $k(773) = 3.06 \times 10^{-3} \text{ s}^{-1}$. The calculated k value at 773 K is approximately three orders of magnitude greater than that at 573 K and one order of magnitude greater than that at 673 K. The results show that the rate-determining step is kinetically more favourable at 773 K.

The calculated ΔG values for the rate-determining step are +42.3, +44.4 and +46.5 kcal/mol at 573, 673 and 773 K for the formation of Int_1 , respectively. From the attached supplementary material, the lowest enthalpy ($\Delta H = +29.7$ kcal/mol) and entropy magnitude ($T\Delta S = -12.6$ kcal/mol) contributions

were calculated at 573 K and highest values were obtained at 773 K ($\Delta H = +30.9$ and $T\Delta S = -15.6$ kcal/mol). The ΔH contributions to the ΔG values are the dominant factors at all temperatures and are approximately 2.5 times the magnitude values of $T\Delta S$. Clearly, 573 K is the thermodynamically more favourable temperature for the formation of Int₁ in the rate-determining step. It is important to mention that similar trends were also observed in our previous study of the same reaction over H₃VO₄ [24].

For other reaction pathways, we calculated negative ΔG^\ddagger and ΔG values for the H-migration pathway (TS₉) at all temperatures, whereas, positive values of ΔG^\ddagger and ΔG , which increase with temperature, were obtained for the H-transfer step (TS₁₀). This shows that the H-migration pathway is kinetically and thermodynamically favourable at all temperatures, and the H-transfer pathway is kinetically more favourable at 773 K and thermodynamically favourable at 573 K. The large negative ΔG^\ddagger and ΔG values for the reoxidation of V(III) to V(V) pathway also indicate that this step is kinetically and thermodynamically favourable at all the three temperatures.

Hence, the formation of 1- and 2-hexene from activation of *n*-hexane by H-abstraction with surface H₄V₂O₇ followed by the second H-abstraction from either a different surface H₄V₂O₇ or from gas-phase O₂, is likely to be more kinetically more favourable at 773 K and thermodynamically more favourable at 573 K.

3.3 Natural Bond Orbital Analyses

NBO calculations [33], [34] at the B3LYP/6-311+G(d,p) level were conducted on the selected TSs of the most likely pathways. The TSs, the highest occupied NBOs (HONBOs) representing the donor orbitals, and the lowest unoccupied NBOs (LUNBOs) representing acceptor orbitals are illustrated in Figure 6. Table 2 lists the selected TSs, the atomic charges of the interacting atoms, the NBOs and the stabilization energies.

The HONBO (Lewis-type donor orbital) for the activation of *n*-hexane through the RDS (TS₁) is a lone pair O of *s*(7.5%) *p*(92.5%) type character. The LUNBO (non-Lewis-type acceptor orbital) is the lone pair H of *s*-type character. The transfer of electron density between the two orbitals is associated with the stabilization energy of +164.1 kcal/mol. The calculated atomic charges of the interacting atoms are O (-0.577), H (+0.362) and C (-0.239), indicating a stronger attraction of the positive H atom by the negative O atom. The donor and acceptor orbitals describing the propagation pathway barriers for the formation of 2-hexene (TS₄) through H-abstraction by an adjacent vanadyl O are the O *s*(80.1%) *p*(19.9%) nonbonding hybrid and the V *s*(13.1%) *p*(81.0%) *d*(5.9%) antibonding hybrid, respectively. The calculated stabilization energy is +39.2 kcal/mol. The distribution of atomic charges on interacting atoms are C (-0.506), H (+0.317) and O (-0.460). An alternative pathway that may lead to 2-hexene is H-abstraction by a different vanadyl O site (TS₅), and the associated donor orbital is the O *s*(80.9%) *p*(19.1%) nonbonding hybrid and the acceptor orbital is the V *s*(13.0%) *p*(81.2%) *d*(5.8%) antibonding hybrid, with stabilization energy of +41.6 kcal/mol. The atomic charges on interacting atoms follow a similar trend, with C (-0.507), H (+0.310) and O (-0.432).

The calculated donor orbital for the intramolecular H-migration pathway within the HOHOV₂O₅H₄ unit to produce H₂O and H₄V₂O₆ (TS₉) comprises two bonded atoms, namely, V *s*(2.8%) *p*(15.8%) *d*(81.4%) and O *s*(1.2%) *p*(98.8%) nonbonding hybrid. The acceptor orbital is H *s*(100%) and O *s*(27.8%) *p*(72.2%) antibonding hybrid, with an energy of +33.1 kcal/mol. As expected the positive charge is on the H atom (+0.515) and the negative charges on the two O atoms, the -0.658 charge on the O atom that releases the H atom and the -0.867 on the O atom that receives the H atom. Similarly, the donor-acceptor orbitals describing the intermolecular H-transfer between two HOV₂O₆H₄ units to produce H₂O, H₄V₂O₆ and H₄V₂O₇ (TS₁₀) are O *s*(16.2%) *p*(83.8%) and a combination of H *s*(100%) O *s*(20.9%) *p*(79.1%) antibonding hybrid, respectively. The related stabilization energy is +14.5 kcal/mol and the atomic charges on the interacting atoms are H (+0.512) and O (-0.654) that releases the H atom and the O (-0.916) that receives the H atom.

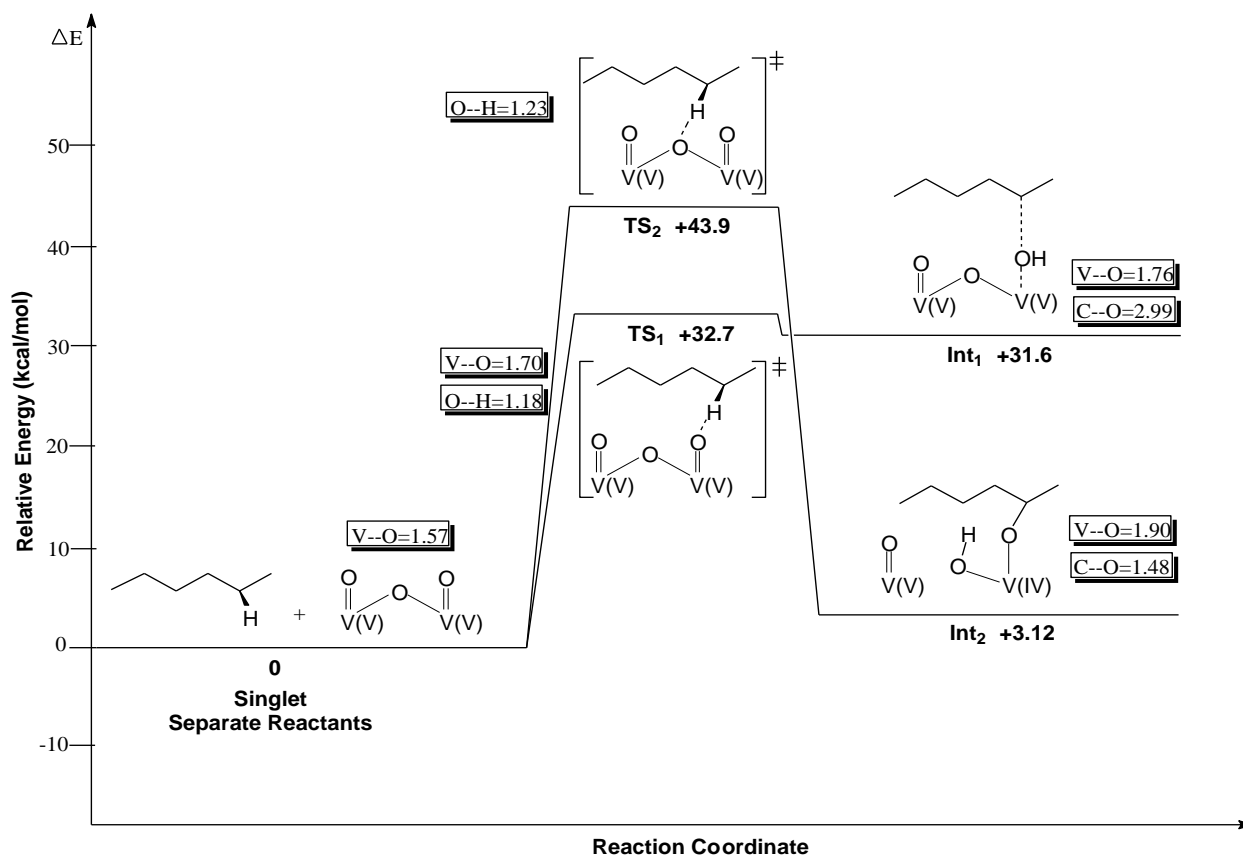


Figure 3 Zero-point corrected relative electronic energy (ΔE) diagram for activation of *n*-hexane over $\text{H}_4\text{V}_2\text{O}_7$ at 673 K. B3LYP/6-311+g(d,p) for the C, O and H atoms, and Stuttgart ECPs for the V atom. The indicated bond distances are in Å. Cartesian coordinates of all TSs are provided as supplementary material.

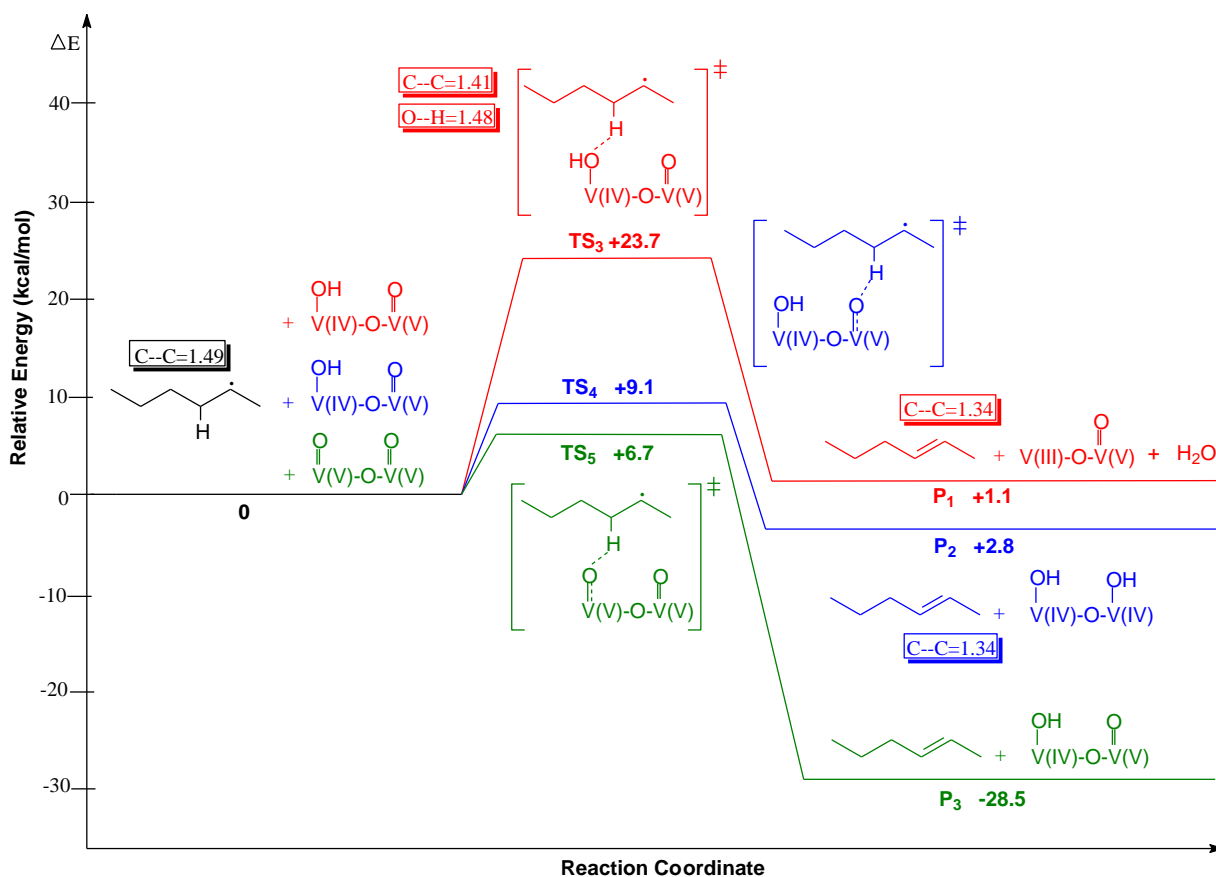


Figure 4 Zero-point corrected relative electronic energy (ΔE) diagram for propagation pathways for the formation of 2-hexene at 673 K. The red colour indicate the kinetically unfavourable pathway for H-abstraction from $\cdot C_6H_{13}$ by OH group in Int₁. The blue colour represents the kinetically and thermodynamically favourable pathway for H-abstraction from an adjacent vanadyl O in Int₁ and the green colour displays a kinetically and thermodynamically favourable pathway for H-abstraction from a different vanadyl O site. B3LYP/6-311+g(d,p) for the C, O and H atoms, and Stuttgart ECPs for the V atom. The indicated bond distances are in Å. Cartesian coordinates of all TSs are provided as supplementary material.

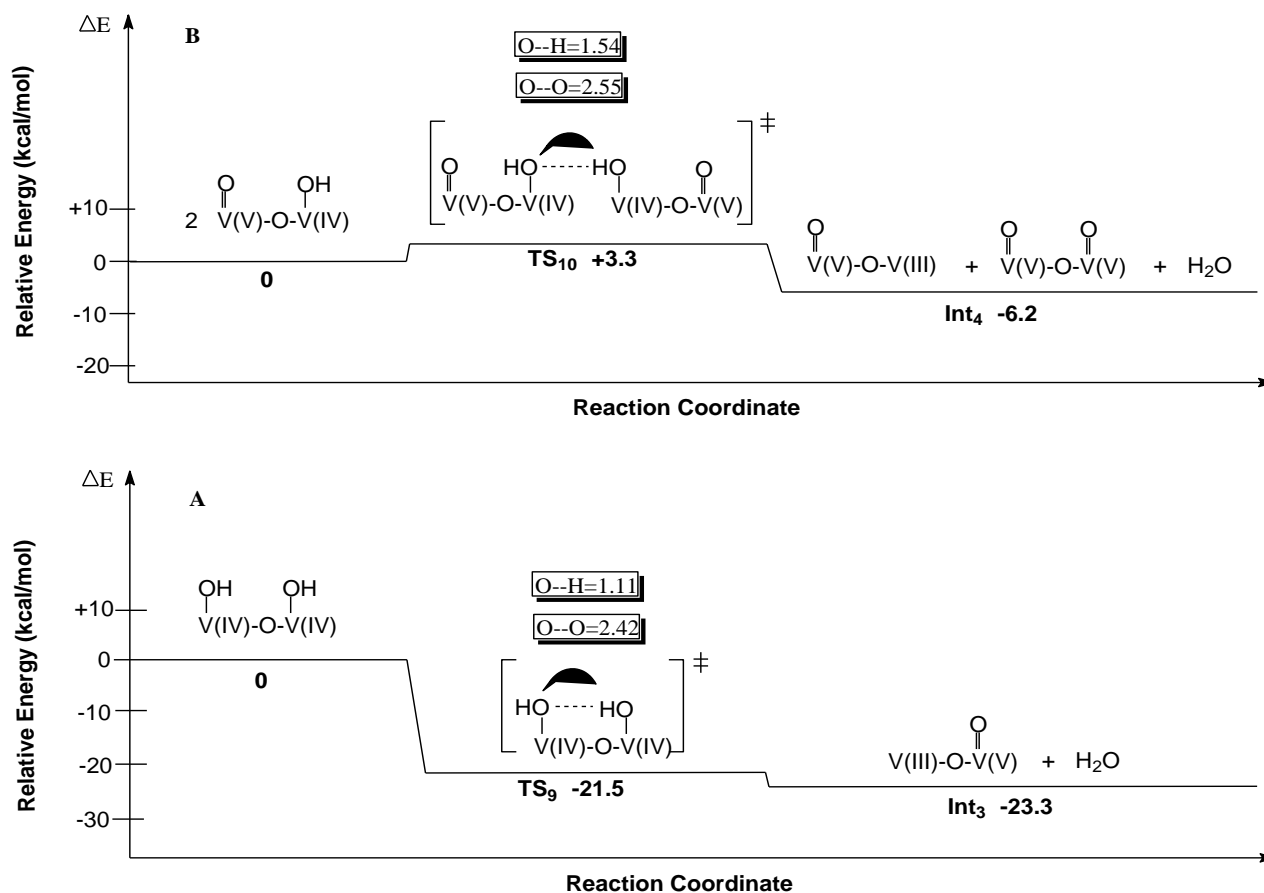


Figure 5. Zero-point corrected relative electronic energy (ΔE) diagrams for intramolecular H-migration in $\text{HOHOV}_2\text{O}_5\text{H}_4$ to produce H_2O and the V(III)-O-V(V) species (pathway A) and intermolecular H-transfer between two $\text{HOV}_2\text{O}_6\text{H}_4$ units to produce H_2O , V(III)-O-V(V) and regenerated V(V)-O-V(V) species (pathway B), at 673 K. B3LYP/6-311+g(d,p) for the C, O and H atoms, and Stuttgart ECPs for the V atom. The indicated bond distances are in Å. Cartesian coordinates of all TSs are provided as supplementary material.

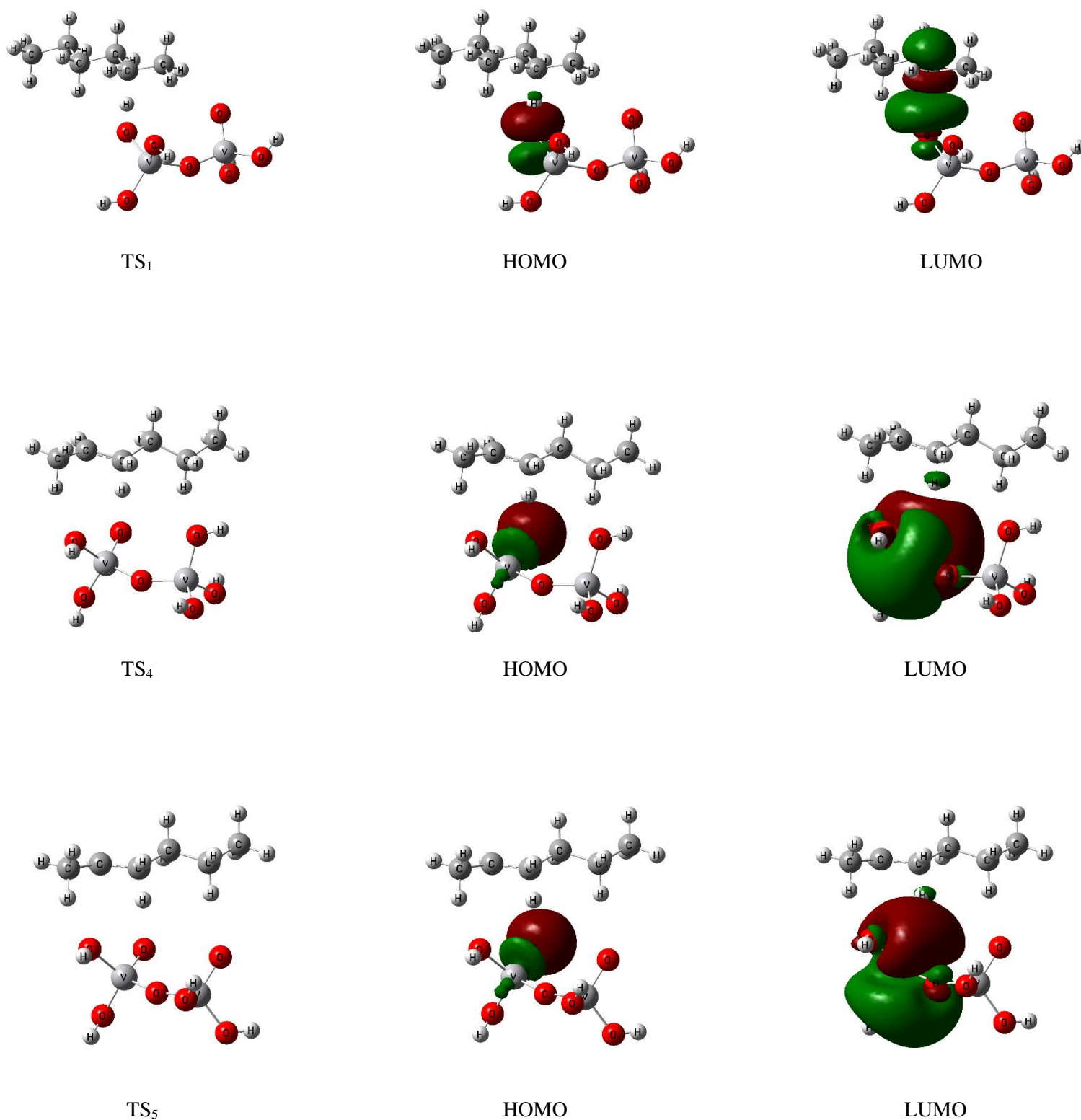
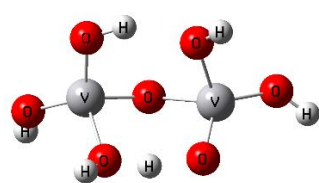
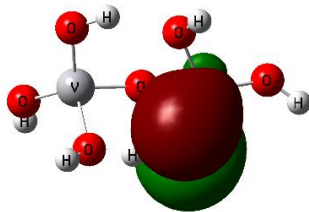
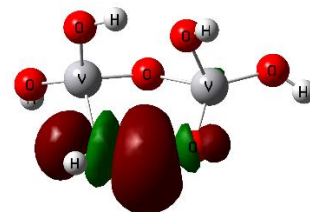


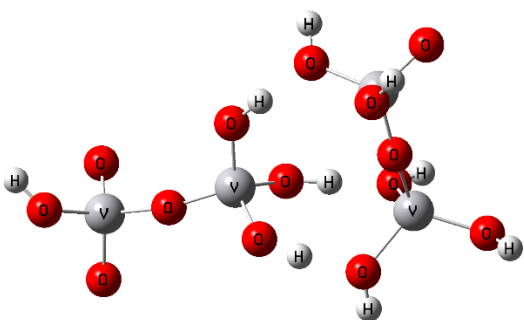
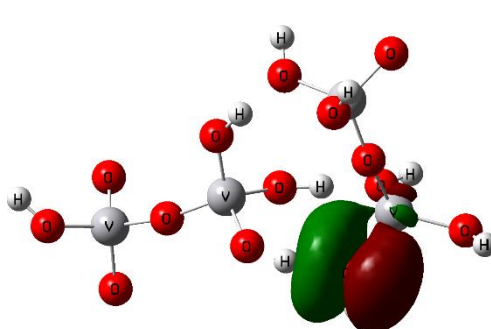
Figure 6 Selected TS structures and the NBO calculated frontier orbitals for the likely mechanistic pathways for the formation of 2-hexene. The orbital lobes are oriented for better clarity in each case and correspond to the reaction coordinate. B3LYP/6-311+g(d,p) for all the atoms. Cartesian coordinates of all TSs are provided as supplementary material.

TS₉

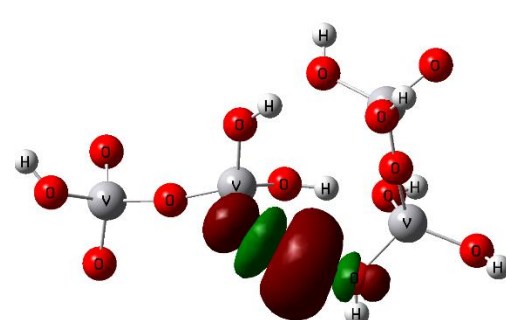
HOMO



LUMO

TS₁₀

HOMO



LUMO

Figure 6 Continuing, Selected TS structures and the NBO calculated frontier orbitals for the likely mechanistic pathways for the formation of 2-hexene. The orbital lobes are oriented for better clarity in each case and correspond to the reaction coordinate. B3LYP/6-311+g(d,p) for all the atoms. Cartesian coordinates of all TSs are provided as supplementary material.

Table 1: Relative Energies (ΔE) and Gibbs Free Energies (ΔG) for the reaction of *n*-hexane with $H_4V_2O_7$ to produce 1- and 2-hexene^a. B3LYP/6-311+g(d,p) for the C, O and H atoms, and Stuttgart ECPs for the V atom. Cartesian coordinates of all TSs are provided as supplementary material.

Reaction Pathway	ΔE	ΔG		
		573	673	773
Initiation				
<i>s</i> - $C_6H_{14}+H_4V_2O_7$	0	0	0	0
<i>s</i> - $C_6H_{14}-H_4V_2O_7$ (TS ₁) – vanadyl O	+32.7	+49.3	+52.5	+55.6
<i>s</i> -TS ₁ → $C_6H_{13}-HOV_2O_6H_4$ (Int ₁)	+31.6 (-1.1)	+42.3 (-7.0)	+44.4 (-8.1)	+46.5 (-9.1)
<i>s</i> - $C_6H_{14}-H_4V_2O_7$ (TS ₂) – bridging O	+43.9	+62.7	+67.3	+72.7
<i>s</i> -TS ₁ → $C_6H_{13}-HOV_2O_6H_4$ (Int ₂)	+3.1 (-40.8)	+26.0 (-36.7)	+30.2 (-37.1)	+34.3 (-38.3)
Propagation from $HOV_2O_6H_4$				
<i>s</i> - $C_6H_{13}+HOV_2O_6H_4$	0	0	0	0
<i>s</i> - $C_6H_{13}-HOV_2O_6H_4$ (TS ₃)	+23.7	+43.2	+55.0	+53.6
<i>s</i> -TS ₃ → $C_6H_{12}+H_4V_2O_6+H_2O$ (P ₁)	+1.1 (-22.6)	+18.6 (-24.6)	+23.5 (-31.5)	+25.3 (-28.3)
<i>s</i> - $C_6H_{13}-HOV_2O_6H_4$ (TS ₆)	+24.4	+48.0	+56.7	+60.7
<i>s</i> -TS ₆ → $C_6H_{12}+H_4V_2O_6+H_2O$ (P ₄)	-13.1 (-37.5)	+8.0 (-40.0)	+7.9 (-48.8)	+16.3 (-44.4)
Propagation from adjacent vanadyl O				
<i>s</i> - $C_6H_{13}+HOV_2O_6H_4$	0	0	0	0
<i>s</i> - $C_6H_{13}-HOV_2O_6H_4$ (TS ₄)	+9.1	+29.3	+33.4	+36.8
<i>s</i> -TS ₄ → $C_6H_{12}+HOHOV_2O_5H_4$ (P ₂)	+2.8 (-6.3)	-7.9 (-37.2)	+10.1 (-23.3)	-0.8 (-37.6)
<i>s</i> - $C_6H_{13}-HOV_2O_6H_4$ (TS ₇)	+9.6	+28.6	+33.1	+35.8
<i>s</i> -TS ₇ → $C_6H_{12}+HOHOV_2O_5H_4$ (P ₅)	-23.0 (-32.6)	-4.0 (-32.6)	+1.0 (-32.1)	+3.1 (-32.7)
Propagation from different vanadyl O				
<i>d</i> - $C_6H_{13}+H_4V_2O_7$	0	0	0	0
<i>d</i> - $C_6H_{13}-H_4V_2O_7$ (TS ₅)	+6.7	+25.3	+28.5	+32.3
<i>d</i> -TS ₅ → $C_6H_{12}+HOV_2O_6H_4$ (P ₃)	-28.5 (-35.2)	-11.9 (-37.2)	-8.8 (-37.3)	-5.6 (-37.9)
<i>d</i> - $C_6H_{13}-H_4V_2O_7$ (TS ₈)	+7.2	+25.3	+29.4	+32.0
<i>d</i> -TS ₈ → $C_6H_{12}+HOV_2O_6H_4$ (P ₆)	-25.3 (-32.5)	-9.8 (-35.1)	-5.5 (-34.9)	-3.9 (-35.9)
H-migration within $HOHOV_2O_5H_4$				
<i>s</i> - $HOHOV_2O_5H_4$	0	0	0	0
<i>s</i> - $HOHOV_2O_5H_4$ (TS ₉)	-21.5	-6.7	-15.6	-2.8
<i>s</i> -TS ₉ → $H_4V_2O_6+H_2O$ (Int ₃)	-23.3 (-1.8)	-11.4 (-4.7)	-21.4 (-5.8)	-9.8 (-7.0)
H-transfer between two $HOV_2O_6H_4$				
<i>s</i> - $HOV_2O_6H_4+HOV_2O_6H_4$	0	0	0	0
<i>s</i> - $HOV_2O_6H_4-HOV_2O_6H_4$ (TS ₁₀)	+3.3	+28.5	+35.0	+37.8
<i>s</i> -TS ₁₀ → $H_4V_2O_7+H_4V_2O_6+H_2O$ (Int ₄)	-6.2 (-9.5)	+19.6 (-8.9)	+24.3 (-10.7)	+29.1 (-8.7)
Reoxidation of $H_4V_2O_6$ to $H_4V_2O_7$				
<i>s</i> -“surface O”+ $H_4V_2O_6$	0	0	0	0
<i>s</i> -“surface O”→ $H_4V_2O_6$ (TS ₁₁)	-177.3	-156.5	-154.9	-149.4
<i>s</i> -TS ₁₁ → $H_4V_2O_7$ (P ₇)	-253.3 (-76.0)	-231.5 (-75.0)	-227.5 (-72.6)	-223.5 (-74.1)

^a ΔE and ΔG are zero-point corrected electronic energy and Gibbs free energy at standard pressure, relative to separate reactants respectively, in kcal/mol. The energies in parentheses are for the indicated reaction pathways. The temperature is in K and ΔE values are at 673K. Prefixes *s*- and *d*- indicate singlet and doublet states, respectively.

Table 2: Selected NBO atomic charges, HONBO and LUNBO orbital types, and orbital energies for the TSs of the *n*-hexane to 2-hexene pathway. B3LYP/6-311+g(d,p) for all the atoms. Cartesian coordinates of all TSs are provided as supplementary material.

TS	Atomic charges on interacting atoms	HONBO type (donor)	LUNBO type (donor)	Stabilization Energy (kcal/mol)
1	C = -0.239 H = +0.362 O = -0.577	O <i>s</i> (7.5%) <i>p</i> (92.5%) nonbonding hybrid	H <i>s</i> (100%) antibonding	+164.1
4	C = -0.506 H = +0.317 O = -0.460	O <i>s</i> (80.1%) <i>p</i> (19.9%) nonbonding hybrid	V <i>s</i> (13.1%) <i>p</i> (81.0%) <i>d</i> (5.9%) antibonding hybrid	+39.2
5	C = -0.507 H = +0.310 O = -0.432	O <i>s</i> (80.9%) <i>p</i> (19.1%) nonbonding hybrid	V <i>s</i> (13.0%) <i>p</i> (81.1%) <i>d</i> (5.8%) antibonding hybrid	+41.6
9	O = -0.658 H = +0.515 O = -0.867	V <i>s</i> (2.8%) <i>p</i> (15.8%) <i>d</i> (81.4%) and O <i>s</i> (1.2%) <i>p</i> (98.8%) bonding hybrid	H <i>s</i> (100%) and O <i>s</i> (27.8%) <i>p</i> (72.2%) antibonding hybrid	+33.1
10	O = -0.654 H = +0.512 O = -0.916	O <i>s</i> (16.2%) <i>p</i> (83.8%) nonbonding hybrid	H <i>s</i> (100%) and O <i>s</i> (20.9%) <i>p</i> (79.1%) antibonding hybrid	+14.5

4 Conclusions

The gas-phase activation of *n*-hexane over $\text{H}_4\text{V}_2\text{O}_7$ has been modelled using DFT methods. The following mechanistic pathways are proposed for the formation of 1- and 2-hexene,



The interaction of *n*-hexane with $\text{H}_4\text{V}_2\text{O}_7$ leads to β -H abstraction by vanadyl O in $\text{H}_4\text{V}_2\text{O}_7$ to produce the $\cdot\text{C}_6\text{H}_{13} + \text{HOV}_2\text{O}_6\text{H}_4$ complex intermediate. This is the rate-determining step with a barrier height of $\Delta E^\ddagger = +32.7$ kcal/mol (TS_1). This value is higher than that obtained in our previous work on gas-phase ODH by vanadyl O in H_3VO_4 ($\Delta E^\ddagger = +27.4$ kcal/mol). The complex intermediate (Int_1) stabilizes with $\Delta E = -1.1$ kcal/mol, relative to TS_1 (Figure 3 and Table 1).



γ -H abstraction occurs through vanadyl O that is adjacent to the V(IV)-OH unit of the $\text{HOV}_2\text{O}_6\text{H}_4$ fragment in Int_1 . The calculated energy barrier is $\Delta E^\ddagger = +9.1$ kcal/mol (TS_4) and the produced P_2 (2-hexene) complex stabilizes to $\Delta E = -6.3$ kcal/mol, relative to TS_4 (Figure 4 and Table 1).



The propagation pathway described in (ii) above is likely to compete with the γ -H abstraction by vanadyl O on a different site. This step has $\Delta E^\ddagger = +6.7$ kcal/mol (TS_5) and the P_3 (2-hexene) complex stabilize to $\Delta E = -35.2$ kcal/mol, relative to TS_5 . The pathway that is likely to occur between (ii) and (iii) may depend on proximity of the $\cdot\text{C}_6\text{H}_{13}$ radical intermediate to either the adjacent vanadyl O or the vanadyl O on a different site (Figure 4 and Table 1).



The propagation pathway described in (ii) above leads to the formation of two OH groups and two V(IV) centres in $\text{HOHOV}_2\text{O}_5\text{H}_4$. The pathway for the migration of the H atom from one OH group to the other has a barrierless $\Delta E^\ddagger = -21.5$ kcal/mol (TS_9) and the complex intermediate (Int_3), containing a V(III) centre, stabilizes to $\Delta E = -1.8$ kcal/mol, relative to TS_9 (Figure 5A and Table 1).



Similarly, the propagation pathway (iii) described above is likely to lead to the formation of an OH group and one V(IV) centre in $\text{HOV}_2\text{O}_6\text{H}_4$. Therefore H-transfer may occur between two $\text{HOV}_2\text{O}_6\text{H}_4$ units, and we calculated a barrier of $\Delta E^\ddagger = +3.3$ kcal/mol (TS_{10}), with the complex intermediate (Int_4), containing separate V(III) and V(V) centres stabilizing to $\Delta E = -9.5$ kcal/mol, relative to TS_{10} (Figure 5B and Table 1).



The generated V(III) complex ($\text{H}_4\text{V}_2\text{O}_6$) from pathways (iv) and (v) above, undergoes reoxidation by “surface O” (NBO atomic charge = -0.988) to produce $\text{H}_4\text{V}_2\text{O}_7$. The calculated barrier-less energy for this pathway is $\Delta E^\ddagger = -177.3$ kcal/mol (TS_{11}) and P_7 stabilizes to $\Delta E = -76.0$ kcal/mol, relative to TS_{11} (Table 1).

Acknowledgments

This work was supported by the NRF, SASOL and Johnsson Matthey. We would like to thank the Centre for High Performance Computing (CHPC) in Cape Town, South Africa, for providing the computational resources necessary to conduct this work.

References

- [1] H.J. Freund, J. Libuda, M. Bäumer, T. Risse, A. Carlsson, **Cluster, facets, and edges: Site-dependent selective chemistry on model catalysts**, Chem. Rec. 3 (2003) 181-201.
- [2] M. Baeumer, H.J. Freund, **Metal deposits on well-ordered oxide films**, Prog. Surf. Sci. 61 (1999) 127-198.
- [3] G.A. Somorjai, **Introduction to surface chemistry and catalysis**, Wiley, N.Y., 1994.
- [4] D.P. Woodruff, T.A. Delchar, **Modern techniques of surface science**, Cambridge University Press, N.Y., 1986.
- [5] R.A. van Santen, P. Sautet, **Computational methods in catalysis and materials science**, Wiley-VCH, 2009.
- [6] B. Hammer, **Theoretical surface science and catalysis-calculations and concepts**, Adv. Catal. 45 (2000) 71-129.
- [7] P. Eisele, R. Killpack, **Ullmann's encyclopedia of industrial chemistry**, Wiley-VCH, 2000.
- [8] T. Blasco. J.M. López Nieto, **Oxidative dehydrogenation of short chain alkanes on supported vanadium oxide catalysts**, Appl. Catal. A 157 (1997) 117-142.
- [9] B. Beck, M. Harth, N.G. Hamilton, C. Carrero, J. Uhlrich, A. Trunschke, S. Shaikhutdinov, H. Schubert, H.J. Freund, R. Schlögl, J. Sauer, R. Schomäcker, **Partial oxidation of ethanol on vanadia catalysts on supporting oxides with different redox properties compared to propane**, J. Catal. 296 (2012) 120-131.
- [10] A. Corma, J.M. López Nieto, N. Paredes, **Influence of the preparation methods of V-Mg-O catalysts on their catalytic properties for the oxidative dehydrogenation of propane**, J. Catal. 144 (1993) 425-438.
- [11] M.A. Chaar, D. Patel, H.H. Kung, **Selective oxidative dehydrogenation of propane over V-Mg-O catalysts**, J. Catal. 109 (1988) 463-467.
- [12] F.D. Hardcastle, I.E. Wachs, **Raman spectroscopy of chromium oxide supported on Al₂O₃, TiO₂ and SiO₂: A comparative study**, J. Mol. Catal. 46 (1988) 173-186.
- [13] I.E. Wachs, B.M. Wechuysen, **Structure and reactivity of surface vanadium oxide species on oxide support**, Appl. Catal. A 157 (1997) 67-90.
- [14] F. Hui, L. Zhi-Pan, L. Zhen-Hua, W. Wen-Ning, F. Kang-Nian, **Periodic density functional theory study of propane oxidative dehydrogenation over V₂O₅(001) surface**, J. Am. Chem. Soc. 128 (2006) 11114-11123.
- [15] A.M. Prakash, M. Hartmann, Z. Zhu, L. Kevan, **Incorporation of transition metal ions into MeAPO/MeAPSO molecular sieves**, J. Phys. Chem. B 104 (2000) 1610-1616.

- [16] K.D. Chen, A.T. Bell, E. Iglesia, **The Relationship between the electronic and redox properties of dispersed metal oxides and their turnover rates in oxidative dehydrogenation reactions**, *J. Catal.* 209 (2002) 35-42.
- [17] S.T. Oyama, **Adsorbate bonding and the selection of partial and total oxidation pathways**, *J. Catal.* 128 (1991) 210-217.
- [18] K. Mori, A. Miyamoto, Y. Murakami, **Catalytic reactions on well-characterized vanadium oxide catalysts. 4. Oxidation of butane**, *J. Phys. Chem.* 89 (1985) 4265-4269.
- [19] J.G. Eon, R. Olier, J.C. Volta, **Oxidative dehydrogenation of propane on γ -Al₂O₃ supported vanadium oxides**, *J. Catal.* 145 (1994) 318-326.
- [20] R. Ramirez, B. Casal, L. Utrera, E. Ruiz-Hitzky, **Oxygen reactivity in vanadium pentoxide: Electronic structure and infrared spectroscopy studies**, *J. Phys. Chem.* 94 (1990) 8960-8965.
- [21] A. Fahmi, C. Minot, **A theoretical investigation of water adsorption on titanium dioxide surfaces**, *Surf. Sci.* 304 (1994) 343-359.
- [22] X. Rozanska, R. Fortrie, J. Sauer, **Oxidative dehydrogenation of propane by monomeric vanadium oxide sites on silica support**, *J. Phys. Chem. C* 111 (2007) 6041-6050.
- [23] M. Cheng, K. Chenoweth, J. Oxgaard, A. van Duin, W. Goddard, **Single-site vanadyl activation, functionalization, and reoxidation reaction mechanism for propane oxidative dehydrogenation on the cubic V₄O₁₀ cluster**, *J. Phys. Chem. C* 111 (2007) 5115-5127.
- [24] N.E. Damoyi, H.B. Friedrich, H.G. Kruger, D. Willock, **A DFT Study of the ODH of *n*-hexane over isolated H₃VO₄**, (2017) unpublished.
- [25] P. Mars, D.W. van Krevelen, **Oxidations carried out by means of vanadium oxide catalysts**, *Chem. Eng. Sci.* 3 (1954) 41-59.
- [26] M.J. Frisch, G.W. Trucks, H.B. Schlegel, G.E. Scuseria, M.A. Robb, J.R. Cheeseman, G. Scalmani, V. Barone, B. Mennucci, G.A. Petersson, H. Nakatsuji, M. Caricato, X. Li, H.P. Hratchian, A.F. Izmaylov, J. Bloino, G. Zheng, J.L. Sonnenberg, M. Hada, M. Ehara, K. Toyota, R. Fukuda, J. Hasegawa, M. Ishida, T. Nakajima, Y. Honda, O. Kitao, H. Nakai, T. Vreven, J. Montgomery, J. A., J.E. Peralta, F. Ogliaro, M. Bearpark, J.J. Heyd, E. Brothers, K.N. Kudin, V.N. Staroverov, R. Kobayashi, J. Normand, K. Raghavachari, A. Rendell, J.C. Burant, S.S. Iyengar, J. Tomasi, M. Cossi, N. Rega, N.J. Millam, M. Klene, J.E. Knox, J.B. Cross, V. Bakken, C. Adamo, J. Jaramillo, R. Gomperts, R.E. Stratmann, O. Yazyev, A.J. Austin, R. Cammi, C. Pomelli, J.W. Ochterski, R.L. Martin, K. Morokuma, V.G. Zakrzewski, G.A. Voth, P. Salvador, J.J. Dannenberg, S. Dapprich, A.D. Daniels, Ö. Farkas, J.B. Foresman, J.V. Ortiz, J. Cioslowski, D.J. Fox, **Gaussian 09, Revision B.01**, Gaussian, Inc., Wallingford, 2010.
- [27] A.D. Becke, **Density functional thermochemistry III - The role of exact exchange**, *J. Chem. Phys.* 98 (1993) 5648-5652.
- [28] C. Lee, W. Yang, R.G. Parr, **Development of the Colle-Salvetti correlation energy formula into a functional of the electron density**, *Phys. Rev. B: Condens. Matter* 37 (1988) 785-789.
- [29] M. Dolg, U. Wedig, H. Stoll, H. Preuss, **Energy-adjusted ab initio pseudopotentials for the first row transition elements**, *J. Chem. Phys.* 86 (1987) 866-872.

- [30] J.M.L. Martin, A. Sundermann, **Correlation consistent valence basis sets for use with the Stuttgart-Dresden-Bonn relativistic effective core potentials: The atoms Ga-Kr and In-Xe**, *J. Chem. Phys.* 114 (2001) 3408-3420.
- [31] C. Gonzales, H.B. Schlegel, **An improved algorithm for reaction path following**, *J. Chem. Phys.* 90 (1989) 2154-2161.
- [32] C. Gonzales, H.B. Schlegel, **Reaction path following in mass-weighted internal coordinates**, *J. Phys. Chem.* 94 (1990) 5523-5527.
- [33] J.E. Carpenter, F. Weinhold, **Analysis of the geometry of the hydroxymethyl radical by the "different hybrids for different spins" natural bond orbital procedure**, *J. Mol. Struct. THEOCHEM* 169 (1988) 41-62.
- [34] J.E. Carpenter, F. Weinhold, **The natural bond orbital Lewis structure concept for molecules, radicals, and radical ions**, in: R. Naaman, Z. Vager (Eds.), *The structure of small molecules and ions*, Plenum, N.Y., 1988, pp. 227-236.
- [35] K.D. Chen, A.T. Bell, E. Iglesia, **Kinetic isotopic effects in oxidative dehydrogenation of propane on vanadium oxide catalysts**, *J. Catal.* 192 (2000) 197-203.
- [36] M.D. Argyle, K. Chen, E. Iglesia, A.T. Bell, **Effect of catalyst structure on oxidative dehydrogenation of ethane and propane on alumina-supported vanadia**, *J. Catal.* 208 (2002) 139-149.
- [37] K. Tamara, S. Yoshida, S. Ishida, H. Kakioka, **Spectroscopic studies of catalysis by vanadium pentoxide**, *Bull. Chem. Soc. Jpn.* 41 (1968) 2840-2845.
- [38] K. Devriendt, H. Poelman, L. Fiermans, G. Creten, G.F. Froment, **Angular resolved XPS applied to V₂O₅-based catalysts**, *Surf. Sci.* 352-354 (1996) 750-754.
- [39] M. D. Argyle, K. Chen, C. Resini, C. Krebs, A. T. Bell, E. Iglesia, **Extent of reduction of vanadium oxides during catalytic oxidation of alkanes measured by in-situ UV-Visible spectroscopy**, *J. Phys. Chem. B* 108 (2004) 2345-2353.
- [40] K. Alexopoulos, M. Reyniers, G.B. Marin, **Reaction path analysis of propane selective oxidation over V₂O₅ and V₂O₅/TiO₂**, *J. Catal.* 289 (2012) 127-139.
- [41] L. Cheng, G.A. Ferguson, S.A. Zygmunt, L.A. Curtiss, **Structure-activity relationships for propane oxidative dehydrogenation by anatase-supported vanadium oxide monomers and dimers**, *J. Catal.* 302 (2013) 31-36.

CHAPTER 5

Summary and Proposed Mechanism

The reaction mechanism for the activation of *n*-hexane to 1- and 2-hexene is proposed based on kinetic and thermodynamic properties that were calculated under laboratory experimental conditions of 573 to 773 K, utilising DFT modelling studies. The first part of the project (Chapter 2) relates to homogeneous activation of *n*-hexane by gas-phase molecular O₂. The second and third parts (Chapters 3 and 4) involve heterogeneous catalytic activation of *n*-hexane by isolated H₃VO₄ and H₄V₂O₇ clusters, respectively. It is important to add that the methodology chosen for heterogeneous catalysis is oversimplified in two aspects. Calculations were conducted on ground electronic states of reactants and other multiplicities were not incorporated to investigate spin-crossing possibilities. And the overall modelling was conducted in gas-phase while heterogeneous catalytic systems involve gas-solid interactions. However, the use of cluster models in gas-phase DFT calculations is common in modelling heterogeneous catalytic systems because of the advantages of reasonable computational costs compared to DFT periodic systems, and the possibility of acquiring quicker insight pertaining to reaction mechanisms of such systems.

The catalytic (H₃VO₄ and H₄V₂O₇ models) ODH radical reaction mechanism for the conversion of *n*-hexane to 1- and 2-hexene is proposed thus,



The rate-determining step is β -H abstraction with electronic energy change, $\Delta E^\ddagger = +27.4$ kcal/mol, from *n*-hexane by vanadyl O atom in monomeric H₃VO₄ to produce the $\cdot\text{C}_6\text{H}_{13} + \text{HOVO}_3\text{H}_3$ complex intermediate ($\Delta E = -3.4$ kcal/mol) with reduced V(IV). Activation by dimeric H₄V₂O₇ (vanadyl O and bridging O) or molecular O₂ is unlikely because of higher ΔE^\ddagger values, namely, +32.7 for vanadyl O, +43.9 for bridging O and +42.4 kcal/mol for O₂. The higher activity of isolated and monomeric VO₄ species, rather than dimeric V₂O₇ species, is in agreement with many publications as discussed in Chapter 3 of the thesis.

The corresponding values for Gibbs free energy of activation (ΔG^\ddagger) for monomeric H₃VO₄, dimeric H₄V₂O₇ and O₂ are +48.7, +55.6 and +57.9 kcal/mol at the most favourable temperature of 773 K. The values of ΔG^\ddagger translate to the respective rates per active site as follows, $k(773) = 2.7 \times 10^{-1}$, 3.1×10^{-3} and $6.8 \times 10^{-8} \text{ s}^{-1}$. Between H₃VO₄ and H₄V₂O₇, there is a difference of about two orders of magnitude in reaction rates at the same temperature, suggesting that the structural differences between H₃VO₄ and H₄V₂O₇ may affect the turnover frequency more positively for the monomeric catalytic site.

For both the monomeric H₃VO₄ and dimeric H₄V₂O₇ species, the NBO interactions for β -H abstraction in the rate-determining step are characterised by donation of electron density from a largely *p*-type orbital associated with C (in *n*-C₆H₁₄ + H₃VO₄ interaction) and O (in *n*-C₆H₁₄ + H₄V₂O₇ interaction), to the H *s*-type antibonding orbital. The difference in electronegativity of the donor-atom (O more electronegative than C) may be related to more orbital stability in the interaction involving H₃VO₄ (+272.4 kcal/mol) than that involving H₄V₂O₇ (+164.1 kcal/mol). Furthermore, there is secondary electron distribution through the bridging O atom between the two V atoms in H₄V₂O₇, which decreases the electron density in the vicinity of the reaction coordinate, and this is clearly absent in H₃VO₄. As a result, there is more stability for the TS associated with the H₃VO₄ species than that with H₄V₂O₇, which may explain the higher activity of the monomeric H₃VO₄ species.



The formation of 1- and 2-hexene from the same site (within the complex intermediate, $\cdot\text{C}_6\text{H}_{13} + \text{HOVO}_3\text{H}_3$) is likely to be hindered by high reaction barriers ($\Delta E^\ddagger > 30$ kcal/mol). The hexenes may readily form on a different H₃VO₄ site, with the $\cdot\text{C}_6\text{H}_{13}$ radical releasing a H atom to a nearby vanadyl

O atom, with $\Delta E^\ddagger = +0.3$ kcal/mol and the products stabilize to $\Delta E = -33.5$ kcal/mol for 2-hexene formation. The possibility of the $\cdot\text{C}_6\text{H}_{13}$ radical to emanate to the gas-phase for the second H-abstraction by O_2 (barrier-less $\Delta E^\ddagger = -3.0$ kcal/mol) to produce 2-hexene + $\text{HO}_2\cdot$ radical ($\Delta E = -14.7$ kcal/mol) is likely, albeit the pathway may be limited by low O_2 concentrations and high VO_4 surface areas. However, chemisorption of the $\cdot\text{C}_6\text{H}_{13}$ radical onto either the vanadyl O on the VO_4 site or gas-phase O_2 is also likely, and may lead to -C-O-V- and -C-O-O- complex-like intermediate species, respectively. Chapters 3 and 4 show that such pathways may produce bi-products like oxygenates, through side reactions. This is because the formation of the hexenes through the -C-O-V- and -C-O-O- like species may be inhibited by higher reaction barriers, as demonstrated by the low ΔE^\ddagger values for chemisorption of the $\cdot\text{C}_6\text{H}_{13}$ radical on to vanadyl O and gas-phase O_2 , being -4.9 and $+2.6$ kcal/mol, respectively. Such kinetically favourable values for chemisorption processes may be the reason why low yields of the hexenes are obtained in laboratory experiments.

Disproportionation:
$$\text{HOVO}_3\text{H}_3 + \text{HOVO}_3\text{H}_3 = \text{H}_3\text{VO}_4 + \text{H}_3\text{VO}_3 + \text{H}_2\text{O}$$

The produced V(IV) intermediates (HOVO_3H_3) disproportionate through intermolecular H-transfer ($\Delta E^\ddagger = +3.6$ kcal/mol) between two nearby OH groups to regenerate V(V) as H_3VO_4 , reduced V(III) intermediate (H_3VO_3) and H_2O with $\Delta E = -9.5$ kcal/mol. Although the disproportionation pathway is facile, it may be limited by large surface distances between any two HOVO_3H_3 species, highlighting the importance of a large surface area for monomeric VO_4 species.

Reoxidation and Termination:
$$\text{H}_3\text{VO}_3 + \text{“surface O”} = \text{H}_3\text{VO}_4$$

The V(V) site (H_3VO_4) is regenerated through barrier-less reoxidation (Mars van-Krevelen) of V(III) in H_3VO_3 by “surface O” ($\Delta E^\ddagger = -119.4$ and $\Delta E = -120.3$ kcal/mol). The NBO analysis shows that the atomic charge on the oxidising O is -0.860 . As stated above, the formation of the hexenes through H-abstraction by gas-phase O_2 will lead to the production of $\text{HO}_2\cdot$ radicals, which disproportionate kinetically and thermodynamically favourably to produce O_2 and H_2O .

Examination of the theoretical calculations further show that the entropy contributions for all the proposed pathways are negligible as a result of the slightly negative calculated values of ΔS^\ddagger and ΔS that range from -0.015 to -0.045 kcal/mol K (supplementary material). This signifies that the enthalpy effects (ΔH^\ddagger and ΔH) are the driving forces behind the kinetically and thermodynamically favourable mechanistic pathways.

Therefore, the highest olefin yields are likely to be obtained on catalysts containing isolated monomeric VO_4 sites at high surface areas, rather than dimeric V-O-V sites. Although the involvement of gas-phase O_2 may lead to olefins through pathways in (gas-phase) homogeneous reactions, high concentration of the former are likely to lead to chemisorption that may produce undesired products.

While the presented work can be regarded as successful and with a valid mechanism that is proposed through DFT calculations with cluster models in the gas-phase, it still needs to be substantiated by further studies with, for example, DFT-periodic systems, for thorough gas-solid interpretations. It is essential to mention that in our laboratory experiments we also characterised some hexadienes and aromatic compounds, for example, benzene. Our research group is presently engaged in modelling mechanistic pathways for the 1- and 2-hexene routes to benzene, and more future publications are planned in this regard.

All optimised output structures of the reactants, TSs, intermediates and products are attached on a CD that can be accessed through the Gausview 5.0 graphics interface as implemented in the Gaussian 09W code.